Reliability of Power Electronics Based Power Systems

From Component to System Level Reliability

Fernando Canales, 5672848

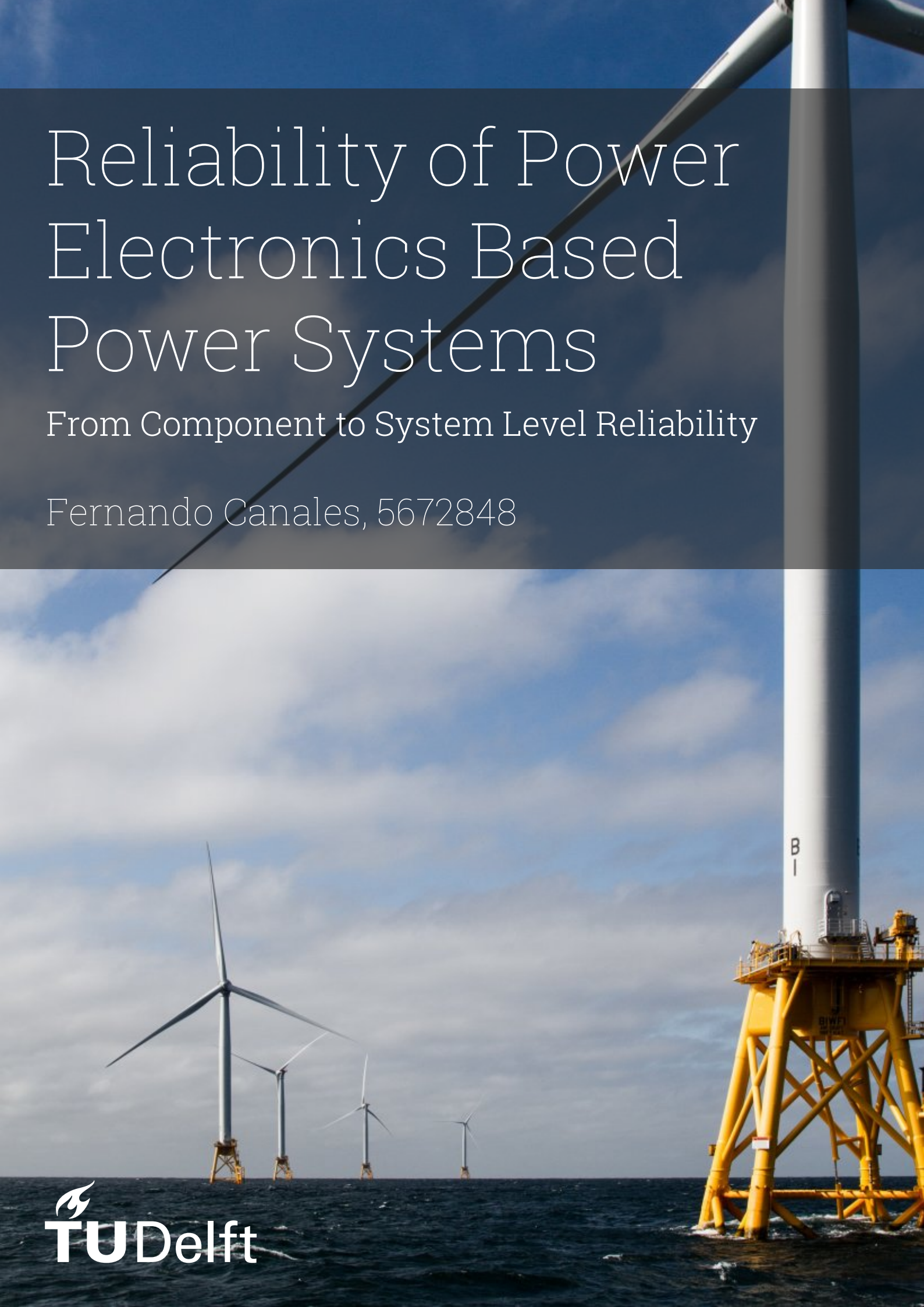

TU Delft

Reliability of Power Electronics Based Power Systems

From Component to System Level Reliability

Fernando Canales, 5672848

University:	Delft University of Technology, Delft
Study Programme:	MSc. Sustainable Energy Technology
	MSc. Electrical Engineering
Thesis Committee:	Dr. Jose Rueda Torres
	Dr. Aditya Shekhar
	Dr. Pedro Vergara
	Dr. Marieke Kootte
	Mr. Miad Ahmadi
Date:	August 19, 2024

Cover: US Department of Energy. (2023). *Wind Energy Technologies Office*. Retrieved from https://www.energy.gov/eere/wind/articles/top-10-things-you-didnt-know-about-offshore-wind-energy

TU Delft

Preface

This report was written by a Delft University of Technology student as part of the Double Degree Master's Thesis project, culminating in master's degrees in Electrical Power Engineering and Sustainable Energy Technologies. It assesses the reliability of AC/VSC-MTDC systems, with a particular focus on enhancing this reliability by balancing redundancy, modularity, and maintenance costs of the system components.

The report assumes that readers possess a basic understanding of probability theory and the electrical engineering principles related to power systems.

Readers with a specific interest in the development and analysis of offshore wind systems and converter reliability modelling are encouraged to focus on chapters 3 and 4. Those more interested in the broader impacts of sustainable energy penetration and power electronics on the overall power system should refer to Chapter 5.

I would like to dedicate this work to my grandmother, a cancer survivor.

Thanks

Fernando Canales, 5672848
Delft, August 2024

Abstract

This research aims to tackle the dual challenges of power electronic uncertainties and the intermittency of renewable energy sources by developing a comprehensive reliability model and conducting a probabilistic evaluation of VSC-MTDC-based hybrid AC/DC power systems. With a specific focus on the North Sea region, the study emphasises enhancing the reliability of these systems, which are increasingly utilised for the efficient transmission of offshore wind power. The objective is to optimise key factors such as redundancy, modularity, and maintenance costs, which are crucial for the reliable integration of these systems into existing power grids.

While Modular Multilevel Converters (MMCs) within these systems offer multiple advantages, the proliferation of power electronic components introduces substantial uncertainties, compounding reliability concerns alongside the inherent variability of renewable energy sources. To address these challenges, the proposed composite probabilistic models account for wind speed variability, turbine drivetrain reliability, and the stochastic behaviour of component failures, providing a detailed reliability model.

The findings highlight substantial opportunities for improving system performance through targeted design and maintenance strategies. By investigating the reliability of offshore wind power, MMCs, DC transmission system and the overall AC/DC system, this research provides valuable insights into optimising system performance and ensuring the efficient integration of renewable energy. The research outcomes include a composite (generation and transmission) model, reliability and cost assessment, an optimal cost-reliability strategy for MMC systems, and a constant risk-minimised cost method of substituting conventional generators with offshore wind power contributing to more resilient and cost-effective renewable energy integration.

The outcomes of this study provide crucial insights into enhancing methods for the reliability of hybrid AC/DC systems. The methodologies and results not only align with global sustainability goals but also bolster energy security by laying a strong foundation for future power grid designs that increasingly depend on sustainable energy sources and advanced power electronics.

Keywords: Adequacy, composite power system, multi-state model, offshore wind power, power electronics, reliability evaluation, VSC-MTDC

Contents

Preface i

Abstract ii

1 Introduction 1

1.1 Literature Overview . . . 1

1.2 Study Case . . . 2

1.3 Research Question . . . 5

1.4 Thesis Outline . . . 6

2 Reliability Evaluation Methodology 9

2.1 Reliability Engineering . . . 9

2.1.1 Reliability Functions . . . 10

2.1.2 Reliability Network Modelling . . . 12

2.1.3 Redundant Systems . . . 14

2.1.4 Maintenance and Asset Management . . . 15

2.1.5 Repairable Systems . . . 16

2.1.6 Frequency and Duration Methods . . . 19

2.2 Reliability Evaluation of Power Systems . . . 20

2.2.1 Available Capacity Model . . . 21

2.2.2 Recursive Algorithm for Capacity Model Building . . . 22

2.2.3 Load Model . . . 23

2.2.4 System Reliability Indices . . . 24

2.3 Summary and Final Remarks . . . 25

3 Reliability Modelling of Offshore Wind Farms 27

3.1 Wind Speed Characteristics . . . 28

3.2 Probabilistic Model of a Wind Turbine Considering Failures . . . 30

3.2.1 Component Downtime and Reliability . . . 31

3.2.2 Amalgamation of Wind Speed and Failure Characteristics . . . 35

3.3 Probabilistic Model of a Wind Farm . . . 36

3.4 Analysis of Wind Farm Model . . . 38

3.4.1 Rounding and Location Effects . . . 38

3.4.2 Drive Train Configuration . . . 39

3.5 Summary and Conclusions . . . 42

4 Reliability Modelling of DC Transmission Systems 44

4.1 Components in DC Transmission Systems . . . 45

4.2 Probabilistic Model of a Power Converter . . . 46

4.2.1 Reliability Function of an MMC's Arm . . . 47

4.2.2 Maintenance Model of an MMC's Arm . . . 49

4.2.3 Reliability Model of an MMC Considering Periodic Maintenance . . . 51

4.3 Reliability Model of a DC Transmission End . . . 52

4.4 Analysis of the DC Transmission Model . . . 54

4.4.1 Converter Sensitivity to Reliability Strategy . . . 55

4.4.2 Cost Optimal Converter Reliability Strategy . . . 56

4.4.3 Converter Reliability Effects on Transmission Capacity . . . 57

4.5 Summary and Conclusions . . . 58

5 Reliability Evaluation of AC/DC Power Systems 60

5.1 Composite Model of Offshore VSC-MTDC-Based Wind Power Supply . . . 61

5.1.1 Reliability Modelling of MTDC systems . . . 61

5.1.2 HLII Composite Model of Offshore Wind Energy 64
5.2 Reliability Evaluation of a Hybrid AC/DC Power System 65
5.3 Reliability Evaluation Analysis 68
5.3.1 Effect of Coupling Degrees on MTDC Reliability 68
5.3.2 Expected Offshore Storage Capacity and Surplus Wind Energy 70
5.3.3 Reliability-Sustainability-Affordability Trilemma in Hybrid AC/DC Power Systems 71
5.4 Summary and Conclusions 72

6 Discussion **74**

7 Conclusion **77**

References **80**

Nomenclature

Variable	Definition	Variable	Definition
α_-	Transition rate to lower capacity state	α_+	Transition rate to higher capacity state
$\boldsymbol{\alpha}$	Transition matrix	λ	Failure rate
λ_{SM}	Failure rate of a sub-module	μ	Repair rate
ρ	Air density	A	Availability
C_p	Power coefficient of a wind turbine	C_g	Generation capacity
C_t	Transmission capacity	C_t	Wind turbine output capacity
C_{gt}	Composite generation and transmission capacity	CTV	Crew Transfer Vessel
EIR	Energy Index of Reliability	$ESWE$	Expected Surplus Wind Energy
$EWEA$	Expected Wind Energy Available	f	Frequency
$HBSM$	Half-Bridge Sub-Module	HLV	Heavy Lift Vessel
h	Hazard rate	k_{max}	Maximum sub-module voltage ripple
l	Number of operational sub-modules required per arm	L_i	Load state i
$LOEE$	Loss of Energy Expected	$LOLE$	Loss of Load Expectation
$LOLP$	Loss of Load Probability	M_k	Margin state k
MMC	Modular Multilevel Converter	$MTTF$	Mean Time To Failure
$MTTR$	Mean Time To Repair	n	Number of redundant sub-modules per arm
N_t	Number of turbines in the wind farm	P_i	Probability of state i
$Q(t)$	Unreliability function	$R(t)$	Reliability function
$R_{stand-by}$	Reliability of stand-by redundancy	$R_{k/n}$	Reliability of k out of n redundancy
R	Number of receiving transmission ends	S	Number of sending transmission ends
SM	Sensitivity to maintenance	SR	Sensitivity to redundancy
T	Duration (Period)	T_m	Maintenance interval
U	Unavailability	v	Wind speed
$V_{dc-link}$	DC transmission voltage	V_{IGBT}	IGBT switch rating

1

Introduction

The global shift towards renewable energy is critical for addressing climate change and ensuring future sustainable energy systems. Offshore wind power, with its vast potential, especially in regions like the North sea, represents a key part of this transition. Therefore, the EU has set an ambitious goal of reaching 111 GW of offshore renewable capacity by 2030, with countries like the Netherlands playing a significant role in this effort. However, harnessing and transmitting offshore wind power over long distances introduces unique reliability challenges to existing power grids.

To efficiently transmit offshore wind power, Voltage Source Converter-based Multi-Terminal Direct Current (VSC-MTDC) systems, particularly those incorporating Modular Multilevel Converters (MMCs), have emerged as a promising solution. These systems offer enhanced power control, flexibility, and the capability to integrate large-scale renewable energy sources. However, the reliability of VSC-MTDC systems is dominated by the stochastic nature of its electronic components failures and the inherent variability of wind power, making reliability analysis and optimisation crucial.

This research addresses these challenges by developing a comprehensive reliability model and conducting a probabilistic analysis of VSC-MTDC-based hybrid AC/DC power systems. The primary motivation is to enhance the reliability of these systems while balancing redundancy, modularity, and maintenance costs. By focusing on the reliability of offshore wind power, MMCs, and the overall AC/DC system, this study provides insights into optimising system performance and ensuring a robust and efficient integration of renewable energy. The findings will contribute to more reliable power systems and support the broader adoption of renewable energy, aligning with global sustainability goals and energy security objectives.

1.1. Literature Overview

The reliability of power systems incorporating wind energy has been a significant area of research, with extensive studies exploring various approaches to assess and enhance system reliability in the presence of intermittent renewable sources. Key contributions in this domain have utilised both analytical models and simulations to evaluate the reliability of generating systems that include wind power. Foundational

works by Billinton et al. [17, 16] and Singh et al. [53] introduced probabilistic methods for reliability evaluation, highlighting the challenges posed by the variability of wind energy. Further studies by Sayas and Allan [49] and Leite da Silva et al. [41] expanded on these methodologies, integrating more complex probabilistic models to better capture the stochastic nature of wind power. However, despite the advancements made, these methods often do not capture the complete particularities of offshore wind energy regarding offshore distance, drivetrain configuration and maintenance costs. Moreover simulation approaches tend to be computationally intensive, making them less compatible with conventional power system reliability evaluation practices.

In the context of DC transmission systems, particularly those based on Voltage Source Converters (VSC), reliability research has also seen considerable development. Studies by Guo et al. [31, 32] and Shen et al. [52] have examined the reliability of VSC-based DC transmission systems, emphasising the need for robust models that account for the unique failure modes and operational characteristics of these systems. MacIver et al. [43] contributed to this field by analysing the reliability impacts of various components and configurations within DC transmission networks. Additionally, significant attention has been given to the reliability of power converters within these systems, with researchers like Wang et al. [63] and Yu et al. [68] focusing on the failure rates and maintenance strategies for converters. However, despite these efforts, comprehensive models that integrate detailed analysis of power converters with overall system reliability remain underdeveloped, indicating a gap in the current literature.

While compositing models that integrate various system components have been well-researched [3], the specific challenge of combining detailed models of offshore wind energy generators and power converters for DC transmission into a single, comprehensive reliability assessment model remains largely unaddressed. This gap is particularly evident when evaluating the adequacy of hybrid AC/DC power systems where conventional generators are replaced by renewable sources such as offshore wind energy. The current research addresses this gap by developing a composite model that incorporates both offshore wind generators and DC transmission systems, assessing its impact on the reliability of an existing AC system. This work builds upon the established foundation of reliability studies while introducing a novel approach to evaluating hybrid power systems, integrating detailed component models into a unified framework that better reflects the complexities of modern power networks.

1.2. Study Case

As stated previously, using VSC-MTDC systems is envisaged to be an effective way to transmit renewable power across long distances. Such is the case for the transmission of wind power generated deep offshore. Such a system is illustrated in Figure 1.1. This figure labels the protagonist components and focus of this thesis. At the subsystem level, the reliability and characteristics of individual elements influence the overall system reliability. This thesis emphasises in developing models from component level of the generating components, specifically wind turbines and their drivetrains, and the AC/DC power converter to power system level. The topology of such a system consists of sending ends, where wind power is generated, and receiving ends, where the system connects to the onshore AC grid. The number of sending and receiving ends represents freedom in designing an HVDC transmission network which also have implications on the power system reliability.

Aside from the chosen system topology and elements a setting is chosen: The North Sea. the immense potential of offshore wind power in the North Sea is particularly significant to the European Union,

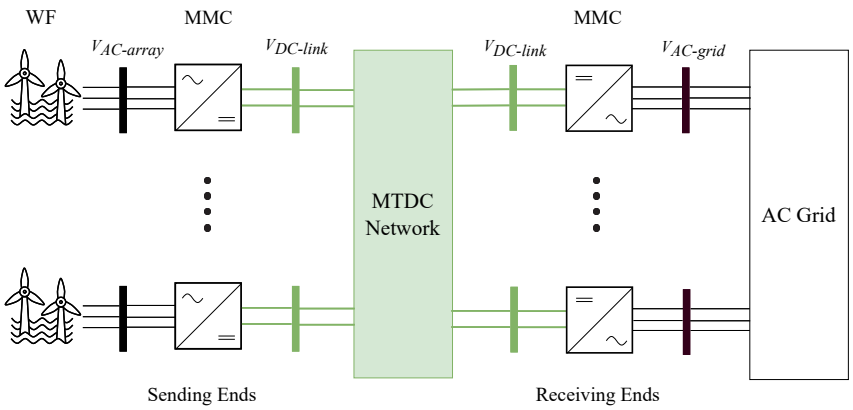

Figure 1.1: VSC-MTDC-Based hybrid AC/DC power system

which has set the ambitious goal of reaching 111 GW of offshore renewable capacity by 2030 [25]. The Netherlands is actively contributing to this effort, with its transmission system operator (TSO) planning to install 16 GW of offshore capacity by 2031 [58]. Figure 1.2 illustrates the intended locations for these offshore wind farms in the North Sea. Therefore, motivated by the high wind resource availability in these locations, the meteorological conditions of these sites have been chosen as the setting.

Figure 1.2: TenneT NL Offshore Wind 2 GW Program Plan [58]

On the transmission side, it has long been known that bulk power transmission through traditional AC systems is less economically attractive at long distances. This is so even though DC transmission requires higher initial capital investment costs, mainly due to the requirement of more expensive converter stations at both the sending and receiving ends, as shown in Figure 1.1. On the other hand, the main

advantages of DC transmission are the reduced number of conductors required to transmit the same amount of power and lower transmission losses. All of these factors result in an approximately 50 km break-even distance for submarine cable transmission [35] [50].

The most simple topology for a DC transmission system is a point-to-point transmission with a converter station at each end. This is indeed the plan stated in the Netherlands' TSO 2GW program by 2030, as shown in Figure 1.3. A topology like this requires only one direct link between sending and receiving end, with no meshing with other ends. Nevertheless, extending this simple interconnection into a meshed topology, namely an MTDC grid, is still an attractive future possibility for reliability purposes. Therefore the reliability gains from this meshed topology will be analysed in this system.

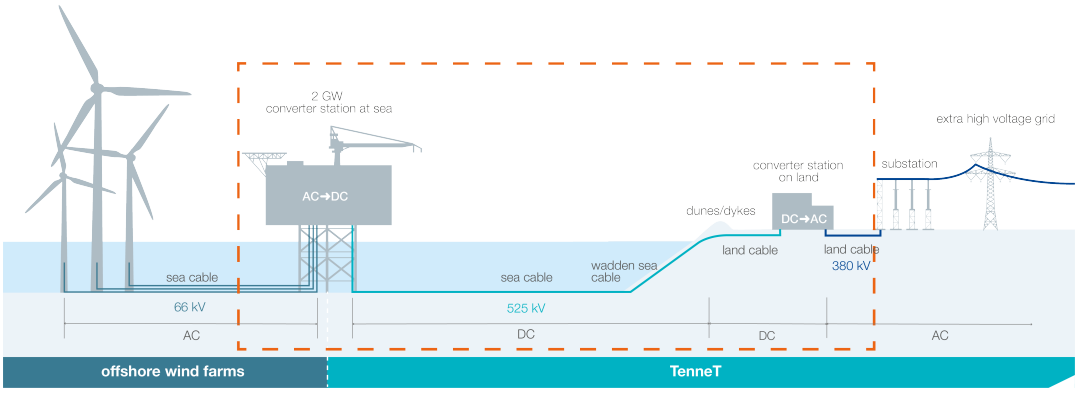

Figure 1.3: TenneT's 2GW Program Grid Connection [58]

HVDC interconnections can be configured in different forms suiting distinct desired performance and operational requirements. The most popular of these is the bipolar configuration with two independent poles. This configuration is very attractive since it can operate at half power capacity with one pole out of service. Due to its popularity and attractiveness, it has been the selected configuration for this thesis [35].

A diagram of a bipolar configuration is shown in Figure 1.4. Each pole can be operated independently using a single pole with the ground as a return path. The fact that HVDC systems can operate at partial capacity means that its model has multiple possible states.

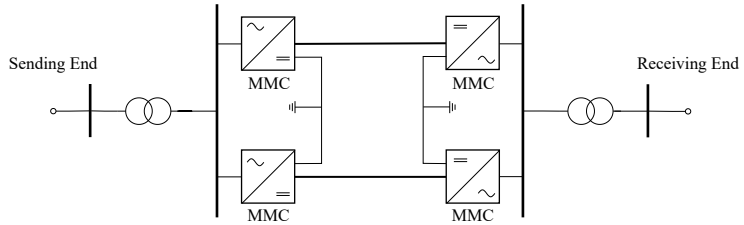

Figure 1.4: HVDC Bipolar Configuration with earth return

The power converter is a main component in these HVDC transmission systems. Two primary conversion technologies are used: line-commutated current source converters (CSCs) and self-commutated voltage source converters (VSCs). The main difference between these technologies lies in the valve type used: CSCs are thyristor-based, while VSCs are transistor-based, as illustrated in Figure 1.5. Both converter types can accomplish the required conversion function, nevertheless some advantages of VSC based HVDC are its self-commutation, superior control, and black-start capabilities.

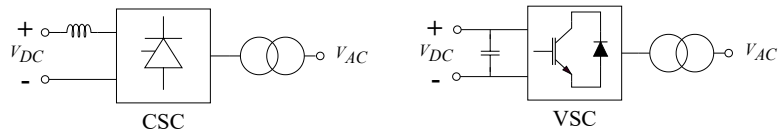

Figure 1.5: Illustrative example of converter technologies

Large remote wind farms require active and reactive power support. Therefore, with its superior power control capabilities, VSC-based HVDC transmission is ideal for long-distance submarine cable transmission. Furthermore, there is no need for communication between terminals since power flow balancing is achieved by monitoring the system voltage. Therefore, VSC-HVDC technology is better suited for MTDC grids [55].

The advantages of VSCs over CSCs have already been stated; nevertheless, multiple VSC topologies exist. The modular multilevel converter (MMC) topology is the most common technology used as VSCs in HVDC. This topology is based on either half-bridge (HB) or full-bridge (FB) structured sub-modules (SM). This means the converter comprises many series-connected sub-modules, each adding to different voltage levels.

In Figure 1.6, it can be seen that the main difference between both SM options is in their output voltage levels and, therefore, the required number of switches. The FB, having four different switches, creates two different voltage levels instead of one. This, however, comes at the cost of increased losses and lower reliability. Because of these disadvantages, the chosen SM topology for the rest of this thesis is a half-bridge-based modular multilevel converter.

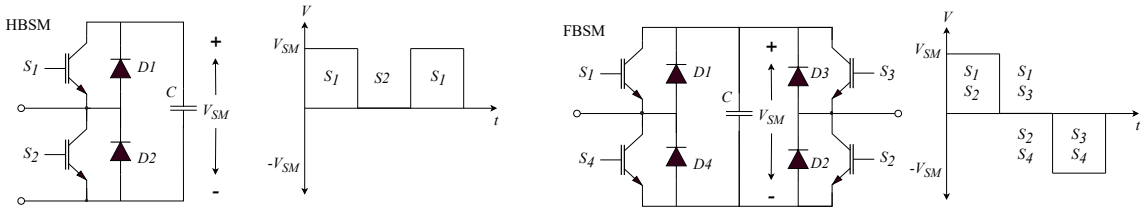

Figure 1.6: Half-Bridge and Full-Bridge SM topologies

1.3. Research Question

Building on the motivation and study case outlined previously, this thesis develops a reliability model and conducts a probabilistic reliability analysis of a VSC-MTDC-based hybrid AC/DC power system. Additionally, it aims to evaluate and propose measures to improve reliability at both the converter and system levels. This research addresses uncertainties associated with the stochastic nature of failures and

the variability of renewable energy sources on the reliability of future power systems. Consequently, the primary research question is defined as follows:

> *"How can the reliability of an AC/VSC-MTDC system based on MMC technology for offshore wind energy generation and transmission be assessed and enhanced while balancing redundancy, modularity, and maintenance costs?"*

Given that this master's thesis contributes to two-degree programs, the main research question is divided into two sets of sub-questions tailored to each program.

For the master's degree in Sustainable Energy Technologies (SET), the sub-questions are:

1. What methods can be used to probabilistically model an offshore wind energy generator's expected available capacity given any chosen meteorological condition setting?
2. What impacts do drivetrain turbine technology and offshore distance have on the output and costs of offshore wind farms?
3. How does the penetration of offshore wind energy in a power system affect overall system adequacy when other conventional generators are decommissioned?
4. How can the surplus wind energy, in instances where curtailment is required, be quantified using probabilistic indices?

For the Electrical Power Engineering (EPE) degree, the sub-questions are:

5. What approaches can be used to model the reliability of an MMC considering different redundancy schemes and preventive maintenance frequencies?
6. How can the reliability of an MMC be optimised in a cost-effective manner?
7. In what way can the reliability of a complete multi-terminal HVDC system be modelled, and how sensitive is this model to coupling degrees?
8. To what extent does the availability of an HVDC transmission system limit the capacity of offshore energy supply, and how does this affect the overall reliability of a power system?

1.4. Thesis Outline

This thesis explores the reliability of power electronics-based power systems, with a particular focus on both component-level and system-level reliability. The research is structured across several chapters, each contributing to a comprehensive understanding of the topic building up to the overall evaluation of a hybrid AC/DC power system. The methodology for reliability analysis is established in Chapter 2, which begins with a detailed discussion of reliability engineering principles. This includes network modelling, redundancy strategies, and maintenance approaches, along with probabilistic modelling techniques that are crucial for evaluating the reliability of complex power systems.

Chapter 3 shifts focus to the reliability modelling of offshore wind farms. It begins by characterising wind speed and the failure probabilities of wind turbines. The chapter then integrates these characteristics

into a probabilistic model that accounts for downtime, rounding effects, and different drivetrain configurations. The reliability model developed here provides essential insights into the broader system reliability discussed in subsequent chapters.

In Chapter 4, the thesis delves into the reliability modelling of DC transmission systems, with a special emphasis on power converters. This chapter explores the reliability functions of Modular Multilevel Converters (MMCs) and examines how periodic maintenance influences overall system reliability. These findings are critical for understanding and evaluating the reliability of multi-terminal HVDC systems, which are analysed later in the thesis.

Chapter 5 integrates the models of offshore wind farms and DC transmission systems developed in earlier chapters to evaluate the reliability of a hybrid AC/DC power system. A composite model of the offshore power system, which includes both AC and DC elements, is introduced in this chapter. This model is used to assess the impact of various factors, such as offshore wind energy penetration and transmission capacity availability, on the overall reliability of the system.

Following the technical evaluations, Chapter 6 discusses the broader implications of the findings, considering both the technical and economic aspects of reliability in power electronics-based systems. The chapter addresses potential trade-offs and examines the relevance of the research to real-world applications, particularly in the context of increasing renewable energy integration.

Finally, the thesis concludes in Chapter 7 by summarising the key findings and their contributions to the field of power system reliability. The conclusion also outlines future research directions, highlighting areas where further investigation could enhance our understanding of reliability in power electronics-based power systems.

Thesis outline

Chapter 1	**Introduction** 1. Literature Overview 2. Study Case 3. Research Question
Chapter 2	**Reliability Evaluation Methodology** 1. Reliability Engineering 2. Reliability Evaluation of Power Systems
Chapter 3	**Reliability Modelling of Offshore Wind Farms** 1. Wind Speed Characteristics 2. Probabilistic Model of a Wind Turbine Considering Failures 3. Probabilistic Model of a Wind Farm 4. Analysis of Wind Farm Model
Chapter 4	**Reliability Modelling of DC Transmission Systems** 1. Components in DC Transmission Systems 2. Probabilistic Model of a Power Converter 3. Reliability Model of a DC Transmission End 4. Analysis of the DC Transmission Model
Chapter 5	**Reliability Evaluation of AC/DC Power Systems** 1. Composite Model of Offshore VSC-MTDC-Based Wind Power Supply 2. Reliability Evaluation of a Hybrid AC/DC Power System 3. Reliability Evaluation Analysis
Chapter 6 - 7	**Discussion & Conclusion** 1. Discussion 2. Conclusion

2

Reliability Evaluation Methodology

This chapter presents the methodology for the reliability analysis necessary to address the research questions stated in Section 1.3. The core of this analysis involves the multi-state probabilistic modelling of all components, which collectively determine the overall state of the power system. With this purpose, Section 2.1 elaborates on the mathematical methods used to model the reliability of components. Then, Section 2.2 focuses on applying the previous models to analyse power systems. Lastly, Section 2.3 summarises the framework, objective, and method for evaluating the chosen power system.

For readers with a background in the reliability evaluation of power systems, it is sufficient to read only Section 2.3.

2.1. Reliability Engineering

Reliability refers to the ability of a system to perform its intended function within desired performance limits for a specified period of time [38]. In the case of power systems, this "function" is essentially the continuous supply of energy to all customers on demand. This is not a straightforward mission, considering power systems' vast size and complexity.

A power system is in itself a physical system comprised of various physical layers, from the smallest elements (e.g., transistors) to subsystems (e.g., converters) and the interconnecting topology of these subsystems (e.g., MTDC network) like illustrated in Figure 2.1. The reliability of power systems is thus an emergent feature stemming from the individual reliabilities of its component layers. This principle underlies reliability engineering, which aims to prevent the failure of all maintainable components within a subsystem.

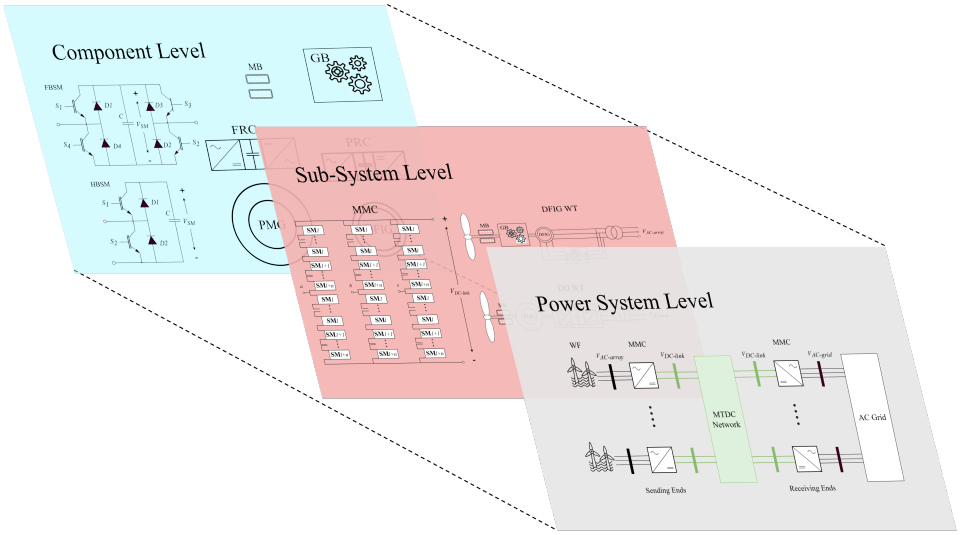

Figure 2.1: Physical Layers of Reliability

Given power systems' continuous and indefinite time operation, their reliability is assessed from the long-term to the short-term. These perspectives are commonly referred to as system *adequacy* and *security* [45]. Adequacy refers to the steady-state availability of sufficient generating capacity to meet consumer demand. Security, conversely, pertains to the system's ability to withstand transient disturbances during its operation [15]. Although this separation exists, a reliable power system must be both adequate and secure. Separating these aspects is only for convenient evaluation purposes, that is adequacy and security can be assessed independently.

From another perspective, a power system reliability evaluation is also subdivided in terms of resolution. That is, separating reliability studies into hierarchical levels depending on the amount of power system levels considered:

- **HLI:** Generators and their ability to supply demand pooled (copper plate transmission).
- **HLII:** The composite capacity of generation and transmission of power to deliver energy at bulk supply points.
- **HLIII:** The complete system capacity, including generation, transmission, and distribution to satisfy the demand of individual consumers.

This thesis focuses on evaluating power system *adequacy* in the context of high penetration of power electronic converter-interfaced and transmitted offshore wind energy based on the probabilistic model building of composite (*HLII*) offshore wind generation and VSC-based MTDC transmission systems. The methods for conducting this evaluation are further detailed in the following sections.

2.1.1. Reliability Functions

The failure probability of a complete device or system is determined using system reliability evaluation techniques. Two primary categories of reliability evaluation techniques exist: *analytical* and *simulation*. In analytical techniques, a mathematical model is developed to represent the system states. On the other

hand, simulation methods, such as Monte Carlo simulations, estimate the reliability indices of a system by simulating the actual process and random behaviour of the system [15].

Although the failure of any one component is stochastic in nature, there are certain ways in which the reliability of systems can be influenced. There are two main ways by which reliability can be improved: *quality* and *redundancy*. Quality pertains to the physical components' robustness and ability to perform their function under different operating conditions and for longer periods of time. Conversely, redundancy acknowledges that components will inevitably fail over time, so sufficient 'backup' should be available in case any component fails.

In continuously operated systems, like power systems, the probabilities of success i.e., *reliability* $R(t)$, or failure i.e., *unreliability* $Q(t)$, of all its components at any given time are derived from actual operational data or accelerated lifetime tests of its smallest elements. These two complementary measures, $R(t)$ and $Q(t)$, are the primary means of assessing a component's quality in terms of reliability.

Furthermore, statistical data, gathered from historical databases (e.g., NESTOR), are used to fit an empirical *failure density function* $f(t)$. This function describes the probability density of a given component having failed up to a specified time t. In reliability evaluation, the preferred function is the exponential function [61]. This choice is due to the exponential function's property of yielding a constant *hazard rate*, $h(t) = \lambda$. The hazard function can be interpreted as a component's conditional rate of failure at time t, given that it has not failed before. A constant hazard rate then implies that the rate of transitions from a healthy state to a failed state remains constant over time [44]. The relationships between these parameters are illustrated and mathematically represented below.

$$f(t) = \frac{dQ(t)}{dt} = \frac{-dR(t)}{dt} = \lambda e^{-\lambda t} \tag{2.1}$$

$$Q(t) = \int_0^t \lambda e^{-\lambda t}\, dt = 1 - e^{-\lambda t} \tag{2.2}$$

$$R(t) = \int_t^\infty \lambda e^{-\lambda t}\, dt = e^{-\lambda t} \tag{2.3}$$

$$h(t) = \frac{f(t)}{R(t)} = \lambda \tag{2.4}$$

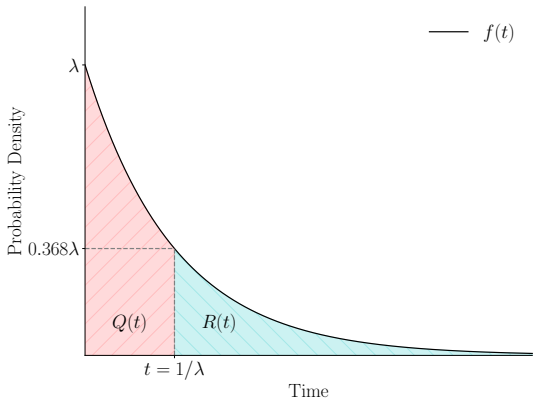

Figure 2.2: Exponential failure density function

An important point is shown in Figure 2.2. At the time $t = 1/\lambda$, both areas and thus probabilities $R(t)$ and $Q(t)$ are equal. In probability theory, this point is regarded as the *mean* of the distribution. It can be regarded as the expected value a random variable would take from this distribution. In reliability theory, this expected value is known as the *Mean Time to Failure* $MTTF$, and the constant hazard rate is generally known as the *failure rate* λ. Mathematically, the expectation or mean, given an exponential distribution, is equated, as shown below. In addition, it is also demonstrated that the expectation of an exponential function is, as mentioned above, equal to $1/\lambda$ and that this can be determined from the integration of the reliability function $R(t)$ alone.

$$\mathbb{E}(t) = \int_0^\infty t f(t)\,dt = \int_0^\infty t\frac{-dR(t)}{dt}\,dt = \cancel{[-tR(t)]_0^\infty} + \int_0^\infty R(t)\,dt = \int_0^\infty e^{-\lambda t}\,dt = \frac{1}{\lambda} = MTTF \quad (2.5)$$

A fundamental tenet of reliability theory is that the hazard function resembles the shape of a bathtub throughout time, as shown in Figure 2.3. This curve, conveniently named "bathtub curve", represents the idea that the rate of failure can be separated into three distinct periods:

- **I** an initial early failure period with decreasing hazard rate, hereby named *de-bugging* period.
- **II** a random failure period where the hazard rate remains constant, named *normal operating life*.
- **III** a final period where the failure rate increases over time, rationally named *wear-out* period.

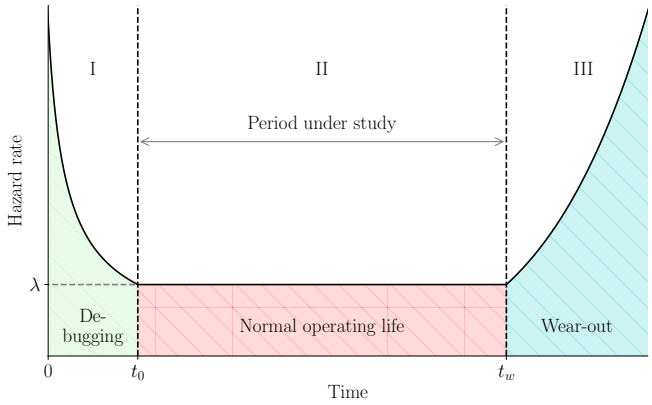

Figure 2.3: Component hazard rate bathtub curve

The general validity of this kind of behaviour for all components can be questioned. Nevertheless, the bathtub curve occupies a place of great importance in reliability evaluation. Thus, the assumption of a constant hazard rate during normal operating life is one backed up by the general literature [39]. Based on the assumptions of constant hazard rate and exponential reliability functions, the reliability modelling of networks can be carried out. This is explained in the following subsections.

2.1.2. Reliability Network Modelling

In the most basic arrangement, components can be "connected" in either series or parallel. In this definition, "connection" is not equivalent to the physical connection of components. In reliability networks, a *series* system is a system in which *all components in the system must work* to have system *success*. In contrast, in *parallel* systems *all components must fail* to have system *failure*. Given these basic arrangements, decomposition techniques are often applied to separate and evaluate system reliability in terms of series and parallel components. These decomposition techniques can be used to evaluate the whole system's reliability comprehensively and to create reduced equivalent reliability networks [15].

The equations used to reduce a series of connected components are shown below. The most important conclusion from this derivation is that the equivalent reliability function of the whole series system is still exponential. Thus, an equivalent constant hazard (failure) rate can be defined as λ_s. Furthermore,

for analysis purposes, Figure 2.4 plots the sensitivity of series system reliability (at any one single instant) to the number n of identical components in series for different cases of individual component reliabilities R_i.

$$R_s(t) = \prod_{i=1}^{n} R_i(t) = \prod_{i=1}^{n} e^{-\lambda_i t} = e^{-\sum_{i=1}^{n} \lambda_i t} \quad (2.6)$$

$$Q_s(t) = 1 - R_s = 1 - e^{-\sum_{i=1}^{n} \lambda_i t} \quad (2.7)$$

$$MTTF_s = \frac{1}{\sum_{i=1}^{n} \lambda_i} \quad (2.8)$$

$$\lambda_s = \sum_{i=1}^{n} \lambda_i \quad (2.9)$$

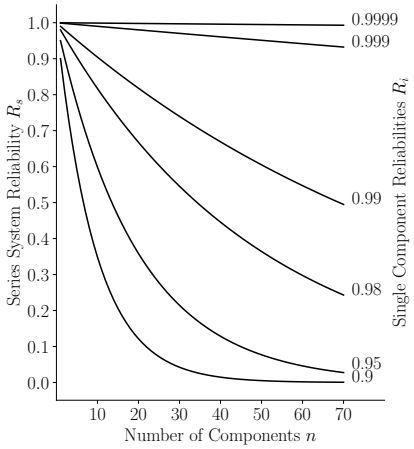

Figure 2.4: Effect of increasing number of series components

The case of parallel systems is shown below. In contrast, in this case, the resultant reliability function is non-exponential. Therefore, the resulting equivalent hazard rate is no longer constant but a function of time. Figure 2.5 depicts the sensitivity of the incremental gains in reliability (again at any one single instant) to a number n of identical parallel components for the same cases of individual component reliabilities R_i.

$$Q_p(t) = \prod_{i=1}^{n} Q_i(t) = \prod_{i=1}^{n} 1 - e^{-\lambda_i t} \quad (2.10)$$

$$R_p(t) = 1 - Q_p(t) = 1 - \left(\prod_{i=1}^{n} 1 - e^{-\lambda_i t} \right) \quad (2.11)$$

$$MTTF_p = \sum_{i=1}^{n} \frac{1}{\lambda_i} - \sum_{1 \le i \le j \le n} \frac{1}{\lambda_i + \lambda_j} + \cdots + (-1)^{n-1} \frac{1}{\sum_{i=1}^{n} \lambda_i} \quad (2.12)$$

$$\lambda_p = \lambda(t) \quad (2.13)$$

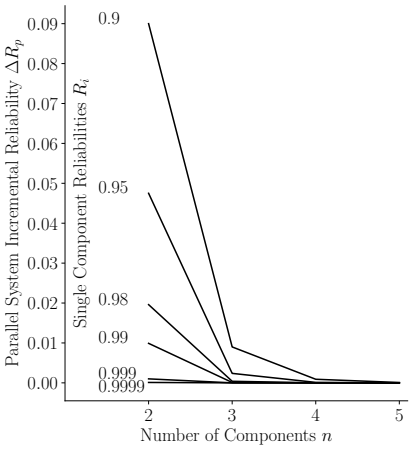

Figure 2.5: Effect of increasing number of parallel components

From these two basic examples, it can be stated that any system composed of many series components (e.g., MMC with many series SMs) will face reliability challenges that cannot be solved only by increasing component reliability (quality). Further, it is also possible to see that the reliability increment per added parallel component is not linear. Thus, choosing the optimal number of parallel redundancies becomes

a complex engineering decision. Choosing a cost optimal redundancy level for an MMC is part of Chapter 4.

2.1.3. Redundant Systems

Power systems (and some converter topologies) are large and complex. Thus, naturally, a power system requires many components in series to realise its function. This fact underlines the necessity for parallel redundancy.

Regarding redundancy, two possibilities exist: *active* or *stand-by* redundancy. In active redundancy, all components work at the same time. In standby redundancy, however, the backup components only initiate working once required. Both of these possibilities stem from basic parallel redundancy. Nevertheless, in real systems sometimes having complete redundancy is not economically feasible, thus they are designed to be *partially redundant*.

More commonly, partial redundancy is called *k-out-of-n* redundancy. This means only a subset k out of a total number of n components is required for system success. Moreover, if all components in the system are identical, then any combination with *at least k* components working would be sufficient for success. The sum of the probabilities of all the possible successful combinations would give the reliability function of the system and can be expressed as follows. In addition, since it was demonstrated in Equation 2.5 that the mean time to failure can be derived from the integration of the reliability function, the mean time to failure expression derived in [64] is shown below.

$$R_{k/n}(t) = \sum_{i=k}^{n} \binom{n}{i} \cdot R_i(t) \cdot Q_{n-i}(t) = \sum_{i=k}^{n} \frac{n!}{i!(n-i)!} \cdot e^{-i\lambda t} \cdot (1 - e^{-\lambda t})^{n-i} \tag{2.14}$$

$$MTTF_{k/n} = \int_0^\infty R_{k/n}(t)\, dt = \int_0^\infty \sum_{i=k}^{n} \frac{n!}{i!(n-i)!} \cdot e^{-i\lambda t} \cdot (1 - e^{-\lambda t})^{n-i} = \sum_{i=k}^{n} \frac{1}{i \cdot \lambda} \tag{2.15}$$

One advantage of active redundancy is that the total burden is divided into equal parts by the total number of components in parallel. This can be considered as correction factors applied to the failure rate of electronic components [12]. On the other hand, the main disadvantage is that all components are exposed to wear and tear throughout the system operation since all components are active at the same time.

Conversely, stand-by redundancy places redundant components into operation until they are needed. Initiating the operation of n *stand-by* backup components sequentially after each preceding one has failed means that a series of conditional probabilities give the system success. This is equivalent to a system that can fail n number of discrete times. This logic implies that its probabilities can modelled through a Poisson distribution. With this in mind, the reliability function and mean time to failure can be mathematically modelled as follows.

$$R_{stand-by}(t) = R(1) \cdot R(2|1) \cdots R(n|n-1) = e^{-\lambda t}\left[1 + \lambda t + \frac{(\lambda t)^2}{2!} + \cdots + \frac{(\lambda t)^n}{n!}\right] = \sum_{x=0}^{n} \frac{(\lambda t)^x e^{-\lambda t}}{x!} \tag{2.16}$$

$$MTTF_{stand-by} = \int_0^\infty R_{stand-by}(t)\,dt = \int_0^\infty \sum_{x=0}^{n} \frac{(\lambda t)^x e^{-\lambda t}}{x!} = \frac{n+1}{\lambda} \tag{2.17}$$

The key assumption here is that the switching system, which senses and changes over components when needed, operates perfectly. Additionally, it is assumed that components do not fail when they are inactive and that the probability of two or more components failing simultaneously is very small [67]. In reality, however, switching systems are not perfect. Moreover, their sensing and control parts add complexity and probabilities of failure to the system. A comparison of the performance of both of these redundant strategies is part of Chapter 4.

2.1.4. Maintenance and Asset Management

In practical systems, other methods of improving reliability, such as different *maintenance strategies* and *stocking spares*, also play a crucial role. Maintenance involves performing activities to ensure that a system remains in a condition that meets the required performance and reliability standards. While the effect of stocking spares is fundamentally the same as that of stand-by redundancy but without automatic switching.

Preventive maintenance aims to reduce the chances of failure by avoiding wear-out of components. Similarly, in power systems, the debugging period is avoided by testing components preventively before commissioning. As a result, the bathtub curve of an asset that is maintained periodically would become discontinuous. Figure 2.6 depicts the effects of maintenance on the hazard rate bathtub curve.

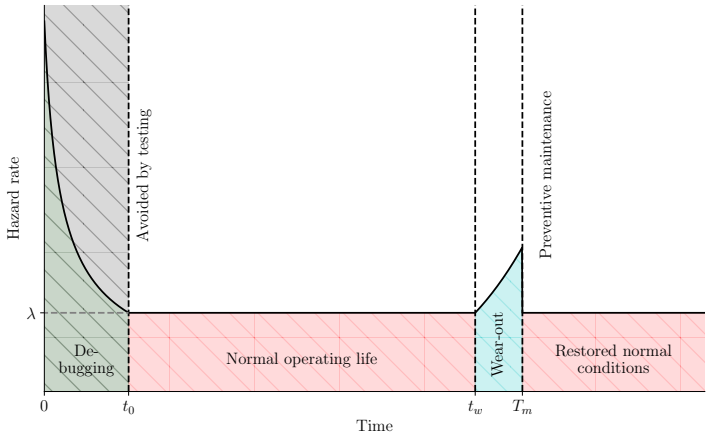

Figure 2.6: Component hazard rate considering asset management

In practice, if proper preventive maintenance strategies are in place, the system can achieve high-reliability values for extended periods of time. This has to be reflected in the reliability function of a

component and, thus, its mean time to failure. Given a periodic maintenance interval T_m, the reliability function would also become discontinuous at the same periodic time interval for each number of discrete activities i. The equations below mathematically express the effect of maintenance.

$$R_{maintained}(t) = \begin{cases} R_x(t) & \text{if } 0 \leq t \leq T_m \\ R_x^i(T_m) \cdot R_x(t - iT_m) & \text{if } iT_m \leq t \leq (i+1)T_m \end{cases} \tag{2.18}$$

$$MTTF_{maintained}(T_m) = \frac{\int_0^{T_m} R_x(t)\,dt}{1 - R_x(T_m)} \tag{2.19}$$

In Equation 2.18, the factor $R_x^i(T_m)$ reflects the quality of the maintenance activity. This factor, ranging from 0 to 1, quantifies the success of the maintenance activity in reinstating the operational conditions to their original "normal" state, $R_x(0)$. Additionally, the exponent i reflects the diminished effectiveness of subsequent maintenance interventions following the initial activity.

The choice of an optimal maintenance interval would intuitively be a shorter interval, which would yield a higher performance. Nevertheless, on a practical basis, time and resource constraints limit this choice. This aspect is further analysed in Chapter 4.

So far, preventive maintenance has been discussed. However, maintenance activities can also be executed to restore the operating state of a component once it has failed. The method for modelling and evaluating systems with this quality of "repairability" is the subject of the next section.

2.1.5. Repairable Systems

Until this moment, the reliability of a system has only been addressed one way: how long it would take to fail. But the reverse direction is possible. The transition from a failed to an operating state is called repair. Similarly to failure, repair can be represented in terms of *mean time to repair* $MTTR$, and *repair rate* μ.

If we assume that the repair rate remains constant in time, i.e., repair of components does not become more difficult as they age, then this implies that repair is also associated with an exponential distribution. Considering these two-way transitions, the probabilities of finding any component in an available state $P_A(t)$ or unavailable state $P_U(t)$, as shown in Figure 2.7, obeys the Kolmogorov forward differential equations [47].

$$\begin{bmatrix} \dot{P}_A(t) & \dot{P}_U(t) \end{bmatrix} = \begin{bmatrix} P_A(t) & P_U(t) \end{bmatrix} \begin{bmatrix} -\lambda & \lambda \\ \mu & -\mu \end{bmatrix} \tag{2.20}$$

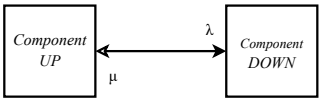

Figure 2.7: Repairable component 2-state space

In this previous equation, the last matrix is conveniently named *transition matrix* $\boldsymbol{\alpha}$. This matrix can

be interpreted as the departure rates of *state i* to *state j*, where i is the row number and j is the column number. Meanwhile, the diagonal of the matrix represents the likelihood that no transitions will occur. This diagonal is always given by the negative sum of the rates of departure to other states, i.e., $\alpha_{i,i} = -\sum_{j\neq i}^{\forall j} \alpha_{i,j}$.

The solutions and behaviour of these differential equations, otherwise called *Markov Process*, are shown below. To solve these equations, we must consider that the initial state is binary, e.g., $P_A(0) = 1$ and $P_B(0) = 0$, and that there is independence between these states, i.e., $P_A(t) + P_B(t) = 1$, In addition, for comparison, the time-dependent success probabilities $R(t)$ of an unrepairable system is also plotted in Figure 2.8.

$$P_A(t) = \frac{\mu}{\lambda+\mu} + \frac{\lambda}{\lambda+\mu} \cdot e^{-(\lambda+\mu)t} \tag{2.21}$$

$$P_U(t) = \frac{\lambda}{\lambda+\mu} - \frac{\lambda}{\lambda+\mu} \cdot e^{-(\lambda+\mu)t} \tag{2.22}$$

$$A = \frac{\mu}{\lambda+\mu} = \frac{MTTF}{MTTR+MTTF} \tag{2.23}$$

$$FOR = U = \frac{\lambda}{\lambda+\mu} = \frac{MTTR}{MTTR+MTTF} \tag{2.24}$$

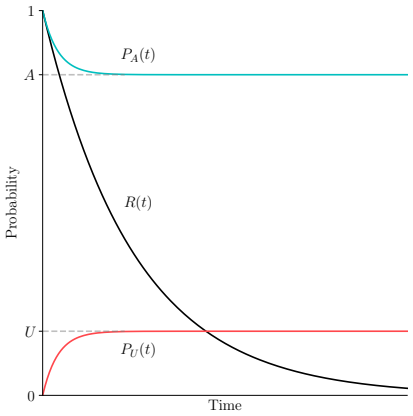

Figure 2.8: Time dependent and limiting states probabilities

The previous plot illustrates that the probability of the system being in either a successful or failed state gradually converges to the steady-state probabilities A and U. These probabilities are determined solely by the system's repair and failure rates. Moreover, since these rates follow an exponential distribution, the steady-state probabilities can also be expressed in terms of mean times to failure and repair. Therefore, in the context of repairable systems, these steady-state probabilities are more commonly referred to as *availability* A and *unavailability* U. The term unavailability is also sometimes called the *force outage rate* FOR.

In more complicated systems, obtaining specific time-dependent expressions for each state becomes increasingly difficult. Thus, a general time dependant solution to the Kolmogorov forward differential equations can be found below.

$$\dot{\mathbf{P}}(t) = \mathbf{P}(t) \cdot \boldsymbol{\alpha} \Rightarrow \mathbf{P}(t) = \mathbf{P}(0) \cdot e^{\boldsymbol{\alpha} t} \tag{2.25}$$

In this equation, $\mathbf{P}(t)$ represents the state probability vector, $\mathbf{P}(0)$ is the initial state vector of the system, and $\boldsymbol{\alpha}$ is the transition matrix. Since a system can have many different configurations and topologies, it is useful to represent this transition matrix with a *state space diagram*.

A state space diagram depicts the operating states of a system and the way these states are connected by their corresponding transition rates. A simple example of a two-component system is shown in

Figure 2.9. In addition, the equations for the time-dependent probabilities for available system states in series and parallel configurations and the probabilities of partial availability, or derated state, in a partially redundant configuration, are shown below.

$$P_{A_{series}}(t) = P_1(t) \tag{2.26}$$

$$P_{A_{parallel}}(t) = P_1(t) + P_2(t) + P_3(t) \tag{2.27}$$

$$P_{D_{partial}}(t) = P_2(t) + P_3(t) \tag{2.28}$$

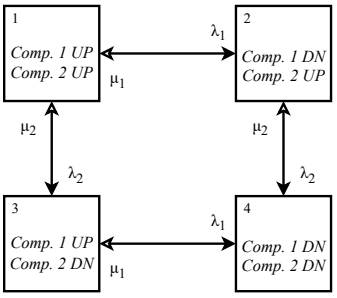

Figure 2.9: State space of 2 repairable components

In systems composed of many components, finding simplified and reduced state space diagrams becomes very useful. This can be achieved by merging equivalent states. For example, in Figure 2.10, states 2 and 3 in Figure 2.9 are considered equivalent, since all components are identical. To ensure that the reduced state space representation is equivalent, the following equations are used to find the new probabilities and transition rates for each new state S composed of merging original states z.

$$P_S(t) = \sum_{z \in S} P_z(t) \tag{2.29}$$

$$\alpha_{S_1 \to S_2}(t) = \frac{\sum_{z_1 \in S_1} P_{z_1}(t) \cdot \alpha_{z_1 \to S_2}}{\sum_{z_2 \in S_2} P_{z_2}(t)} \tag{2.30}$$

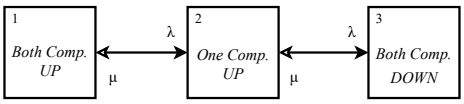

Figure 2.10: Equivalent state space of 2 repairable components

Given that a single unit, e.g., wind turbine, can be composed of a series of repairable components, approximate methods can be utilised to find reduced approximate equivalent series failure λ_s and repair μ_s rates from its components individual rates[30]. The equations for such approximate transition rates are shown below.

$$\lambda_s = \sum_{i=1}^{n} \lambda_i \tag{2.31}$$

$$\mu_s = \frac{\sum_{i=1}^{n} \lambda_i}{\sum_{i=1}^{n} \frac{\lambda_i}{\mu_i}} \tag{2.32}$$

The equivalent failure rate expression is the same as Equation 2.9; nevertheless, the repair rate is an approximation. The main assumption behind this approximation is that no subsequent component

can fail after one component has failed. This is a valid assumption for a system with no inactive failures. Thus, these are the main equations used to find the equivalent model of a single wind turbine considering all of its components in series in Chapter 3.

Lastly, since the steady-state solution is of more relevance in repairable systems, a general mathematical formulation of the steady-state solution is presented. The steady-state probability vector $\mathbf{P}_\infty$ can be determined using the fact that in steady state $\dot{\mathbf{P}}(t) = 0$. Thus, at this time, the differential equations reduce to:

$$0 = \mathbf{P}_\infty \cdot \boldsymbol{\alpha} \tag{2.33}$$

From this last equation, we can conclude that the steady-state probability vector $\mathbf{P}_\infty$ is related to the left eigenvector corresponding to the 0 eigenvalue of the transition matrix $\boldsymbol{\alpha}$. The fact is that $\boldsymbol{\alpha}$ will always have an eigenvalue 0 due to the matrix's singularity of all rows adding to zero, which arises from the conservation of probability [47].

2.1.6. Frequency and Duration Methods

Any physical event that evolves continuously and randomly over time and space can be mathematically modelled as a random variable. In practical applications, these continuous processes are often approximated into a discrete state space, e.g., wind speed states. When combined with the assumptions of a Markovian system, this approximation—where governing equations follow an exponential distribution and transition rates are constant—forms the foundation of frequency and duration methods. These methods are essential for analysing and predicting the reliability and performance of systems over time [49].

The general idea behind this method is that the mean residence time (or duration) of a system in a discrete state T_i over a mean cycle time period T of encountering each individual state i provides insight into the steady state probabilities of finding the system in such state at any other time. Furthermore, the expected transition rate α_{ij} from state i to another state j can be estimated by counting the number of transitions N_{ij} observed during the total duration of state T_i. The relevant mathematical expressions are shown below, and Figure 2.11 illustrates an example of a binary mean time/state diagram.

$$P_i = \frac{T_i}{T} = \frac{m}{T} \tag{2.34}$$

$$\alpha_{ij} = \frac{N_{ij}}{T_i} = \frac{1}{m} \tag{2.35}$$

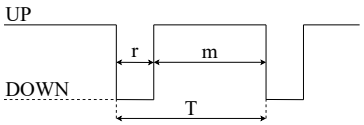

Figure 2.11: Single repairable component state time duration

It has already been stressed that there is a fundamental relationship between transition rates and the mean time duration of each state when using exponential reliability functions. Nevertheless, like in Figure 2.10, some states have more than one other state they can transition towards. Thus, the mean time of residence of each such state becomes a function of adding all of these departure rates going into

another state.

In power systems, it becomes convenient to order the states based on the different levels of system outcomes, e.g., available capacity. Given this order then, the departure rates can be merged into just two directions: transitions going to higher capacity states α_{+i} and transitions going to lower capacity states α_{-i} using Equation 2.30 which reduce to equations Equation 2.36 and Equation 2.37. Another important fact is that the mean cycle time period T is inversely proportional to each state's occurrence frequency f_i. Then Equation 2.34 can be re-written like Equation 2.38.

$$\alpha_{+i} = \sum_{j>i}^{n_j} \alpha_{ij} \tag{2.36}$$

$$\alpha_{-i} = \sum_{j<i}^{n_j} \alpha_{ij} \tag{2.37}$$

$$f_i = P_i(\alpha_{+i} + \alpha_{-i}) \tag{2.38}$$

Frequency and duration methods are most useful for finding reliability indices at specific load connection points, e.g., receiving ends in MTDCs. Henceforth, this method is used to build the probabilistic model of the system. Furthermore, these last equations are fundamental to the recursive algorithm used for a power system's capacity model building, which is the subject of the next section and Chapter 5.

2.2. Reliability Evaluation of Power Systems

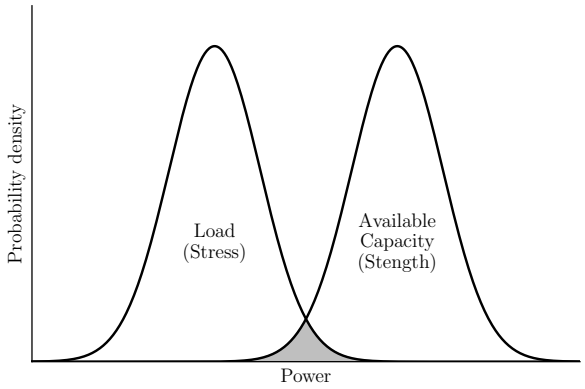

Figure 2.12: Stress-strength model of power systems

The main objective of a power system is to provide a reliable and economical supply of electricity to its customers. This objective's reliability aspect underlies the necessity of redundancy in the system. On the other hand, this redundancy has to be commensurate with its economic objective. Two approaches exist to assess this reliability-cost dilemma: *deterministic* or *probabilistic*.

Usually, deterministic approaches are applied by real system operators because of their simplicity. Some of these deterministic approaches are the percentage reserve margin, largest unit reserve, and the n-1 or n-2 criteria. Nevertheless, these approaches do not correctly represent a power system's stochastic

nature and often lead to over-investments.

Probabilistic approaches were thus developed to consider probabilistic aspects such as forced outage rates of generators, failure rates in the function of circuit length for transmission systems, and probabilistic load models. This form of evaluation is often depicted as a probabilistic stress-strength model, like in Figure 2.12. In this model, the probabilistic distribution of the load (stress) and available capacity (strength) is the means of assessing the probabilities of failure, given by the area between both curves [7].

2.2.1. Available Capacity Model

The *generation capacity model* can be represented by a state space diagram like the one shown in Figure 2.9. In this state space, each unique system state probability P_i is derived from the combination (joint probability) of each generator's independent state g probabilities that compose state i. From another perspective, the generation model is simply a probabilistic model with many discrete (derated) states with probabilities that stem from the product of each component's probability, as shown in Equation 2.39. Then equations (2.36) to (2.38) are used to determine the departure rates and frequency of each individual system capacity state i.

$$P_i(P_1 \cap P_2 \cap \cdots \cap P_g \cap \cdots \cap P_{n_g}) = \prod_{g=1}^{n_g} P_g \tag{2.39}$$

This procedure can create multiple identical generating capacity states, which can be ordered in descending capacity. Moreover, reducing the state space by rounding original capacity states into new merged capacity states C_k is useful for practical and computational expense reasons. This procedure can be carried out using the following equations where it is assumed that state x originally represents a lower capacity than state y but is rounded together into the same capacity state k.

$$C_k \approx C_1 \approx C_2 \approx \cdots \approx C_i \tag{2.40}$$

$$P_k = \sum_{i \in k} P_i \tag{2.41}$$

$$f_k = P_k(\alpha_{+k} + \alpha_{-k}) \tag{2.42}$$

$$\alpha_{+k} = \frac{\sum_{i \in k} P_i \alpha_{+i} - \sum_{(x,y) \in k} P_x \alpha_{xy}}{P_k} \tag{2.43}$$

$$\alpha_{-k} = \frac{\sum_{i \in k} P_i \alpha_{-i} - \sum_{(x,y) \in k} P_y \alpha_{yx}}{P_k} \tag{2.44}$$

This procedure is used to derive *capacity output probability tables*. These tables store each system generation capacity state's probability distribution and transition rates. This is carried out in Chapter 3 to model the capacity output of a wind farm given the aggregation of multiple turbines and their probabilistic model.

A similar procedure can be followed to develop the *available transmission capacity model*. In this model, the probabilities of available transmission capacity considering all its possible configurations are determined and, similarly, are also presented in a *transmission capacity probability table*. In reality, for a power system to fulfill its function, there should be an adequate generation and transmission capacity. Thus, a *composite*

generation and transmission model is determined to carry out *HLII* system adequacy studies. This is done in Chapter 5.

The idea behind building composite models of generation and transmission is finding a *minimum distribution*, where the minimum value between both capacities is taken as the capacity of the composite model. A minimum distribution is the resultant probability distribution of the composite capacity C_{gt} given by combining two independent probability distributions for C_g and C_t. As shown below, this can be expressed mathematically for every possible state C_{gt} as a sum of conditional probabilities. The last term in the expression below is subtracted to avoid double counting the probabilities of equal capacities.

$$C_{gt} = min(C_g, C_t) \tag{2.45}$$

$$P_{gt}(C_{gt}) = P(C_g = C_{gt} \cap C_t \geq C_{gt}) + P(C_g \geq C_{gt} \cap C_t = C_{gt}) - P((C_g = C_{gt} \cap C_t = C_{gt}) \tag{2.46}$$

In addition, transition rates and frequency of each combined state can be found through equations (2.36) to (2.38). Given this composite model, the reliability at specific load points can be determined, or what otherwise can be called *nodal reliability*. The complexity of modelling many generators and interconnections can become unmanageable. Therefore, an alternative method of capacity model building is addressed in the following section.

2.2.2. Recursive Algorithm for Capacity Model Building

The capacity model-building procedure becomes too cumbersome in power systems from its state space analysis. Thus, a recursive capacity model-building algorithm, formalised in [14], is usually applied. Fundamentally, this algorithm does the same as the previous procedure; however, it is not necessary to know all the combinations of individual states of generators beforehand, but rather, each generator is added recursively to the model.

This algorithm's logic addresses the problem from an outage X perspective rather than a state space. Thus, in the mathematical expressions for this algorithm, shown below, X represents the equivalent state of available capacity $C_{tot} - X$.

The general mathematical expressions for the probabilities and transition rates for each state X are shown below. In this expression each generator g can have many intermediate (derated) capacity states C_i and a total n states. These expressions are used recursively until all generators have been added to the model. In this expression, all variables with superscript apostrophes represent the previous iteration value. In contrast, the values without the superscript represent the values of each generator being added with capacity C_i, probabilities P_i, and transition rates $\alpha_{\pm i}$ of each state.

$$P_k(X) = \sum_{i=1}^{n} P'_k(X - C_i)P_i \tag{2.47}$$

$$\alpha_{+k}(X) = \frac{\sum_{i=1}^{n} P'_k(X - C_i)P_i(\alpha'_{+k}(X - C_i) + \alpha_{+i}(C_i))}{P(X)} \tag{2.48}$$

$$\alpha_{-k}(X) = \frac{\sum_{i=1}^{n} P'_k(X - C_i)P_i(\alpha'_{-k}(X - C_i) + \alpha_{-i}(C_i))}{P(X)} \tag{2.49}$$

These equations are equally valid if a composite model of generators and its interconnection is aggregated into an existing system. This is part of Chapter 5. However, the composite generation and transmission model is only one side of the reliability coin. The other side, the load side, is discussed in the following subsection.

2.2.3. Load Model

Frequency and duration methods are similarly used to create probabilistic discrete load models. The idea behind discretising the load is that a low load and peak state can represent each day. Furthermore, the mean duration of this peak state for any given day $T_i = e$, called *exposure factor*, can be defined as a factor ranging from 0 to 1 representing the fraction of time during the day in which the peak is present. In addition, it is assumed that the exposure factor is equal every day.

Load is period dependent, i.e., the expected peak load is very different for weekends than weekdays or different for each season. Thus, multiple peak states can be defined to represent these different expected values. The resulting equations to model peak and low load states using frequency and duration methods are presented below. In these equations, T represents the entire duration of the load model, n is the number of occurrences of a specific load level, and L_i is the peak load level i. Variables with subscript L_i represent peak states, and variables with subscript L_0 low load. Lastly, the frequency can be determined simply from Equation 2.38

Peak Load L_i		Low Load L_0	
$T_{L_i} = e$	(2.50)	$T_{L_0} = 1 - e$	(2.54)
$P_{L_i} = \frac{n(L_i)}{T} \cdot e$	(2.51)	$P_{L_0} = 1 - e$	(2.55)
$\alpha_{+L_i} = 0$	(2.52)	$\alpha_{+L_0} = \frac{1}{1-e}$	(2.56)
$\alpha_{-L_i} = \frac{1}{e}$	(2.53)	$\alpha_{-L_0} = 0$	(2.57)

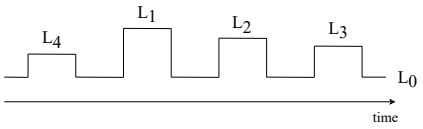

Figure 2.13: Load model state time duration

There is no limit to the number of daily peak load states that can be defined; a value for every day can be defined. Furthermore, the resolution can be increased to model peak loads as hourly ones. The main disadvantage of doing so is the increased computation expense.

Given that the principal focus of this thesis is the modelling and analysis of the composite offshore MTDC system, a given IEEE RTS 24 [8] load model is used to answer the proposed research questions. Nevertheless, it is of utmost importance for real system operators to use realistic load forecast models for a real system reliability evaluation. Furthermore, uncertainty analysis regarding these load forecasts is also relevant since the reliability indices introduced in the next section are very sensitive to the load model [19].

2.2.4. System Reliability Indices

The last step to finally evaluate power system reliability is the capacity and load models combination, as shown in Figure 2.12. The mathematical operation to combine two discrete distributions, creating a convoluted new discrete probability distribution, is called $convolution$. The most simple and commonly used example of a discrete convolution is the distribution of the values given by the sum of a roll of dices, as shown in Figure 2.14 for illustrative purposes.

If generator convention is used, the available capacity values C_{gt} are taken as positive values, and the load state values L_i are taken to be negative, then the sum of states can yield an array of *margin states* M_k. The negative margin states represent the states with a failure condition, i.e., *loss of load*. A convolution in power system reliability evaluation, simply put, yields the probabilities distribution of the new margin states by multiplying the probabilities of each state in one distribution by the probabilities of all the states in another distribution. Then, all the identical margin states are added up to get this new state's probabilities. The mathematical expressions for the values of this new margin state array are shown below.

$$M_k = C_{gt} - L_i \tag{2.58}$$

$$P_M = (P_C * P_L)_M \tag{2.59}$$

$$\alpha_{+M} = \alpha_{+C} + \alpha_{-L} \tag{2.60}$$

$$\alpha_{-M} = \alpha_{-C} + \alpha_{+L} \tag{2.61}$$

$$f_M = P_M(\alpha_{+M} + \alpha_{-M}) \tag{2.62}$$

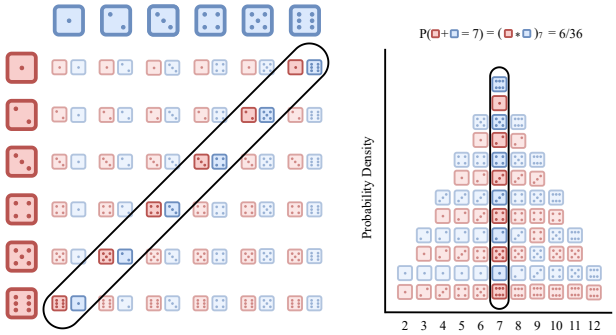

Figure 2.14: Convolution of discrete probability distributions

The margin state array values contain all the information regarding the adequacy of a power system. Thus, it is useful to establish metrics that indicate the system's risk level.

The first index is simply the cumulative probability of any single failure condition event occurring, *loss of load probability* $LOLP$. A second index is related to the expected frequency there is to be loss of load throughout a period of time T in days, *loss of load expectation* $LOLE$ usually measured in days per year. A last common index relates the expected amount of energy that will not be supplied throughout a period of time T in hours, *loss of energy expected* $LOEE$ usually measured in MWh per year. The equations for all of these indices are shown below.

$$LOLP = \sum_{M_k<0} P_M \tag{2.63}$$

$$LOLE = LOLP \cdot \frac{T}{e} \tag{2.64}$$

$$LOEE = \int_0^T \mathbb{E}(M_k)^- \, dt \tag{2.65}$$

Each of these probabilistic indices has its advantages. Nevertheless, for real system operators, a percentage indicator is commonly preferred for its practicality and easier interpretation. The most common percentage reliability index relates the $LOEE$ and the total *expected energy demand* EED throughout a period of time T in hours. This index is adequately called *energy index of reliability* EIR. The following equations determine these indices.

$$EED = \int_0^T \mathbb{E}(L_i)\, dt \tag{2.66}$$

$$EIR = 1 - \frac{LOEE}{EED} \tag{2.67}$$

Lastly, given the variability and sustainability of offshore wind energy, it is also relevant to measure on the other side the *expected surplus wind energy* $ESWE$ [59]. In this case, however, the main focus is on the change of *expected wind energy dispatch* $EWED$ given the wind generators are prioritised by merit order (lowest variable cost) and the *expected wind energy available* $EWEA$.

If the dispatch of wind energy is prioritised, we can determine the $EWED$ by finding the change in $LOEE$ once the wind composite model has been added. On the other hand, the $EWEA$ would be given by integrating the expected available capacity of the model at the same time before compositing the transmission system. Then, we define $ESWE$ as the difference between these two expectations. The equations for these are given below.

$$EWED = LOEE_0 - LOEE_W \tag{2.68}$$

$$EWEA = \int_0^T \mathbb{E}(C_g)\, dt \tag{2.69}$$

$$ESWE = EWEA - EWED \tag{2.70}$$

This surplus indicator references instances where available wind capacity exceeds the demand or the wind energy is curtailed due to lack of transmission capacity. The other metrics indicate adequacy or not, given the probability of having higher demand than the available capacity. It is compelling to see how both of these are related. These results are discussed in Chapter 5.

2.3. Summary and Final Remarks

This chapter introduced the chosen methodology for the reliability analysis tailored to evaluate a hybrid AC/DC power system integrating offshore wind energy and modular multilevel converters. The framework encompasses various probabilistic modelling techniques and reliability evaluation methodologies, each meticulously detailed to address the specific components and their interactions within the power system.

Firstly, the principles of reliability engineering, including the fundamental concepts, were addressed in Section 2.1. The exponential distribution's role in simplifying the reliability analysis was underscored, along with the importance of the bathtub curve in representing the varying failure rates over a component's lifecycle. Then, the reliability network modelling introduced series and parallel systems,

showing how these configurations and strategic redundancy planning improve system reliability. Maintenance strategies, especially preventive maintenance, were discussed in relation to their role in extending component lifespans. The modelling of repairable systems using Markov processes highlighted the transition rates and steady-state probabilities of system availability. Frequency and duration methods were presented as essential tools for analysing power system reliability over time, facilitating the assessment of system performance and reliability indices.

Finally, the reliability evaluation process for power systems was outlined in Section 2.2, focusing on the composite generation and transmission capacity models. The recursive algorithm for capacity model building was presented, providing a practical approach to handling the complexities of large-scale power systems. The load model and its convolution with the capacity model were discussed, leading to the derivation of key reliability indices such as loss of load probability (LOLP), loss of load expectation (LOLE), and loss of energy expected (LOEE).

In conclusion, this chapter has established a robust framework for the proposed HLII reliability analysis, integrating advanced probabilistic modelling techniques and practical methodologies to evaluate the performance and reliability of hybrid AC/DC power systems with significant offshore wind energy penetration. The subsequent chapters will build upon this framework to provide detailed analyses, ultimately contributing to a deeper understanding of the reliability-sustainability-affordability trilemma in modern power systems.

3

Reliability Modelling of Offshore Wind Farms

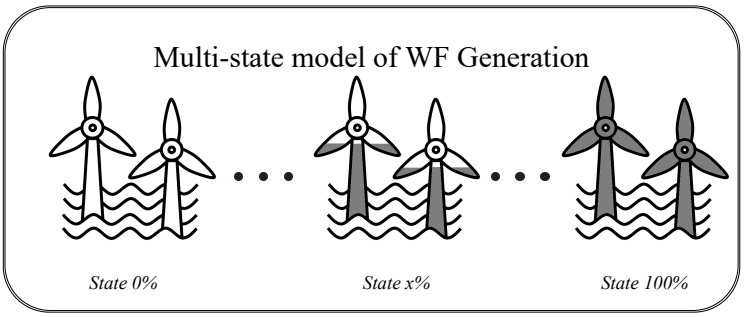

The variability of wind energy resources (wind speed) and the stochastic nature of wind turbine failures are critical factors in the modelling and operation of offshore wind farms. To assess the impact of component failures on wind farm reliability, an advanced probabilistic model based on the methodology outlined in Section 2.1.5 is developed. Additionally, the intermittent nature of wind speed is analytically modelled using the techniques described in Section 2.1.6.

Reliability in the presence of wind power has been extensively studied [17, 16, 53, 49, 41, 18, 59]. These studies utilise both analytical models and simulations, as discussed in Section 1.1. However, simulations require extensive historical hourly wind speed data and are computationally intensive. Moreover, simulations are not always compatible with conventional practices for power system reliability evaluation, as explained in Section 2.2 [24].

The main objective of this chapter is the probabilistic analytical modelling of offshore wind farms, situated in the context described in Section 1.2, addressing sub-research questions 1 and 2 presented in Section 1.3. This chapter is structured as follows: Section 3.1 examines the intermittent nature of wind speed. Section 3.2 develops a probabilistic model of a single wind turbine, incorporating variable wind speed and stochastic component failures. Section 3.3 expands the single wind turbine model to encompass an

entire wind farm. Section 3.4 conducts a sensitivity analysis of the models, considering meteorological conditions, wind turbine drivetrain, and offshore distance. Finally, Section 3.5 summarises the findings and answers the proposed sub-research questions.

3.1. Wind Speed Characteristics

The selected wind sites are all located in the North Sea, as mentioned in Section 1.2. Out of all the locations in the Netherlands' TSO plans of offshore wind farms for 2030 exposed in [58] only 6 have been selected. This is because, as shown in Figure 1.2, these six locations are the most suiting for a future MTDC system since they are relatively close to each other. The exact location of these is tabulated in Table 3.1.

Location	Latitude	Longitude	Offshore Distance (km)
IJmuiden Ver Alpha	52.82	3.73	50
IJmuiden Ver Beta	52.84	3.77	60
IJmuiden Ver Gamma	52.89	3.77	70
Nederwiek 1	53.47	3.07	80
Nederwiek 2	54.04	3.72	90
Nederwiek 3	54.17	3.89	100

Table 3.1: Locations and distances of offshore wind sites

The wind speed series of these locations was extracted from the dutch meteorological institute (KNMI) where hourly data points are registered for all of these locations for 3 years (2019-2021) [40]. The probability distribution of different wind speeds in the Ijmuiden Ver Alpha location is plotted in Figure 3.1. In this figure it is also appreciable to see that the mean wind speed during these three years was 10.38 m/s. This is as significantly high average wind speed, and confirms the attractiveness of this location for offshore wind production.

Another consideration that has not been stated is the relationship between wind speeds and height. Given the existing, although very low, offshore surface roughness at lower heights the measured wind speed is higher at higher altitudes. This effect is called wind shear and can be estimated by two wind profiling methods, logarithmic and power law at higher than 60 m altitudes. The motivation in this case for choosing to plot wind speeds at 150 m height is due to the chosen wind turbine. The designated wind turbine for this model is the *IEA 15 MW offshore reference wind turbine*. Some of the key parameters of this reference turbine are given in Table 3.2 [28].

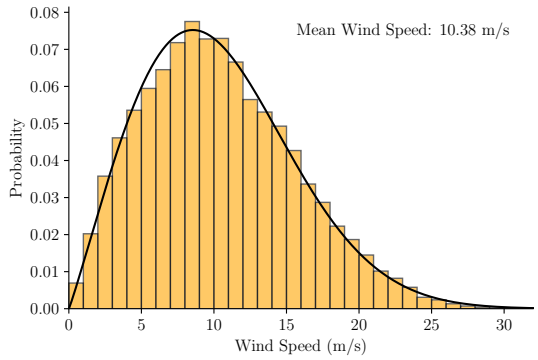

Figure 3.1: Wind speed histogram for IJmuiden Ver Alpha at 150 m height

Parameter	Units	Value
Power rating	MW	15
Turbine class	-	IEC Class 1B
Drivetrain	-	Direct Drive
Cut-in wind speed	m/s	3
Rated wind speed	m/s	10.59
Cut-out wind speed	m/s	25
Rotor diameter	m	240
Hub height	m	150

Table 3.2: Key Parameters for the IEA 15 MW Turbine

The relationship between wind speed and a wind turbine's power output C_t is given by Equation 3.1. Usually this power output is plotted in a power curve for a wind turbine. The curve is defined by two characteristic operating regions:*partial load* and *full load*. The power curve of this reference turbine is shown in Figure 3.2 [1].

$$C_t = \begin{cases} \frac{1}{2}\rho C_p A_r v_t^3 & \text{when } v_{\text{cut-in}} \leq v_t < v_{\text{rated}} \\ P_{\text{rated}} & \text{when } v_{\text{rated}} \leq v_t \leq v_{\text{cut-out}} \\ 0 & \text{otherwise} \end{cases} \tag{3.1}$$

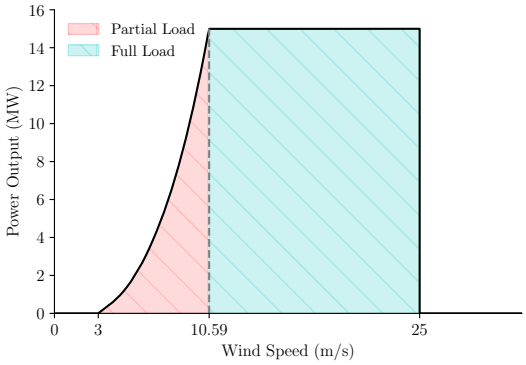

Figure 3.2: IEA 15 MW offshore reference turbine power curve

Since the available power output capacity of a turbine is limited by its uncontrollable primary resource, it is crucial to account for the probabilistic nature of wind speeds during a reliability analysis. By combining the probabilistic wind speed with the power output curves, we can define a model with the probability of discrete output states for a single wind turbine W_t. The number of states used in this model is a trade-off between accuracy and computational and time resources.

In power system reliability studies, often many states for single generators are undesired. Moreover, many of these states yield the same output and can be merged into equivalent states. Therefore, for this thesis the available resources where the primary factor for deciding to round and merge the turbine model into a 5 state model based on the rounding and merging of wind speed states that yield these 5 outputs, like shown in Figure 3.4. Once the wind speeds and thus output power has been rounded and merged into these arbitrary 5 states, frequency and duration methods equations (2.34) to (2.38), like explained in Section 2.1.6, can be used to probabilistically model a single turbine accounting only for the probabilities of wind speeds. The state space representation of this single turbine is shown in Figure 3.3.

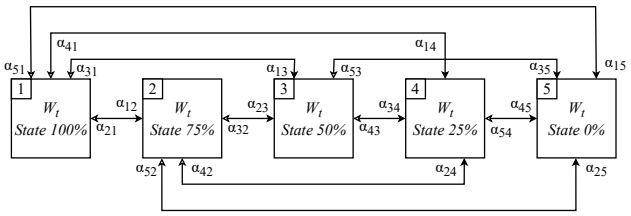

Figure 3.3: Multi state model for a single wind turbine W_t

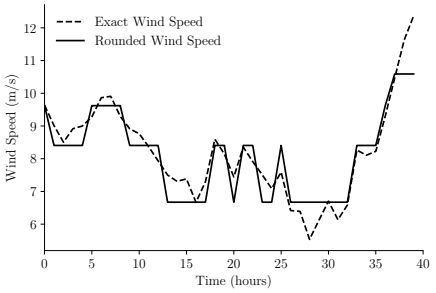

Figure 3.4: 40 hours wind speed sequence rounding

This generation capacity model can be depicted through a *turbine capacity output probability table* $TCOPT$ and a transition matrix representation of its state space, as shown in Table 3.3. The result that the state with the highest probability is the full output state 1 is expected given the mean speed of this location is 10.38 m/s. Furthermore, this is commensurate with the theoretical values of capacity factor for wind turbines offshore which typically achieve a capacity factor of even above 0.5 [10]. In addition, a more visual depiction of the probability distribution contained in the table is shown in Figure 3.5

States	C_t (MW)	v_t (m/s)	P_i (-)	α_{+i} (occ/day)	α_{-i} (occ/day)	f_i (occ/day)
1	15	10.59	0.48	0.00	1.64	0.78
2	11.25	9.62	0.08	6.76	7.15	1.10
3	7.5	8.41	0.11	5.93	5.30	1.25
4	3.75	6.67	0.26	2.65	1.31	1.04
5	0	0.00	0.07	5.58	0.00	0.38
Sum			1.00			

Table 3.3: IEA 15 MW wind speed dependent TCOPT

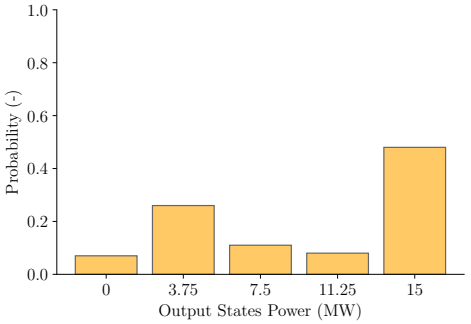

Figure 3.5: IEA 15 MW wind speed dependent turbine model output probability distribution

This initial probabilistic model, which accounts solely for the probabilities of wind states, proves to be overly optimistic. Therefore, the subsequent section addresses the incorporation of stochastic elements related to component failures.

3.2. Probabilistic Model of a Wind Turbine Considering Failures

Determining offshore wind turbine component failure rates and resource requirement for repair are vital for modelling a single turbine as a repairable system. These two vital inputs are both sensitive to the selected turbine technology and the distance offshore. Therefore, an approximate model based on the aggregation of all individual components reliabilities is determined in Section 3.2.1. Then, Section 3.2.2 combines the probabilistic characteristics of both turbine failures and wind speeds into a single wind turbine probabilistic model.

3.2.1. Component Downtime and Reliability

A population analysis based on ~350 offshore wind turbines over a 5-year period was carried out in [20]. Later, the same author created a model for the availability, maintenance and repair of offshore wind turbines considering their offshore distance and drivetrain configuration [21]. The model developed was based on Monte Carlo Markov Chain simulations of 40 hypothetical offshore wind farms. The model developed here is based on the output downtime and failure rates of this model.

The composition of two different wind turbine drivetrains is illustrated in Figure 3.6 and Figure 3.7. These illustrations clearly highlight the key differences between the two configurations. The primary distinctions lie in the presence of the *gearbox* GB, which features *three stages* $3s$ in the first configuration and is entirely absent in the second. Additionally, the *generator* types differ, with the first configuration utilising a *doubly fed induction generator* $DFIG$ and the second employing a *permanent magnet generator* PMG. Lastly, the *converter* varies, with one configuration using a *partially rated converter* PRC and the other a *fully rated converter* FRC.

Given these differences, henceforth, the drivetrain in Figure 3.6 is referred as *3s DFIG PRC*, while the drivetrain in Figure 3.7 is called *DD PMG FRC*.

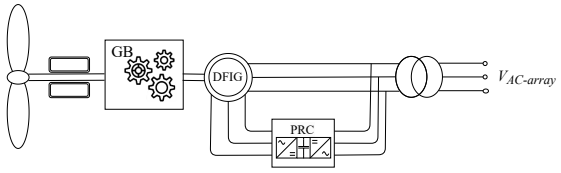

Figure 3.6: 3s DFIG PRC wind turbine drivetrain

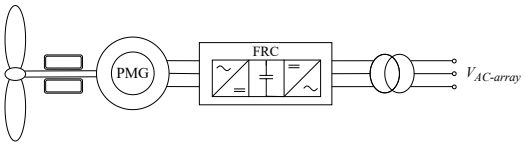

Figure 3.7: DD PMG FRC wind turbine drivetrain

The criticality of each component can be partly assessed through a downtime analysis. Special focus is given to the three components with significant differences between these two drivetrains. Figure 3.8 shows the percentage contribution to downtime for these three components and a combined category for the rest of the turbine components.

Notably, the downtime due to the gearbox is substantial in the $3s$ gearbox, while it is completely absent in the DD. Similarly, the $DFIG$ experiences more downtime compared to the PMG, which is expected given the simpler design of the latter with fewer components. In contrast, the PRC has a much lower share of downtime than the FRC [22].

For simplification, the rest of the components, including but not limited to the turbine's blades, yaw and pitch system, transformer, and circuit breaker, are grouped into a single category labelled as *rest of turbine*. It is important to note that the percentage contribution to downtime for the rest of the turbine category differs between the two drivetrains. Nevertheless, the absolute contribution, measured in downtime hours, is approximately the same.

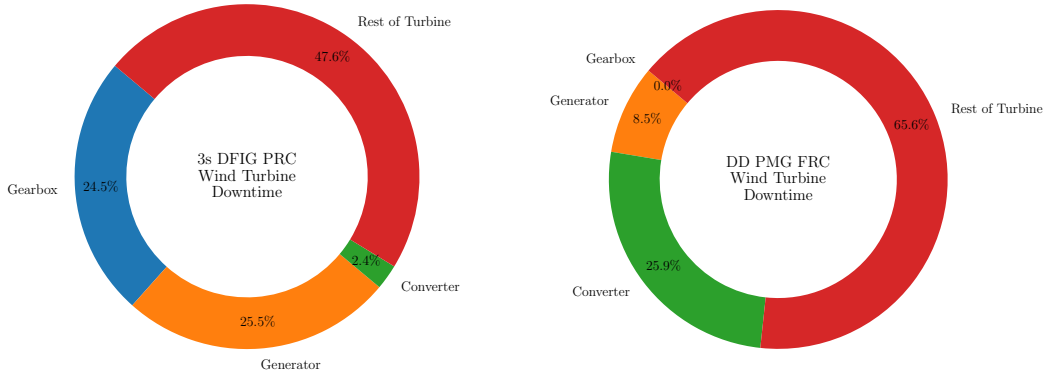

Figure 3.8: DFIG vs DD wind turbine downtime analysis

To accurately model each component as a repairable entity, it is crucial to differentiate between the types of repairs required based on the severity of failure. The severity of a failure significantly impacts the complexity and difficulty of the repair process. Consequently, the effects of component failures are categorised into three distinct types of repair: *major replacement*, *major repair*, and *minor repair*. The severity of these failures is particularly relevant in the context of offshore wind turbines, where the logistical challenges are heightened due to the necessity of marine vessels for transportation and servicing. Therefore, two types of vessels are considered, depending on the severity of the repair required.

For gear box and generator major and minor repairs only *crew transfer vessels CTVs* are required while for major replacement *heavy lift vessels HLVs* are required. In the case of converter repairs only *CTVs* are required for its repair. Having this categorisation considered, then the absolute downtime for each of the component in each drivetrain configuration is plotted in Figure 3.9. Using frequency and duration techniques, the availability of a wind turbine is determined and presented in Table 3.4, where only 8600 operational hours are considered and maintenance is considered scheduled perfectly.

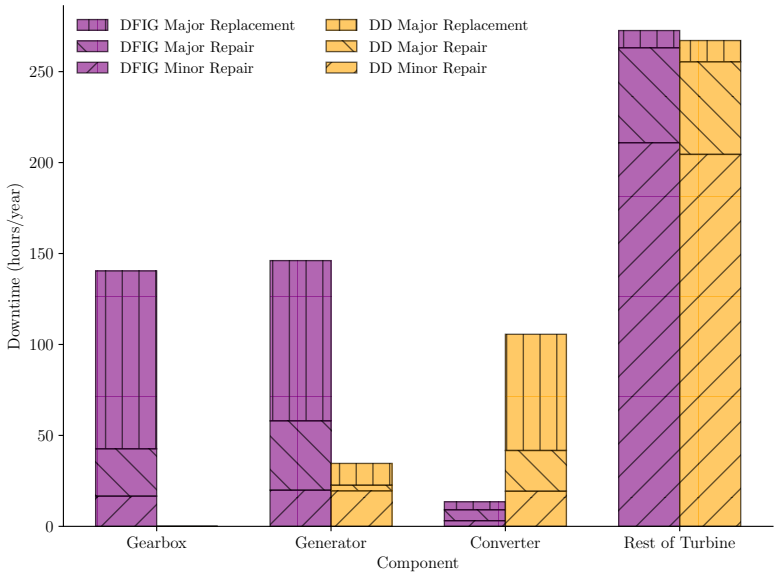

Figure 3.9: Downtime for both drivetrain types at 10 km offshore

Components Downtime	3s DFIG PRC (hours/year)			DD PMG FRC (hours/year)		
	Minor Repair	Major Repair	Major Replacement	Minor Repair	Major Repair	Major Replacement
Gearbox	16.62	26	97.8			
Generator	19.9	38.1	88.1	19.5	3.1	12
Converter	3.1	6	4.4	19.3	22.4	63.9
Rest of turbine	210.9	52.2	9.49	204.5	50.9	11.7
Availability	93.8%			95.5%		

Table 3.4: Downtime hours for each component and failure severity at 10 km offshore

Furthermore, from a frequency duration perspective this total downtime is the result effect of failure rate λ and repair rate μ. Therefore, using the previous downtime and the failure rates given in [21], wind turbines components can be modelled in failure and repair rate terms for each failure severity. Lastly, using equations (2.31) and (2.32), a turbine can be approximated as a single markovian repairable system with series connected components. The resulting approximate rates, λ_t and μ_t, for these configurations are shown in Table 3.5. A good way of verifying these equivalent rates is applying Equation 2.23 to see that they yield the same availabilities as shown in Table 3.4.

Components Rates	3s DFIG PRC (occ/year)						DD PMG FRC (occ/year)					
	Minor Repair		Major Repair		Major Replacement		Minor Repair		Major Repair		Major Replacement	
	λ	μ	λ	μ	λ	μ	λ	μ	λ	μ	λ	μ
Gearbox	0.43	227.26	0.04	14.11	0.06	5.23						
Generator	0.54	236.29	0.36	81.50	0.11	10.73	0.55	244.73	0.03	84.74	0.01	6.56
Converter	0.08	237.28	0.09	131.31	0.01	11.94	0.54	243.65	0.34	131.84	0.08	10.48
Rest of turbine	34.86	1412.90	3.20	534.15	0.09	80.44	33.77	1412.90	3.12	534.15	0.11	80.44
Equivalent	$\lambda_t = 39.86$		$\mu_t = 601.55$				$\lambda_t = 38.54$		$\mu_t = 817.19$			

Table 3.5: Failure and repair rates for each component failure severity at 10 km offshore

Up until now a single 10 km offshore distance has been considered. Nevertheless, the model developed in [21] involves modelling the effect of resource scarcity and offshore distance on wind turbines availability. This relationship is shown in Figure 3.10. In this figure all turbine availabilities drop with increasing distance, however, the rates at which the availability drops differs between configurations and with the distance from the shore.

The motivation for this drops regards to the increased time to repair turbines as they move further from shore. Furthermore, the change in the gradient between different ranges of distance corresponds to the limitation of resources in both workforce and vessel capacity, this is clearly noticeable between 80-90 km.

An interesting conclusion from the behaviour shown in the figure is that: as offshore distance increases the difference in availability between geared and direct drive turbines increases. This is mainly due to the lower failure rates of the direct drive configuration, which leads to a lower loading on vessel and technician resources further offshore.

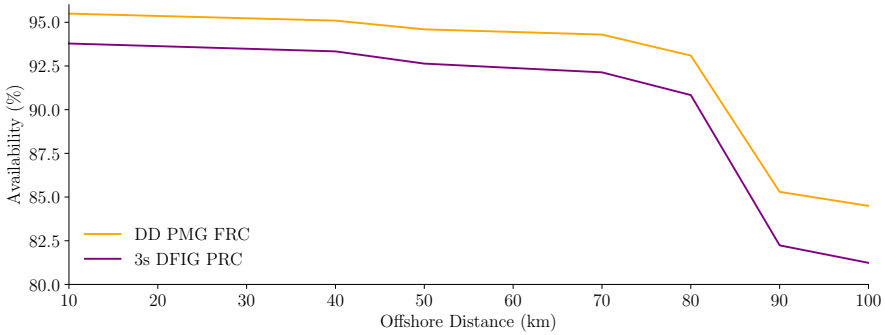

Figure 3.10: Availability of wind turbines as function of offshore distance [21]

On another side, the performance in operation and maintenance $O\&M$ cost terms, which represent around 35% of the levelised cost of electricity $LCOE$ offshore wind farms [69] [56], can also be evaluated given their availability across different offshore distances. Figure 3.11 shows the increasing operation and maintenance $O\&M$ costs for both drivetrain configurations located at near, medium, and far shore distances. In this figure it can be seen that for the $DFIG$ configuration costs attributed to lost production and transport cost have about an equal share of the total cost $\sim$ 45%, while repair and staff both contribute $\sim$ 5%. In the DD configuration in contrast, transport costs has a lower share $\sim$ 33% given the reduced requirement of heavy lift vessels due to the absence of the gearbox component. In relationship to distance the highest increasing costs can be attributed to the increased lost production. This can be directly linked to the drop of availability as offshore distance increases as shown in Figure 3.10.

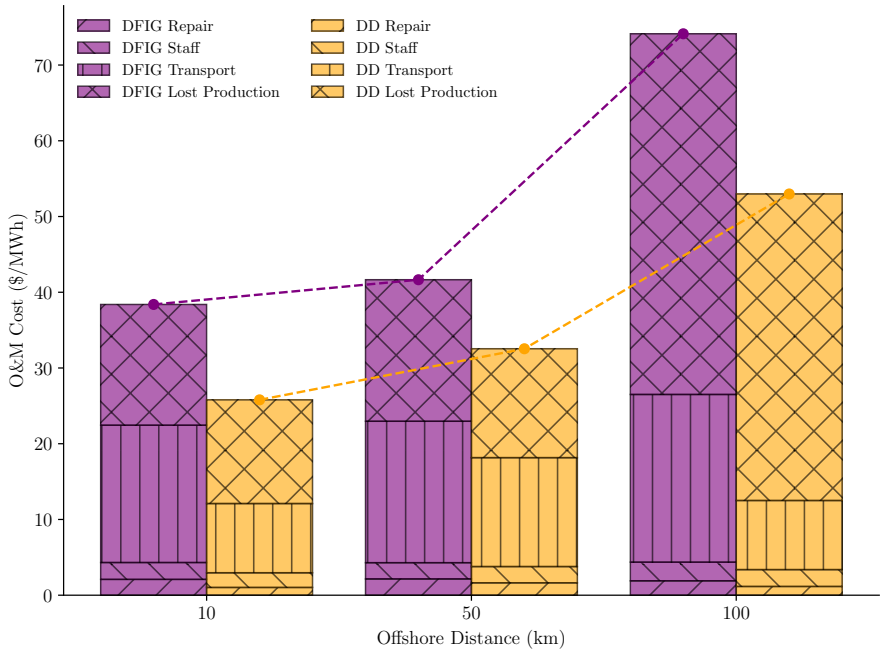

Figure 3.11: O&M costs of wind turbines with at different distances and drivetrain configurations[21]

Under the assumption that failure rates of both turbine types remain constant across varying distances, repair rates become more significant because of longer travel times and resource scarcity. This considerations can be used to create an equivalent two-state probabilistic model for the IEA 15 MW

offshore reference wind turbine, which has a *DD PMG FRC* configuration. Furthermore, continuing with the IJmuiden Ver Alpha located approximately 50 km offshore, the following model was defined.

State	C_t (MW)	P_i (-)	μ_t (occ/day)	λ_t (occ/day)	f_i (occ/day)
Up	15	0.95	0.00	0.11	0.10
Down	0	0.05	1.85	0.00	0.10
Sum		1.00			

Table 3.6: IEA 15 MW failure dependent two-state model at 50 km offshore

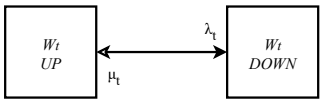

Figure 3.12: Two state model of a wind turbine

3.2.2. Amalgamation of Wind Speed and Failure Characteristics

Until this moment, the probabilistic characteristics of wind speeds and failures have been considered and modelled separately. Therefore, this subsection will address the integration of these two effects into a single model. The mathematical operation to find a composite model was defined in equations (2.45) and (2.46). This operation finds the capacity limiting characteristic and merges all the equivalent capacity states.

Considering the independent probability distribution of availability and wind speed states, the resulting possible state space is shown in Figure 3.13. In this state space however, all the possible states where the wind turbine is down yield the same capacity C_t of 0.

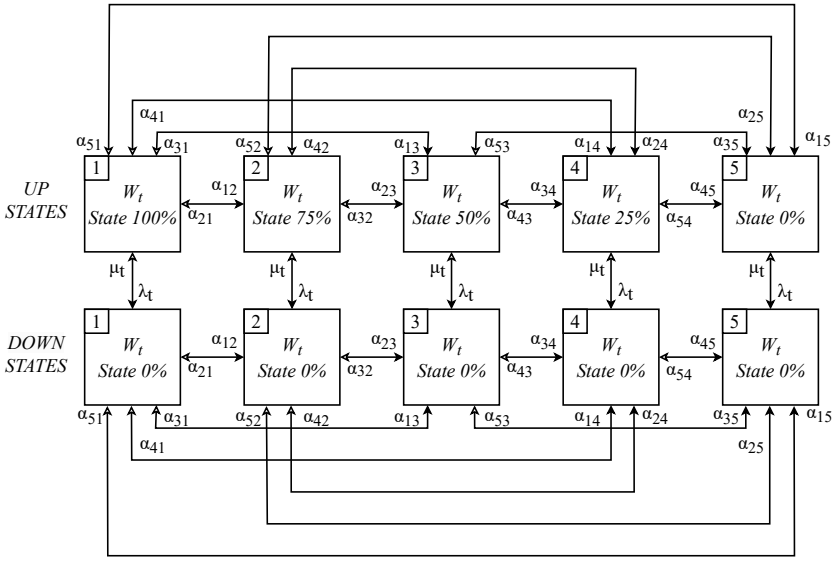

Figure 3.13: State space diagram of a composite wind turbine model

Taking into consideration the equivalence of states, a reduced equivalent state space can be determined using equations (2.29) and (2.30). Which would result in a similar 5-state space like the one shown in Figure 3.3 with a higher probability of residing in the state with 0 capacity. Amalgamating this state space and the combined probabilities of failures and wind speed states yields the composite $TCOPT$

for a single turbine shown in Table 3.7. Similarly the probability distribution is plotted in Figure 4.13.

States	C_t (MW)	P_i (-)	α_{+i} (occ/day)	α_{-i} (occ/day)	f_i (occ/day)
1	15	0.45	0.00	1.74	0.79
2	11.25	0.07	6.76	7.25	1.05
3	7.5	0.11	5.93	5.40	1.12
4	3.75	0.25	2.65	1.42	1.01
5	0	0.12	3.82	0.00	0.45
Sum		1.00			

Table 3.7: IEA 15 MW composite TCOPT

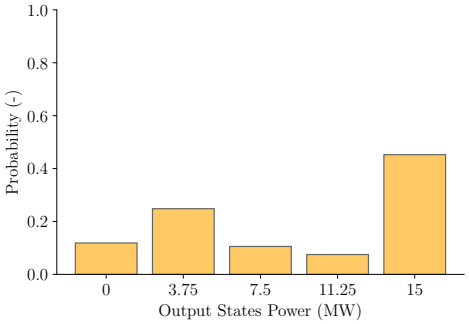

Figure 3.14: IEA 15 MW composite turbine model output probability distribution

3.3. Probabilistic Model of a Wind Farm

A wind farm is composed of multiple identical wind turbines that can be assumed to be subject to the same wind speed regime. In practice, there are wake effects influencing the wind speed and turbulence incident on downstream turbines. Nevertheless, for the sake of simplicity, these effects are ignored under the assumption that turbines are well distributed and distanced enough from each other.

An additional consideration is the array topology and switchgear selectivity of each connected turbine. Two of the most common array configurations are the *string* and *star* topologies, as illustrated in Figure 3.15. The string topology is simpler and more cost-effective. However, it suffers from reliability issues because a cable or switchgear fault at any turbine potentially results in the loss of all downstream turbines. Consequently, the wind farm model will be based on a star array topology. This topology is more reliable and easier to model, as each turbine can be considered identical, and a single failure will only result in the loss of capacity of one individual turbine [9].

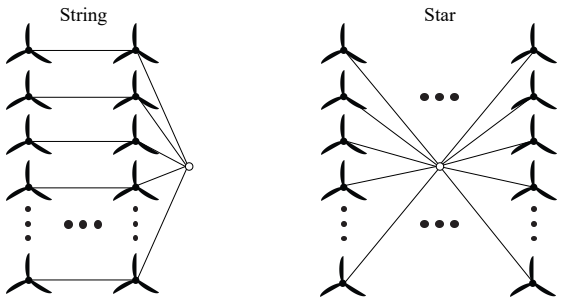

Figure 3.15: Offshore wind farm string and star array topologies

Under these assumptions, a wind farm W_f composed of N_t identical wind turbines W_t can be developed using the recursively adding the previous wind turbine model to a complete wind farm using equations (2.47) to (2.49). Furthermore, given that the wind turbines are identical, the state space diagram for a wind farm is depicted in Figure 3.16.

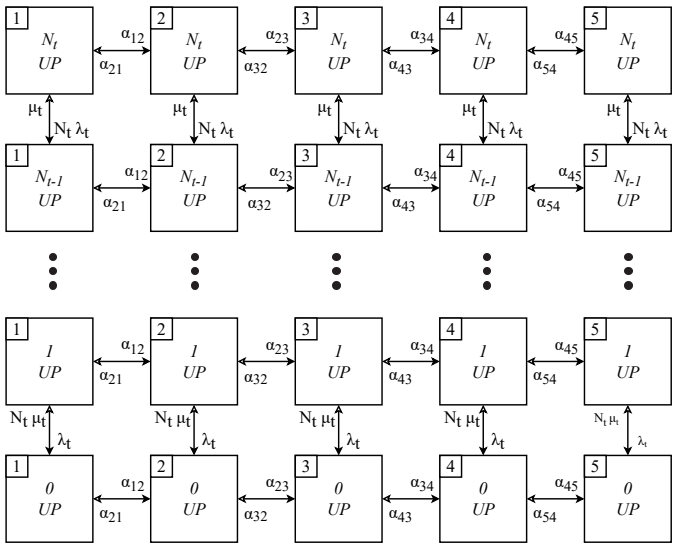

Figure 3.16: State space of a Wind Farm W_f composed of N_t identical wind turbines W_t

The complete discrete state space of a wind turbine consists of $(N_t + 1) \times 5$ total states. As anticipated, this state space is excessively large for practical reliability evaluation. Even after merging equivalent capacity states, the state space remains larger than what is tolerable; for instance, a wind farm with $N_t = 10$ would still have 25 unique states. Consequently, further rounding of states is necessary to reduce the complexity of the model.

The process of rounding and merging together similar unique states follows equations (2.40) to (2.44) and a conservative policy in which no other state is rounded with the 100% state. For the sake of congruence, as before for the wind turbine, a 5 state model was chosen for the wind farm. The resulting state space representation is shown in Figure 3.17 where states and transition rates are labelled with a superscript apostrophe to differentiate them from the previous merged state space.

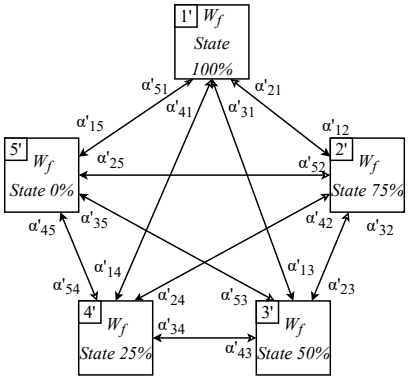

Figure 3.17: Rounded multi state model for a wind farm W_f

The generation capacity model of the whole wind farm can also be depicted through a *farm capacity output probability table* $FCOPT$. Following the chosen setting and wind turbine, a wind farm model with a total capacity of 600 MW, i.e., 40 IEA 15 MW wind turbines, was developed. The resulting

probabilities and transition rates are presented below.

States	C_f (MW)	P_i (-)	α_{+i} (occ/day)	α_{-i} (occ/day)	f_i (occ/day)
1	600	0.05	0.00	5.86	0.30
2	450	0.51	0.055	1.52	1.05
3	300	0.11	5.95	5.28	1.26
4	150	0.26	2.65	1.31	1.04
5	0	0.07	5.58	0.00	0.38
Sum		1.00			

Table 3.8: 600 MW wind farm rounded FCOPT

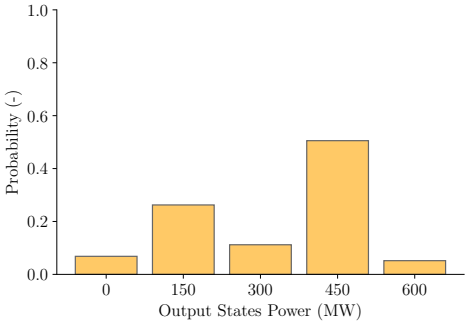

Figure 3.18: 600 MW rounded wind farm output probability distribution

Given the number of wind turbines, $N_t = 40$ it becomes unlikely to find them all in operable state. The probability of this state would be given by the probabilities of finding a single turbine up, or availability $A = 0.95$ like shown in Table 3.6, to the power of the number of turbines A^{N_t}. Furthermore, accounting for the probabilities of being in a wind state that yields a full load output reduces even further the probabilities of the first state of Table 3.8. Therefore, as it is clearly visible in the probability distribution, the full output state is less likely than finding the wind farm operating in an intermediate 75% output state.

The expected value of this distribution becomes a valuable measure of the *expected available capacity*. In other terms, this expected available capacity is simply the average output capacity of a wind farm modelled by this distribution. The ratio between this expected value and the total installed capacity is then an *expected capacity factor*. The capacity factor would thus measure the overall performance of the wind-farm reliability and wind speed dependent output. The subject of how these measures are sensitive to the input parameters of the model is discussed in the following section.

3.4. Analysis of Wind Farm Model

The considerations for the probabilistic modelling of a wind farm have been explained in the previous sections. In this section the relationship and sensitivity of the model to these considerations is evaluated. Therefore, the the effects of rounding and location effects on the wind farm model are analysed in Section 3.4.1. Then, Section 3.4.2 compares the performance relating the expected capacity factor, installed capacity, and $O\&M$ costs of wind farms composed of the two different drivetrain configurations.

3.4.1. Rounding and Location Effects

The output capacity of a wind farm is highly dependent on resource availability, and the availability of a wind farm is influenced by its offshore distance. This underscores the need for a detailed analysis of wind farm performance across the various locations in the North Sea. The analysis focuses on the variation in expected available capacity when a model of a 600 MW wind farm, based on the IEA 15 MW Turbine, is constructed at the different locations. Additionally, the study includes an evaluation of

the loss of accuracy by comparing the expected capacity values across different numbers of states.

The results of the analysis are visible in Figure 3.19. On the first location *IJmuiden Ver Alpha* it is most noticeable the loss of accuracy due to rounding. The expectation is always lower due to the conservative rounding chosen for the models, in which no other states were merged with the 100% output state. Nevertheless, even in this worst case scenario the loss of accuracy for a 5-state model is ~ 10% while this accuracy does not increase linearly to the number of states.

Another evident outcome visible is the reduced expected available capacity as offshore distance location increases. In contrast, this loss of capacity increases the probabilistic model accuracy. This effect of increasing accuracy is mainly due to the higher share of lower capacity states in the distribution due to reduced generator's availability.

Lastly, although different meteorological conditions were extracted from [40], there does not seem to be much difference in the expected output due to wind speed differences between the locations. This is because the locations are close enough to expect similar wind speed distributions in all the locations, as can be seen in Figure 1.2.

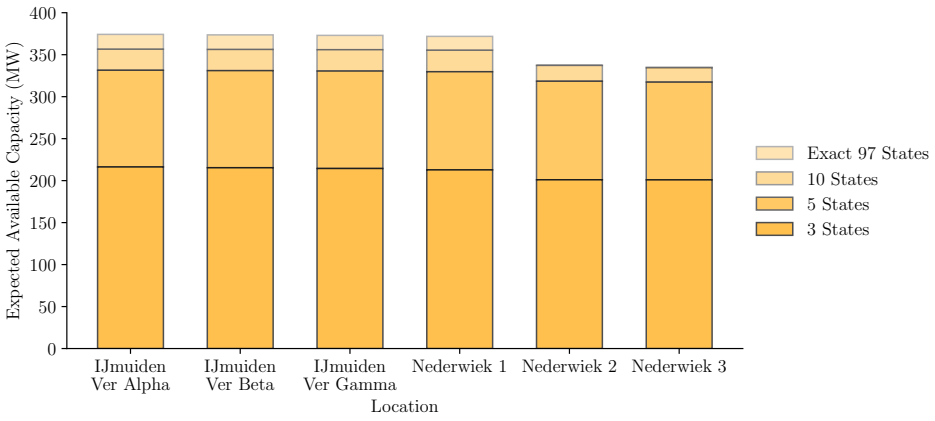

Figure 3.19: Expected available capacity of a 600 *MW* wind farm at different locations

Although this has been evaluated for every single location, the sensitivity of a wind farm performance to installed capacity, i.e., number of wind turbines installed N_t, and the different possible wind turbine drivetrain technologies have not yet been involved. The subject of the analysis of these other factors is the focus of the following subsection.

3.4.2. Drive Train Configuration

In Section 3.2 the component downtime and O&M cost of two different drivetrain configurations were presented. In this subsection the comparison of wind farm models composed of these two wind turbine technologies is compared. For such matter the same *IEA 15 MW* reference turbine is compared with the *DTU 10 MW* reference turbine which is designed to have a *3s DFIG PRC* configuration [65][11]. Therefore, wind farms models for multiple capacities were created considering the characteristics of the DTU reference turbine. The key parameters of this new turbine are shown in Table 3.9. Apart from the drivetrain configuration differences it is also important to notice the differences in cut-in and rated wind

speeds, hub height, and rated power.

The resulting model performance of these two types of wind turbines, measured in capacity factor, is shown in Figure 3.20. The first big noticeable difference is in the gap between both expected capacity factor curves. The gap difference is mainly due to the turbine higher cut-in and rated speeds which reduce the range of wind speeds at which the generator operates and reduces the probabilities of residing in a full output state. Another minor contributor to this change is the lower hub height. As it was mentioned before, wind speeds are height dependant due to wind shear. Nevertheless, the difference between both heights is small, being that at 120 m hub height the mean wind speed difference is meagrely $-0.19\ m/s$. Lastly, the differences in availability also play a role in this gap difference, given that a single DTU turbine has 2% lower availability.

Another interesting observation is the ripple noticeable in the output curves of the models. The ripples are caused due to rounding differences upon increasing number of turbines. Nevertheless, this small ripple effect is not the same as the accuracy loss due to the number of rounding states discussed previously and shown in Figure 3.19. In comparison the frequency of the ripples in the DTU curve is higher just because its power rating is lower, thus more points are plotted for the curve range from 0 to 2010 MW capacity (the least common multiple above 2000 MW between the 15 MW and 10 MW turbine capacities). Moreover, it is appreciable how this ripple effect smooths out as the number of turbines increases. In the real continuous case these curves should be totally smooth.

It is evident that the initial rate of change or decline in the expected capacity factor is lower in the DD case. This can be attributed to the combination of higher availability and greater rated power per wind turbine. In contrast, the DFIG curve begins to converge towards a limiting constant value earlier than the DD curve, primarily due to the higher *modularity* in the system, which employs turbines with lower rated capacities. The convergence of these curves is driven by the increasing *partial redundancy* within the system, which enhances overall system reliability in a non-linear fashion as more parallel components are added, as previously illustrated in Figure 2.5. Consequently, in systems with very high installed capacities, the difference in expected capacity factor will ultimately revert to the initial difference observed in a single turbine.

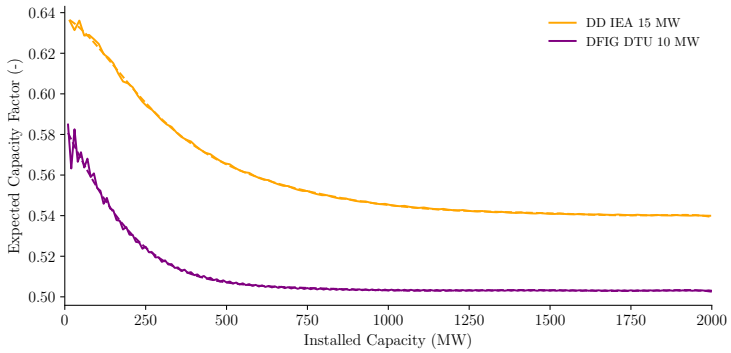

Figure 3.20: Expected capacity factor for wind turbines with different drivetrain configurations located at IJmuden Ver Alpha

Parameter	Units	Value
Power rating	MW	10
Turbine class	-	IEC Class 1A
Drivetrain	-	Geared
Cut-in wind speed	m/s	4
Rated wind speed	m/s	11.4
Cut-out wind speed	m/s	25
Rotor diameter	m	178.3
Hub height	m	119

Table 3.9: Key Parameters for the DTU 10 MW Turbine

Although the difference in expected capacity per drivetrain configuration has been analysed, this analysis alone is insufficient for a comprehensive understanding. It is necessary to compare the cost

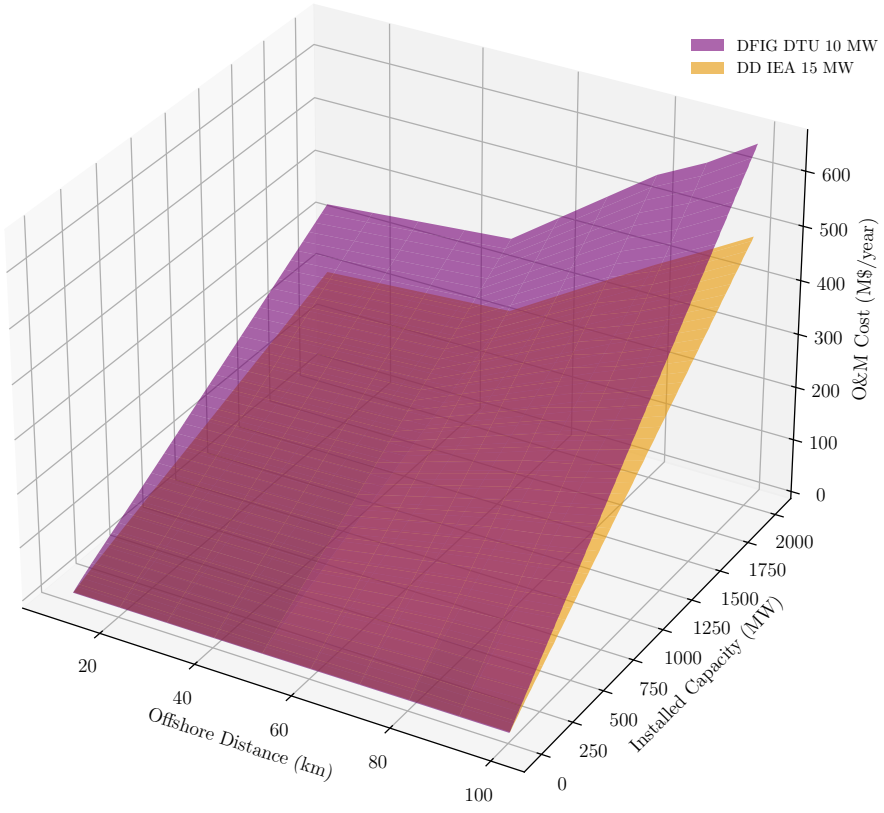

Figure 3.21: O&M costs for wind farms composed of geared DFIG and DD PMG turbines

performance of the drivetrains for different offshore distances and installed capacities. These effects are depicted in Figure 3.21. As anticipated from Figure 3.11, the *DFIG* turbine always incurs higher O&M costs due to the absence of a gearbox in the *DD* turbine. However, the figure shows that the cost difference becomes more significant as installed capacities, and thus the number of turbines, increase substantially. This is further clarified in Figure 3.22, which illustrates the annual cost increment in millions of dollars when comparing both drivetrains.

In the distance sensitivity analysis, near-shore O&M cost differences are not very significant, and capital expense differences may favour DFIG-based wind farms. However, at a certain mid-offshore distance, resource scarcity and vessel availability create a bottleneck that increases repair difficulty and thus the gradient change in costs. Far offshore, the increased unavailability due to gearbox failures and prolonged repair times has a considerable effect on wind farm O&M costs, significantly widening the cost gap between the two technologies.

An intriguing inverse effect emerges when analysing the annual cost difference associated with using either technology, as depicted by the contour lines in Figure 3.22. While the overall trend shows a downward slope for each line, a slight upward slope is noticeable in the 80 to 90 km range, particularly at higher installed capacities. This behaviour arises from the combined effects of a steep decline in availability, driven by resource scarcity as illustrated in Figure 3.10, and the converging nature of the model's expected output, as shown in Figure 3.20. As installed capacity increases, the gap between the

two technologies narrows. Furthermore, the converging effect and the difference between the curves become more pronounced as availability decreases, leading to a smaller cost difference as both curves approach their limit values at higher capacities

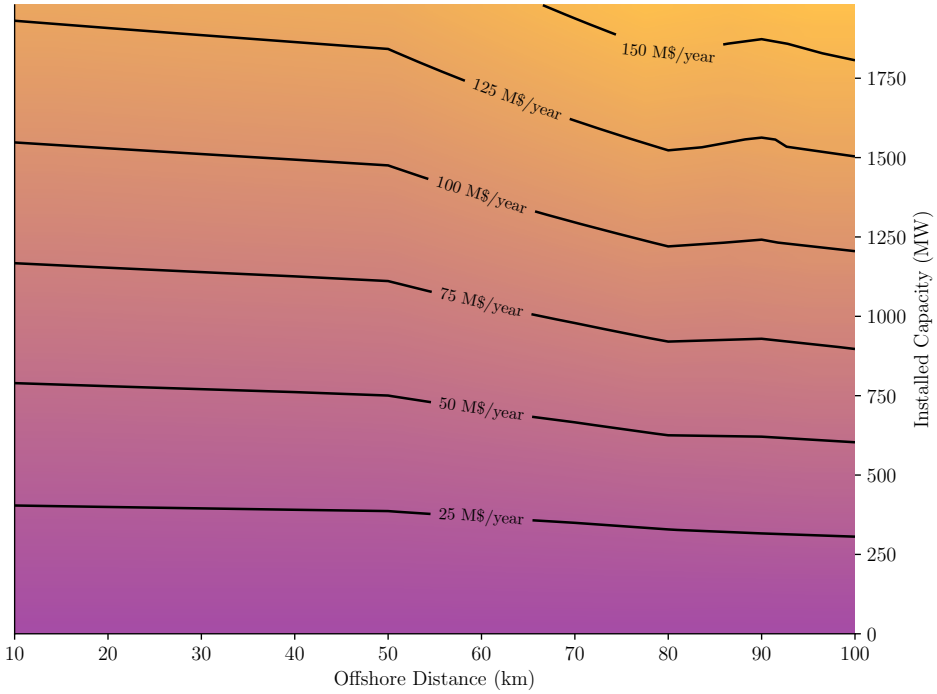

Figure 3.22: Cost difference in O&M comparing DD PMG vs geared DFIG based wind farms

3.5. Summary and Conclusions

In this chapter, focused on addressing sub-research questions 1 and 2 presented in Section 1.3, a comprehensive probabilistic model for offshore wind farms was developed, incorporating wind speed characteristics, turbine power output curves, and component failures. The chapter's structure included examining wind speed variability, modelling probabilistically the emergent behaviour of wind farms from the single turbine state space, and conducting sensitivity analyses regarding meteorological conditions, drivetrain configurations, and offshore distances.

To answer the first question, a composite probabilistic model for offshore wind energy generators was developed. This model integrates wind speed characteristics, turbine power output curves, and the stochastic nature of component failures. Effectively amalgamating the variability of wind energy and the stochastic nature of wind turbine failures was a critical focus in this modelling. By utilising historical data and frequency and duration probabilistic methods, it was possible to model the available capacity of wind turbines through a state space representation, discrete probabilistic distribution and a capacity output table. Furthermore, this approach balances accuracy with computational feasibility by rounding and merging states to create a manageable amount of possible states.

In addressing the second question, the impacts of drivetrain technology and offshore distance on the performance and costs of offshore wind farms were analysed. Two distinct drivetrain configurations were considered: the 3-stage gearbox with a doubly fed induction generator (3s DFIG PRC) and the direct

drive permanent magnet generator with a fully rated converter (DD PMG FRC). The analysis revealed that the DD PMG FRC configuration offers superior reliability and lower operation and maintenance (O&M) costs, especially as offshore distance and installed capacity increases. This is primarily due to the elimination of the gearbox, which is a major contributor to downtime and maintenance costs in the 3s DFIG PRC configuration. This study showed that while near-shore installations might not exhibit significant cost differences between the two configurations, mid and far offshore installations experience a noticeable increase in costs for the 3s DFIG PRC due to higher failure rates and repair complexities.

The comprehensive reliability and cost assessment highlighted the advantages of direct drive systems in terms of higher availability and lower O&M costs, particularly in deep offshore locations. These findings emphasise the importance of considering both drivetrain technology and offshore distance in the planning and development of offshore wind farms to optimise performance and minimise costs. The developed probabilistic model serves as a robust tool for evaluating the expected available capacity of offshore wind energy generators under various meteorological conditions, providing valuable insights for future offshore wind farm projects and its integration and effect on the overall power system reliability.

4

Reliability Modelling of DC Transmission Systems

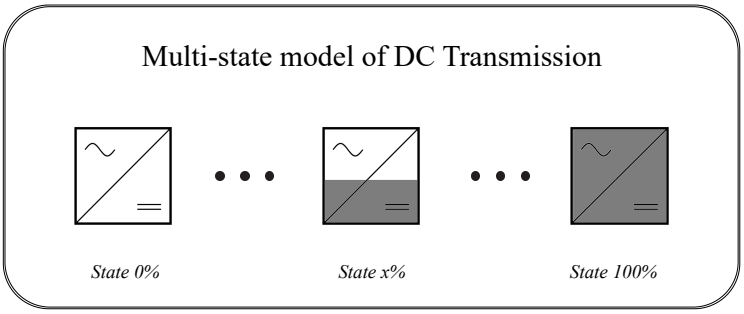

Unless energy is used at the location where it is generated, a connecting physical structure is required to transport it between different points. This is especially relevant for offshore power generation, where the distances from the source to the load are significant. Therefore, in the adequacy study of a power system involving deep offshore wind energy, the DC transmission system must be critically assessed.

The reliability of VSC-based DC transmission systems has been extensively researched [31, 52, 32, 43, 60]. Additionally, multiple studies focus exclusively on converter reliability [63, 68, 2, 6, 5]. However, comprehensive modelling of the system with detailed analysis of the effects of the power converter is still lacking. Thus, this chapter aims to address the transmission layer of an offshore wind energy provider, with a particular focus on the converter component. As discussed earlier in Section 1.2, the chosen power converter is the modular multilevel converter (MMC). Therefore, the reliability model of an MMC is developed with the purpose of answering sub-research questions 5 and 6 of Section 1.3.

With the previous purpose in mind, this chapter is structured as follows: Section 4.1 introduces the components and topology of the transmission system. Section 4.2 focuses on the reliability modelling of the converter component. Section 4.3 integrates the reliability model of the converter with the availabilities of the other components in the system. Finally, Section 4.4 conducts an analysis of the

created model, and Section 4.5 summarises and concludes the key points of this chapter.

4.1. Components in DC Transmission Systems

As mentioned in Chapter 1, there exists a break-even distance for the cost of HVDC transmission systems. Furthermore, all of the subject offshore locations shown in Figure 1.2, tabulated in Table 3.1 and modelled in Section 3.4.1 are located beyond this break-even distance. Therefore, the model of DC transmission ends, i.e., the connecting terminals from which energy is sent and received, is to be developed.

Figure 4.1 shows a typical topology of one DC transmission *sending end*. A *receiving end* would be a mirror image of this exact same topology connecting instead to another AC system or load. The main components of this system are labelled and subdivided into internal sub-systems. Sub-system SA is composed of the following AC components: breaker ACB, converter transformer CT, harmonic filter ACF, coupling reactor CR, and a combined control and protection system component CPD. Sub-system SB is exclusively composed by the chosen power electronic converter MMC and lastly sub-system SC is composed of the DC components, a breaker DCB and transmission cable DCC.

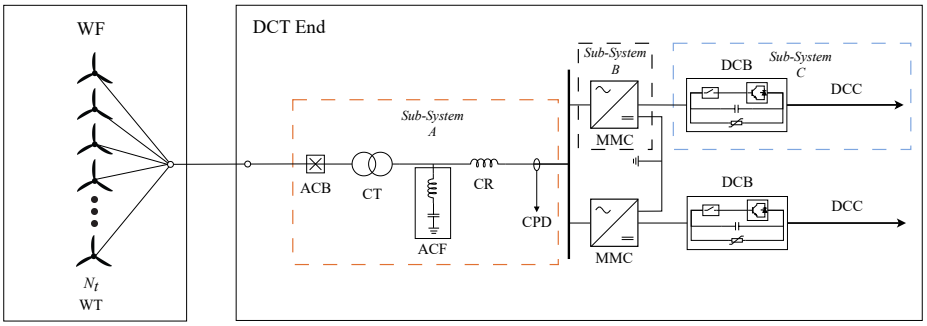

Figure 4.1: DC transmission end topology diagram

Notably, all of the components in each sub-system are connected in series in its electrical and reliability block diagram. Therefore, the methods explained in Section 2.1.5 can be utilised to reduce each sub-system into approximate equivalent failure and repair rates. Another particularity of this topology, as explained before for any bipolar with ground return HVDC topology, is the possibility of operating at partial capacity even when any one component fails in SB or SA. The particularities of modelling these possible derated states is later analysed through a state space representation of the system.

While all components merit detailed analysis, the DCC and MMC components are the most critical in these types of systems [52]. Cable accessories, such as joint and termination points, are the most vulnerable aspects of the DCC. Consequently, the reliability of cables depends on the number of accessories used for their connection. Additionally, it is expected that the failure rate is correlated with cable length. Therefore, the impact of the number of cable accessories is assumed to be included in a linearly dependent failure rate per kilometre of cable distance [62, 60]. In contrast, the reliability of the electronic power converter requires a deeper assessment and is extensively analysed in the following section.

4.2. Probabilistic Model of a Power Converter

Historical operational data of power systems indicate that converters are a common source of failure in power generation and transmission systems [54, 66, 26, 27, 48, 23, 33, 29, 45]. Furthermore, the reliability of any converter is dependent on its operating conditions and topology [34, 46]. Consequently, in this section the probabilistic model of an MMC is modelled considering it's topology and the utilisation of half-bridge sub-modules $HBSM$ for its composition, as shown in Figure 4.2.

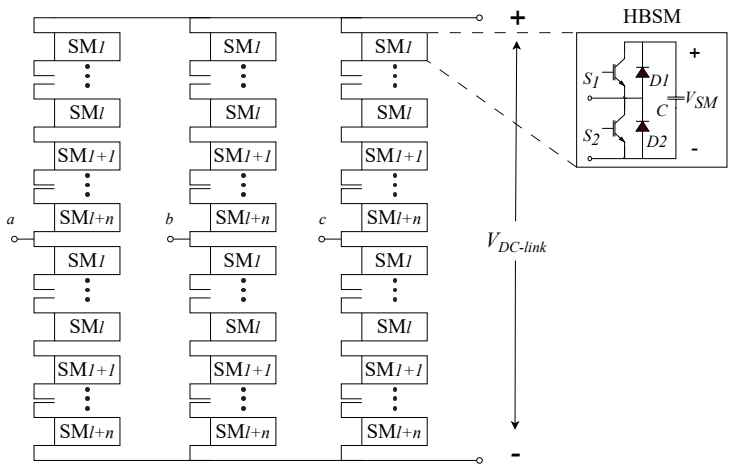

Figure 4.2: HBSM based MMC converter topology

As can be seen from the previous figure the topology of this converter consists on the cascaded connection of several sub-modules SMs with individual driving systems. The logic behind the series connection and individual drive is that each sub-module can be activated such that multiple discrete levels of voltage can be generated from a DC input. The reverse operation is also possible, thus an MMC can be operated as both a rectifier and inverter [51].

It can also be seen that each phase is composed by two *arms*, connected to the positive and negative terminals. Moreover, each arm requires *at least* l number of sub-modules per arm to operate. Furthermore, each one of this sub-modules is composed of two identical IGBT switches (including their diodes), a capacitor bank and a driving mechanism component.

Evidently, the dependency of so many components creates very significant reliability issues for this converter topology. In order to address this issue a reliability model of the converter is developed. Starting from the most fundamental component in the converter, the half-bridge SM reliability model. Since each one of these components are required for the successful operation of the SM and each one of these components can be modelled under the assumption of an exponential failure density function, a simple series reliability network can be devised as shown below. Then, an equivalent SM failure rate λ_{SM} can be found like shown in Table 4.1.

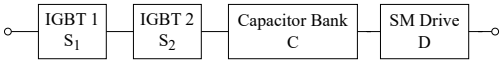

Figure 4.3: Reliability block diagram of a SM

Component	λ (occ/year)
IGBT	8.76×10^{-4}
Capacitor	1.752×10^{-3}
Drive	6.123×10^{-3}
λ_{SM}	9.627×10^{-3}

Table 4.1: Failure rates of SM components [63]

Evidently, the reliability of a SM can be improved only by means of improving component's quality, nevertheless, for the successful operation of a single arm several series connected SMs are required. The number l of SMs required can be determined from the IGBT switch rating V_{IGBT} and the DC transmission voltage $V_{dc-link}$. In addition, a maximum capacitor voltage ripple $k_{max} = 1.1$ and a safety factor $S_f = 0.6$ are considered. Then, this required number of SMs per arm can be determined by Equation 4.1.

$$l = \left\lceil \frac{k_{max} \times V_{dc-link}}{S_f \times V_{IGBT}} \right\rceil \tag{4.1}$$

Evidently, from the previous equation, a higher rated switch will yield a lower amount of required SMs. Nevertheless, other factors, such as operational losses and capital investment costs, must be considered for the optimal choice of modularity in an arm. This study has been carried out in [6] and applied to the case study inspired by the 525 kV DC transmission links planed by the Dutch TSO. This yields an optimal choice switch rating of $V_{IGBT} = 6.5$ kV and a number of required $l = 149$ *SMs per arm*.

As depicted in Figure 2.4, any system depending on this many series connected components will experience serious reliability issues even if each individual SM would have a very high reliability. Therefore, other reliability improvement measures are required to have a feasible reliable system working. One of these measures, *redundancy*, is addressed in the following subsection.

4.2.1. Reliability Function of an MMC's Arm

In order to improve the reliability of a single arm in the MMC, n back-up redundant sub-modules are often installed. As it was previously explained in Section 2.1.3, redundancy can be of two kinds. It is therefore, the subject of this subsection to carry out the modelling and comparison of the reliability model of an arm considering either *stand-by* or *active* redundancy.

An initial consideration is in the different operating conditions each SM is exposed to in the different redundancy schemes. While in stand-by redundancy the load burden is only shared between l operating SMs, in the active redundancy the load is distributed amongst all $l + n$ SMs. This particularity of the active redundancy is why this operating mode is often called *load sharing* mode, while the stand-by operation is referred to as *idle* mode.

In reliability terms the difference between both redundant operating modes can be considered utilising correction factors k_v on the switch and capacitor failure rates to express an equivalent series SM failure

rate λ_{SM}. Where the sub-index v is related to the reduced voltage stress at which both components are exposed to. Taking this constant correction factor and applying equations (2.14) and (2.16) the reliability functions of an arm can be defined as follows.

$$\lambda_{SM} = 2\lambda_{IGBT} k_{v_{IGBT}} + \lambda_C k_{v_C} + \lambda_D \tag{4.2}$$

$$R_{k/n}(t) = \sum_{i=l}^{l+n} \frac{(l+n)!}{i!(l+n-i)!} \cdot e^{-i\lambda_{SM}t} \cdot (1 - e^{-\lambda_{SM}t})^{l+n-i} \tag{4.3}$$

Equations: Load sharing mode

$$\lambda_{SM} = 2\lambda_{IGBT} + \lambda_C + \lambda_D \tag{4.4}$$

$$R_{sby}(t) = \sum_{x=0}^{n} \frac{(l\lambda_{SM}t)^x e^{-l\lambda_{SM}t}}{x!} \tag{4.5}$$

Equations: Idle mode

Although, the reduced voltage stress on each SM changes after each redundant SM fails, this "mission profiling" is out of the scope of the model and in contrast a constant factor k_v is assumed for each level of redundancy as in [63]. Since the sole objective is to compare both operating modes, the correction factors used are given by the ratio between the resulting factor with no redundancy and the redundancy level analysed given by equations (4.6) and (4.7) from [36]. Since a constant factor is taken the number n of redundant SMs is halved to compensate for the time an arm spends below the maximum value of possible redundant SMs as one or more have already failed. This result in an overall lower SM failure rate λ_{SM} for any level of redundancy in load sharing mode.

$$k_{v_{IGBT}} = 0.045 \cdot e^{3.1 \frac{\frac{V_{dc-link}}{l+n/2}}{V_{rated}}} \tag{4.6}$$

$$k_{v_C} = \left(\frac{\frac{V_{dc-link}}{l+n/2}}{0.6 \cdot V_{rated}} \right)^5 + 1 \tag{4.7}$$

The differences between the reliability of these two modes of operation is difficult to interpret simply from their mathematical expressions. Therefore, the reliability functions for both operating modes are compared in Figure 4.4. Evidently, the idle mode or stand-by mode always results in higher reliability even though the SMs failure rate is lower in load sharing mode. This is expected since it is in line with Section 2.1.3 and the general literature [68, 4]. A horizontal grey line at 0.5 probability is also plotted in the figure. Wherever the reliability functions intersect this horizontal line gives the $MTTF$. Evidently, the MTTF of stand-by redundancy is higher for all levels, additionally it is clearly visible that this difference increases as the level of redundancy increases. Therefore, stand-by seems a more attractive operation mode for MMC's redundancy.

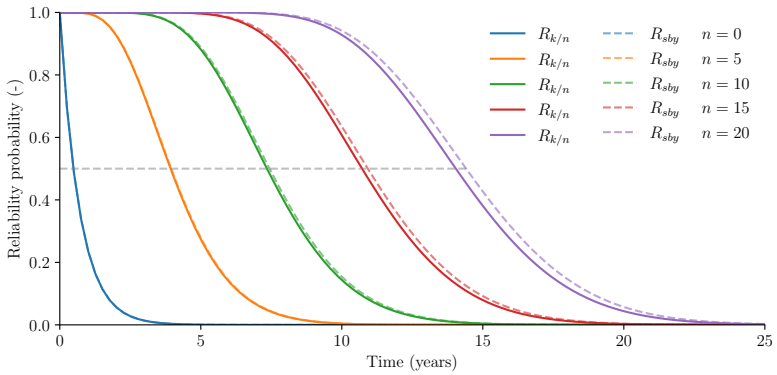

Figure 4.4: Reliability functions of an MMC arm for operating modes and redundancy levels with $l = 149$

Another advantage of stand-by redundancy in MMCs is the reduced losses in the converter. Given that switching and conduction losses result in an approximate 0.5% losses in each SM, having n extra redundant SMs actively operating will increase the losses per arm by $n \cdot 0.5\%$. The main disadvantage of stand-by redundancy is the added complexity and component of the switching system. Nevertheless, in this model perfect switching is assumed and therefore stand-by redundancy is used further to model an MMC arm.

A last notable particularity in this kind of system is that it is, as of yet, an un-repairable system. Therefore, the system can only transition into a failed state. Furthermore, it is simply continuously reducing its chance of success. In real power systems activities to maintain the assets are set on place with the purpose of avoiding this kind of behaviour. The subject of modelling maintenance is therefore the objective of the next subsection.

4.2.2. Maintenance Model of an MMC's Arm

As discussed in Section 2.1.4, the primary objective of maintenance activities is to reduce the probability of system or component failure by *restoring* their normal operating conditions. This restoration significantly impacts the modelling of the reliability of such components. Consequently, the reliability function of a maintained MMC arm is represented by equation Equation 2.18.

In this model, a *periodic perfect* maintenance strategy is assumed, meaning that the reliability function of an arm is fully restored to its initial condition, as illustrated in Figure 4.5. This assumption approximates the real-world scenario in which all SMs are inspected and faulty SMs are replaced at regular intervals. However, in practice, this only restores the initial conditions of the replaced SMs, not the entire arm. This issue is further analysed in [68], where the reliability function's change after each maintenance activity is examined. Despite this, the research demonstrates that the expected error of the model with a perfect maintenance assumption at the desired levels of redundancy is $\leq 0.1\%$. Therefore, for the sake of simplicity, this assumption is tolerated.

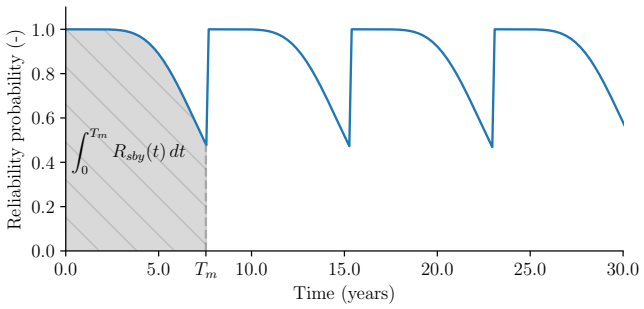

Figure 4.5: Reliability function of an MMC arm considering maintenance renewal with $T_m = 7.67$ years periodicity and $n = 10$ stand-by redundancy

An evident criticism is that the lifetime of a component modelled by this curve would theoretically be infinite, which is obviously unrealistic. However, an important area is highlighted in the previous figure that can be used to model an MMC arm as a single *repairable* component. By considering the MMC arm as a repairable component, practical reliability predictions involving the maintained mean time to failure can be achieved. Thus, as equated in Equation 2.19, the $MTTF$ of an arm can be determined using this shaded area.

Although in this definition the reliability of a stand-by redundant arm is addressed, this same equation can be used for the active redundant case. Moreover, the integration of the reliability functions are not straightforward as they might seem from the figure. A more detailed derivation was carried out in [63], however the resulting expression of the integration of a stand-by redundant arm with any one maintenance interval time T_m is shown below.

$$\int_0^{T_m} R_{sby}(t)\,dt = \int_0^{T_m} \sum_{x=0}^{n} \frac{(l\lambda_{SM}t)^x e^{-l\lambda_{SM}t}}{x!}\,dt = \sum_{x=0}^{n}\left[\frac{1}{l\lambda_{SM}} - \left(\sum_{p=0}^{x}\left\{\frac{(l\lambda_{SM}T_m)^p}{p!}\cdot\frac{e^{-l\lambda_{SM}T_m}}{l\lambda_{SM}}\right\}\right)\right] \tag{4.8}$$

The effect of maintenance on the MTTF of an MMC arm is illustrated in Figure 4.6. This figure compares the MTTF of an arm without maintenance $MTTF_{arm_0}$ to the behaviour of $MTTF_{arm}$ including maintenance as the maintenance interval T_m varies. On the one hand, theoretically unlimited high MTTF values can be achieved with shorter maintenance intervals. On the other hand, if the maintenance interval exceeds the expected lifetime of a single arm, the benefits of maintenance become negligible, as the arm is likely to have failed before the scheduled maintenance. Moreover, it is evident that there is an initial degree of sensitivity of the $MTTF_{arm}$ to the time interval T_m, this is further analysed in Section 4.4.1.

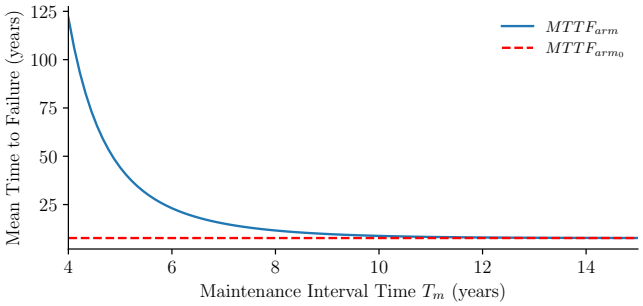

Figure 4.6: Mean time to failure of a maintained arm with $n = 10$ stand-by redundancy

$$MTTF_{arm}(T_m) = \frac{\int_0^{T_m} R_{sby}(t)\,dt}{1 - R_{sby}(T_m)} \tag{4.9}$$

The rules of this renewal process can be applied to define the mean steady availability of a single arm A_{arm} as explained in Section 2.1.5. By applying the previous definition to Equation 2.23 and assuming a constant $MTTR_{arm} = 12$ days, the availability of a single arm can be defined as follows [37].

$$A_{arm} = \frac{\mu_{arm}}{\lambda_{arm} + \mu_{arm}} = \frac{MTTF_{arm}}{MTTR_{arm} + MTTF_{arm}} \tag{4.10}$$

Since the $MTTF_{arm}$ is unbounded, very high availability can be achieved. Therefore, a cost-based decision must be considered to optimally choose the reliability strategy, which is the subject of Section 4.4.2. Now that the availability of a single arm has been defined from the basic SM reliability, the availability of the MMC as whole can be modelled. This is the subject of the following subsection.

4.2.3. Reliability Model of an MMC Considering Periodic Maintenance

In addition to the failure of a converter arm, several other failures can cause the MMC to shut down. These include failures of the central controller, cooling system, power supply, as well as internal converter insulation failures and faults [42]. These kinds of faults can be merged into single series connected block of *converter level components* with availability $A_{con} = 99.78\%$ and failure rate $\lambda_{con} = 2.628 \times 10^{-2}$ occ/year. These converter level components and the total number of arms in the chosen MMC configuration are shown in Figure 4.7. Since any of the failures of a single arm or converter level components causes the total failure of the converter, the availability of the MMC as a whole A_{MMC} can be determined using Equation 4.11. Similarly the failure rate of the converter can be determined by Equation 4.12.

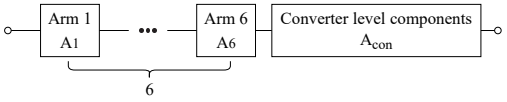

Figure 4.7: Reliability block diagram of an MMC

$$A_{MMC} = A_{arm}^{6} \cdot A_{con} \tag{4.11}$$

$$\lambda_{MMC} = 6\lambda_{arm} + \lambda_{con} \tag{4.12}$$

Figure 4.8 shows the relationship of the availability of an MMC to the maintenance time interval T_m. In this figure it is appreciable that the dependency of the availability of an MMC to maintenance decreases as the redundancy level increases. Moreover, the region of highest sensitivity to changes in T_m is right shifted as redundancy increases. This is due to the fact that as redundancy increases the constant period of ~ 1 reliability also prolongs itself, as shown in Figure 4.4, therefore the greatest sensitivity will be found until the time ranges where the reliability function is decreasing.

This figure shows that the availability of an MMC for any level of redundancy always converges to a maximum $A_{MMC} = 99.91\%$ availability as T_m decreases. Conversely, as T_m increases it is noticeable that again the availability converges to a minimum value which is different for each level of redundancy. The reason for this is that the maintenance is now ineffective since it is executed after the MMC arm has already reached its end of life, i.e., its reliability function at that time is ~ 0. This is commonly called *over* maintenance in the former case or *under* maintenance in the latter case.

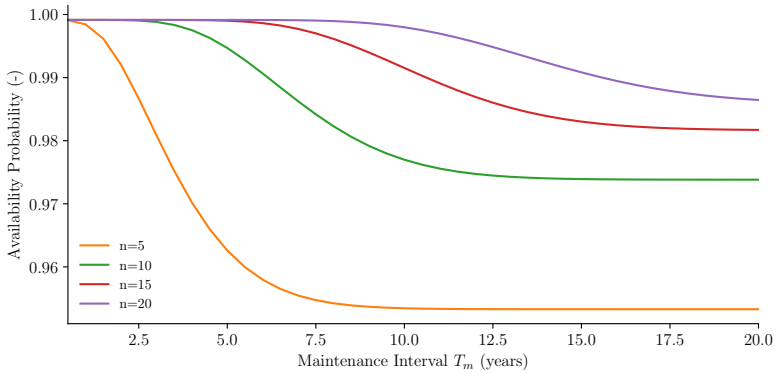

Figure 4.8: Availability of an MMC as function of its maintenance interval T_m

Since the resources for maintenance are not unlimited nor free, the choice of a maintenance interval T_m is often cost-based. Nevertheless, a clear understanding of the ranges at which maintenance is most effective is of upmost importance for making the correct engineering decisions.

4.3. Reliability Model of a DC Transmission End

Up until this point, the focus has been on the converter component of the DC transmission end (DCT end). However, this is not the only component to consider in the probabilistic modelling of the entire transmission system, as discussed in Section 4.1. Figure 4.9 illustrates the reliability network of a single transmission end. By utilising the techniques outlined in Section 2.1.2 and the failure and repair rates of individual components shown in Table 4.3, equivalent failure rates λ_{SA}, λ_{SB} and λ_{SC} and similarly for repair rates μ_{SA}, μ_{SB} and μ_{SC} can be defined.

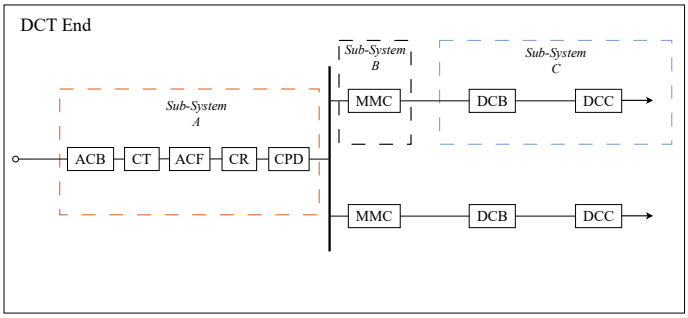

Figure 4.9: Reliability network block diagram of a DCT End

Component	λ (occ/year)	μ (occ/year)
ACB	0.025	52.276
CT	0.037	5.544
ACF	0.200	1459.667
CR	0.116	34.219
CPD	0.088	1446.780
MMC	*MMC model*	
DCB	0.121	121.7
DCC (/cct100km)	0.071	6.083

Table 4.2: Failure and repair rates of DCT end components [31, 60]

Once the merged equivalent rates of each subsystem have been determined, these subsystems can be modelled as equivalent components. The available capacity of the system is then determined by the state of each one of these components and the previously shown network topology. A common way to analyse the possible outcomes of the system is by constructing a *failure tree*, as shown below.

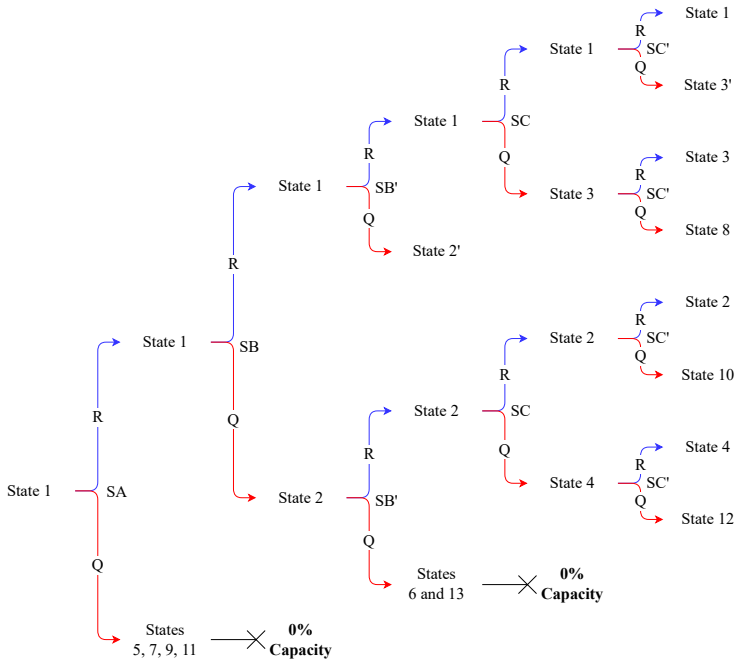

Figure 4.10: Failure Tree of a DCT End

This analysis method involves enumerating the possible states and their resulting capacity outcomes after each subsystem either succeeds R or fails Q. Since in each DCT end, there are two subsystems SB and SC a subscript apostrophe is used to differentiate them. This duality, as previously mentioned, allows for the existence of half-capacity states, which are equivalent for failures of either SB or SB' and SC or SC' failures. Notably, only state 1 results in full capacity, while states 2, 3, and 4 result in partial capacity. The remaining states yield zero capacity, leading to the pruning of the failure tree once zero capacity is reached.

Using the considerations outlined in Section 2.1.5 to create state space diagrams and incorporating the previous failure tree analysis, a possible 13-state space model is developed, as shown in Figure 4.11. In this state space, each down subsystem is depicted by a shaded square. Additionally, the transition rates between these 13 possible states are mapped, taking into account the existence of identical dual states for states 2, 3, and 4. Consequently, some of the rates going into these states are doubled.

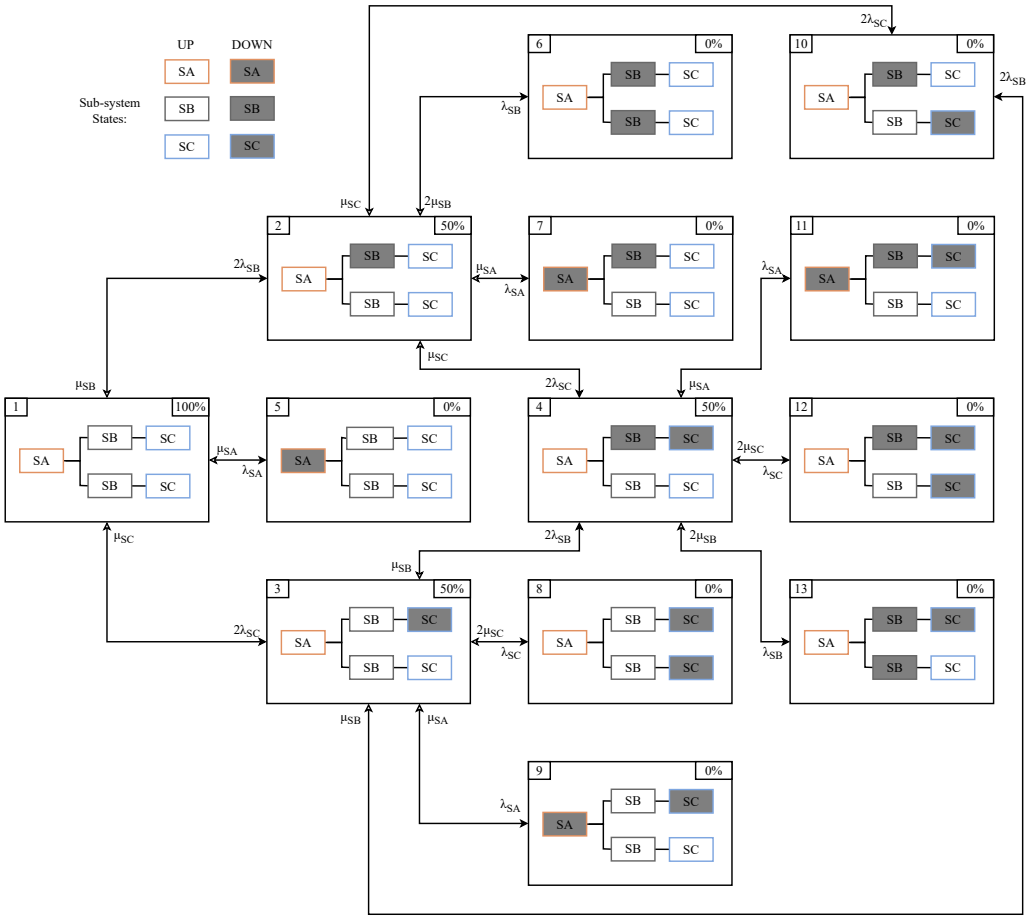

Figure 4.11: 13-State space model of a DCT end

Given that many of the states in the previous diagram yield the same capacity, an equivalent merged 3-state space model can be developed using equations (2.29) and (2.30). Hereby, the three states are named: normal (100% capacity) N state, partial (50% capacity) P state, and failed (0% capacity) F state. The transition rates between these states are denoted with appropriate subscripts, as shown in Figure 4.12 and Table 4.3.

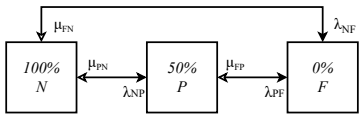

Figure 4.12: Equivalent 3-state space model of a DCT end

λ (occ/year)		μ (occ/year)	
λ_{NP}	1.326	μ_{PN}	15.813
λ_{PF}	1.485	μ_{FP}	8.782
λ_{NF}	0.466	μ_{FN}	32.863

Table 4.3: Transition rates of equivalent 3-state DCT end with $n = 10$ and $T_m = 7.67$ MMC reliability strategy

Lastly, given all the input parameters of the MMC reliability strategy and the rest of the components in the DCT end, numerical values can be assigned to the 3-state model of the transmission model. Similarly to the generation model, these can be stored in a probability table and distribution named *DC transmission capacity output probability table* or DCTCOPT. This is shown and plotted below.

States	C_{DCT} (MW)	P_i (-)	α_{+i} (occ/day)	α_{-i} (occ/day)	f_i (occ/day)
N	2000	0.91	0.00	4.91×10^{-3}	4.47×10^{-3}
P	1000	0.08	1.00×10^{-1}	1.11×10^{-2}	8.51×10^{-3}
F	0	0.01	9.77×10^{-1}	0.00	1.26×10^{-2}
Sum		1.00			

Table 4.4: DCT end capacity output probability table DCTCOPT with $n = 10$ and $T_m = 7.67$ MMC reliability strategy

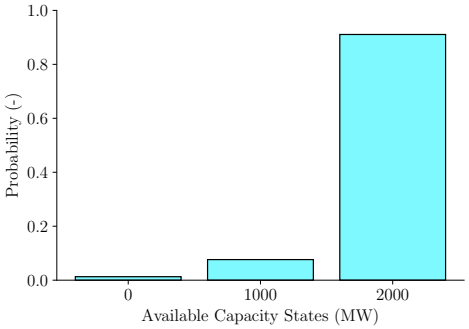

Figure 4.13: DCT end model output probability distribution

This probability distribution is much less spread and thus yields a higher *expected available DCT end transmission capacity* of 1897.82 MW, this is much better in comparison to the distributions encountered for the wind generation model. This is expected since, in the transmission case, derated states of available capacity are much less likely due to the lack of dependency to wind speeds. Although these results might seem positive when comparing them to the previous model, optimisation can further enhance the reliability to a desired transmission system standard. Therefore, the following section analyses and presents the sensitivity of this model to the reliability strategy of the MMC and its cost optimisation.

4.4. Analysis of the DC Transmission Model

The probabilistic model of a DC transmission end has been previously developed with a particular focus on the reliability modelling of its converter. As previously mentioned, this model has multiple degrees of freedom and various perspectives for its analysis. To address these, Section 4.4.1 focuses on the sensitivity analysis of the MMC model. Following this, Section 4.4.2 examines the reliability strategy of an MMC from a cost perspective and formulates a cost-oriented decision for its optimal design. Lastly, Section 4.4.3 explores the impact of an MMC and its reliability strategy on the reliability of the entire DC transmission end.

4.4.1. Converter Sensitivity to Reliability Strategy

The reliability of any component can be influenced by multiple factors, including its operating mode, quality (e.g., SM failure rate), and modularity, which have been addressed previously. In summary, the most reliable choices for an MMC operating at 525 kV DC transmission voltage are the stand-by operation and a 6.5 kV rating for the SM components [6]. Therefore, special focus is given to the effects of redundancy levels in combination with maintenance on the availability of an MMC designed for this system.

To thoroughly analyse the sensitivity of the availability of the converter to these parameters the derivation of the availability function, previously presented in equations (4.10) and (4.11), with respect to the variables n and T_m have to be formulated for both the *redundancy SR* and *maintenance SM* sensitivity functions. The derivations of these equations have been carried out meticulously for both MMC operating modes in [63]. However, the focus is placed on the stand-by operation and thus only this mode is analysed using the equations below.

$$SM(T_m) = \frac{\partial A_{MMC}}{\partial T_m} = 6 \cdot A_{arm}^5 \cdot A_{con} \cdot \frac{\partial A_{arm}}{\partial T_m} \quad (4.13) \qquad SR(n) = \frac{1}{2}\left(A_{MMC}(n+1) - A_{MMC}(n-1)\right) \quad (4.14)$$

In the previous equations, the sensitivity to maintenance SM could be derived directly from the equation of the availability of the MMC. In contrast, the sensitivity to redundancy SR is defined using the difference quotient since n is a discrete integer variable. The results of this sensitivities applied to the designed system with an MMC with $l = 149$ SMs per arm is shown in the figure below.

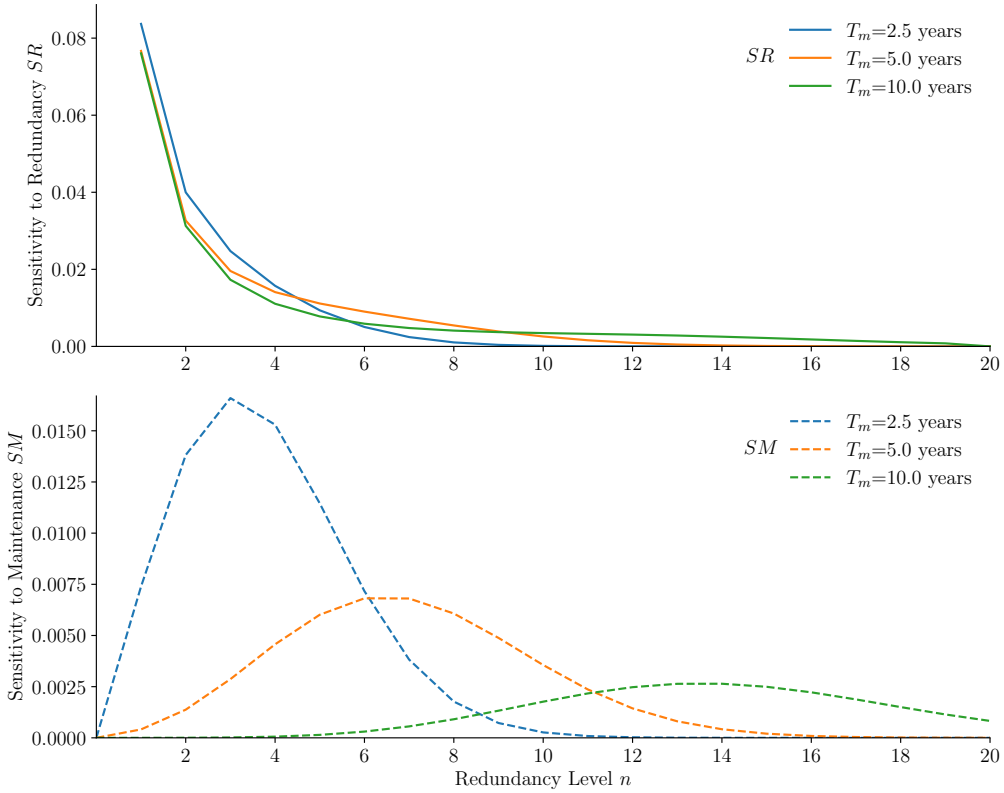

Figure 4.14: Availability sensitivity to the reliability strategy of an MMC with $l = 149$ SMs

The behaviours of the sensitivities for three different maintenance interval periods T_m can be seen in the previous figure. In the first plot, as T_m increases, the rate of decay of SR decreases, and its tail becomes longer. However, it is observed that the sensitivity for higher T_m is initially lower and then becomes higher than in cases of lower values of T_m. This implies that as T_m increases, the initial few redundant SMs have less relevance, but a higher number of SMs remain relevant as the curve takes longer to decay to closely zero, since the MMC takes longer to approach its maximum availability $A_{MMC} = 99.91\%$.

Similarly, the second plot shows that as T_m increases, the initial steepness and peak of the SM curve decrease, but its tail behaviour follows the similar pattern as the previous plot. This indicates that shorter maintenance intervals are more significant for low levels of redundancy. In contrast, higher T_m values have a longer range of relevance of redundancy levels.

Another important aspect of this analysis, apart from the shape of the curves, is their magnitudes. Comparing both plots, it becomes evident that redundancy is the more effective improvement measure for reliability purposes. Nevertheless, the complementary behaviour of maintenance on the model renders higher levels of redundancy unnecessary. Therefore, a careful combination of these reliability strategy parameters is required. This is the subject of the next subsection.

4.4.2. Cost Optimal Converter Reliability Strategy

The relevance of both redundancy and maintenance has been already assessed. Nevertheless, a decision making policy has not been established for the choice of both n and T_m parameters. As it is often the case in engineering systems, this decision is heavily oriented on a cost-based analysis. Therefore, this analysis is carried out in this subsection. To establish this cost-oriented policy, it is necessary to associate costs with the n redundant SMs and the maintenance activities performed periodically at T_m intervals.

Firstly, the cost of each SM can be annualised using a uniform value based on the actual market price and a discount rate. This results in an annual cost increment of 2.975 k$/year for each of the n redundant SMs [63]. Secondly, the cost of a single maintenance activity for an offshore converter can be estimated at 60 k$ per occurrence, with the maintenance carried out at intervals of T_m [13]. By integrating these cost factors Figure 4.15 was plotted.

In this plot, various reliability strategies are represented by bars whose heights correspond to their incremental annual costs. Five different resulting MMC availability ranges are depicted using five different colours, as shown in the colour bar. Establishing a desired minimum MMC availability output of *at least* 99.5%, the most cost-optimal combination of both redundancy level n and maintenance interval period T_m can be determined. The bar for this optimal choice is highlighted in red for clear identification.

Given that the search space of this optimisation problem is small enough to be assessed graphically, the results are clearly visible in the figure below. However, a formal mixed-integer optimisation algorithm could be developed, where n is an integer and T_m is a continuous variable. This approach would provide greater accuracy in determining the optimal maintenance interval T_m. Despite this, obtaining an exact value for T_m would not lead to significant reliability improvements and is less favoured in practical scenarios due to the low and widely dispersed sensitivity to the maintenance interval, which does not yield substantial benefits. Consequently, in this thesis, T_m is evaluated in increments of 0.5 years. This approach results in a cost-optimal reliability strategy with $n = 8$, $T_m = 3.5$ years, and an annual cost

increment of 40.943 k$/year.

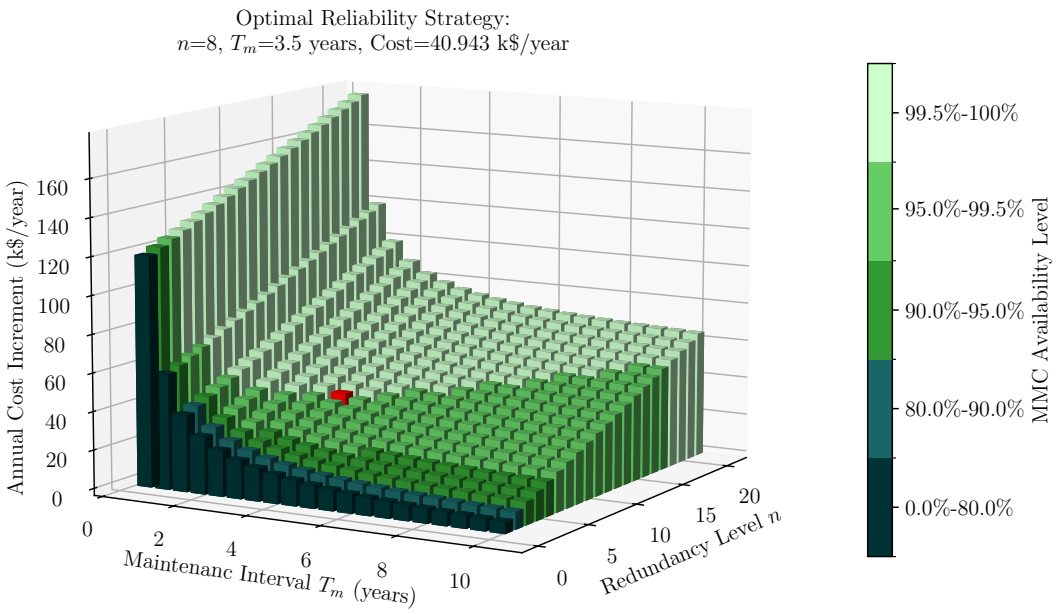

Figure 4.15: Cost optimal reliability strategy design of an MMC with l = 149 SMs

Having established a formal cost-based reliability strategy for the MMC designed for the desired 525 kV DC transmission system, it is important to recognise that this converter is just one of several critical components in the system. Therefore, the following subsection will evaluate the impact of this reliability strategy on the overall expected available transmission capacity of a DCT end.

4.4.3. Converter Reliability Effects on Transmission Capacity

As it has been previously exposed, a DCT end can be modelled as 3-state equivalent probabilistic distribution. This distribution was defined based on the premise of the reliability network diagram of a bipolar DC transmission system and the reliabilities of each of its components. As it has been previously done, the reliability of this kind of probabilistic models is often measured by its expectation. Therefore, given the degree of freedoms which the MMC reliability strategy brings to the model, the effect of multiple strategies is assessed following.

The complete model building process developed before was carried out for multiple reliability strategies. Then the resulting expected available capacity was determined for each of these combinations of n and T_m and plotted as a heat map in Figure 4.16, contour lines were added for its easier interpretation.

Evidently, establishing reliability improvement strategies for the converter significantly benefits the overall reliability of the transmission system. The reliability of a DC transmission system can be improved by approximately ~ 20% by applying the correct MMC strategy. Moreover, analysing the

contour lines reveals that the combination of maintenance and redundancy has a nonlinear impact on the expected capacity. Furthermore, it is clear that as T_m decreases lower levels of redundancy are required to achieve high reliability levels. Conversely, at higher T_m values, redundancy becomes much more critical. This is illustrated by the contour lines being more tightly clustered on the left side of the plot than on the right.

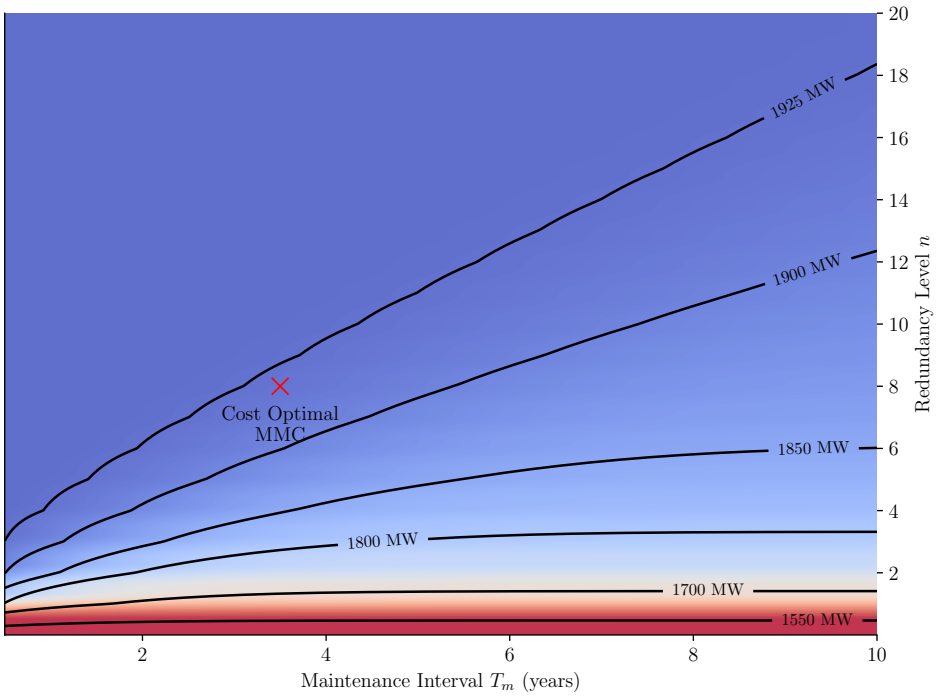

Figure 4.16: Expected available transmission capacity of a DCT end considering possible reliability strategies of an MMC with $l = 149$ SMs

Interestingly, the cost-optimal strategy for an MMC with $l = 149$ and $A_{MMC_{min}} = 99.5\%$, designed for the study scenario of 525 kV DC transmission voltage, yields an expected capacity of 1921.8 MW, which is very close to the maximum achievable capacity of 1930 MW according to this model. The difference between these two values represents the necessary compromise between cost and reliability. To fully assess the impact of this compromise on the reliability of the power system as a whole, a composite model integrating the generation model developed in Chapter 3 and the transmission model developed in this chapter will be examined in the following chapter, considering a multi-terminal topology.

4.5. Summary and Conclusions

This chapter addresses the reliability modelling of DC transmission systems, with a particular focus on the modular multilevel converter (MMC) as a critical component. The research aimed to answer two sub-questions: the modelling approaches for MMC reliability considering different redundancy schemes and preventive maintenance frequencies, and the optimisation of MMC reliability in a cost-effective manner.

To model the reliability of an MMC, a probabilistic model was developed that accounts for the converter's topology and its composition of half-bridge sub-modules (HBSMs). Each sub-module includes critical

components such as IGBT switches, capacitors, and driving mechanisms, whose failure rates were used to calculate the overall sub-module failure rate. Two redundancy schemes were considered: stand-by and active redundancy. Stand-by redundancy, where redundant sub-modules are inactive until needed, was found to be more reliable compared to active redundancy, which shares the load among all sub-modules. The reliability functions for both redundancy schemes were derived and compared, showing that the reliability gains of stand-by redundancy increase even further at high levels of redundancy.

Preventive maintenance was incorporated into the model by assuming periodic perfect maintenance, which restores the reliability function of the MMC to its initial state. The effect of maintenance intervals on the mean time to failure (MTTF) of the MMC was analysed, highlighting the importance of optimal maintenance scheduling.

The cost optimisation of MMC reliability involved balancing the costs of adding redundant sub-modules and performing maintenance activities. Each sub-module's cost was annualised, and the maintenance costs were estimated based on offshore converter maintenance activities. By evaluating various combinations of redundancy levels and maintenance intervals, the most cost-effective strategy that achieves the desired reliability levels was identified.

The sensitivity analysis of the MMC availability to redundancy and maintenance parameters demonstrated that redundancy is more effective in improving reliability. However, a complementary approach combining both redundancy and maintenance yields the best results. The optimal strategy for the case study of a 525 kV DC transmission system involved eight redundant sub-modules and a maintenance interval of 3.5 years, resulting in an annual cost increment of 40.943 k$ and an expected transmission capacity of 1921.8 MW.

In conclusion, this chapter developed a comprehensive reliability model for MMCs, incorporating redundancy and maintenance strategies. The findings highlight the importance of carefully balancing cost and reliability to achieve optimal performance in DC transmission systems. The next chapter will integrate this model with the generation model to evaluate the overall reliability of a composite power system.

5

Reliability Evaluation of AC/DC Power Systems

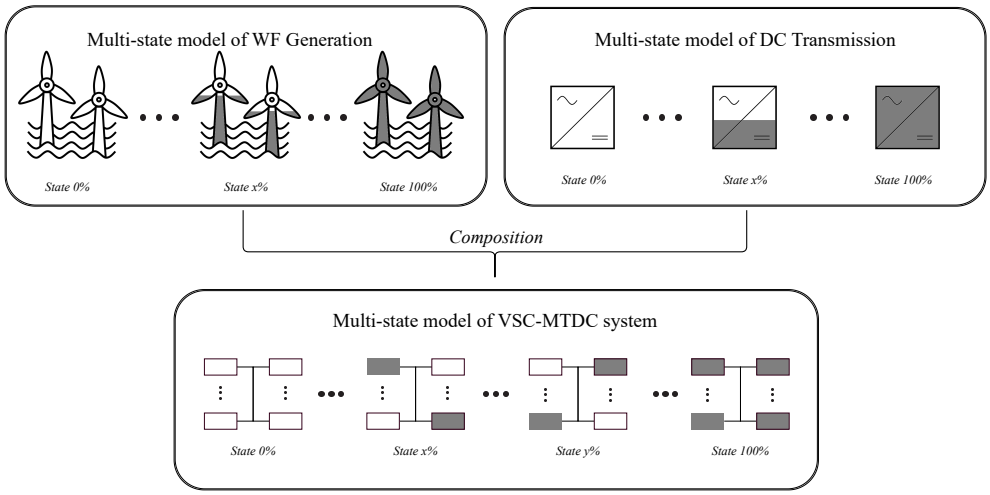

The probabilistic characteristics of offshore wind energy generation and DC transmission systems have been extensively studied separately in previous chapters. This chapter aims to develop a composite model that combines both generation and transmission models. While compositing models is well-researched [3], evaluating a system that combines detailed models of offshore wind energy generators (Chapter 3) and power converters for DC transmission (Chapter 4) is still necessary. This chapter also models the topology of the interconnecting multi-terminal layout and assesses the adequacy of an existing AC system when the composite offshore model replaces conventional generators.

This modelling and reliability evaluation addresses sub-research questions 3, 4, 7, and 8 from Section 1.3. With this purpose, Section 5.1 presents the developed composite generation and transmission model for an offshore wind energy system. Section 5.2 evaluates the impact of this model on the reliability of a hybrid AC/DC power system. Section 5.3 provides an extensive analysis of the results and their implications, and Section 5.4 summarises and concludes the chapter.

5.1. Composite Model of Offshore VSC-MTDC-Based Wind Power Supply

Developing composite generation and transmission systems is necessary for accurately assessing the adequacy of power systems. Furthermore, the reliability of the transmission system is vital for offshore power supply. Therefore, this section develops a composite model in two parts. Section 5.1.1 addresses the complete modelling of a multi-terminal topology HVDC transmission system, and then Section 5.1.2 combines the generation model with the transmission model.

5.1.1. Reliability Modelling of MTDC systems

Previously, the reliability of a single DCT end has been modelled; however, a complete transmission system comprises multiple sending and receiving ends, possibly forming a multi-terminal topology. Figure 5.1 presents the network diagram of such a system. The number of sending and receiving ends affects the number and probability of states of the whole system, each emerging from the state of individual DCT blocks.

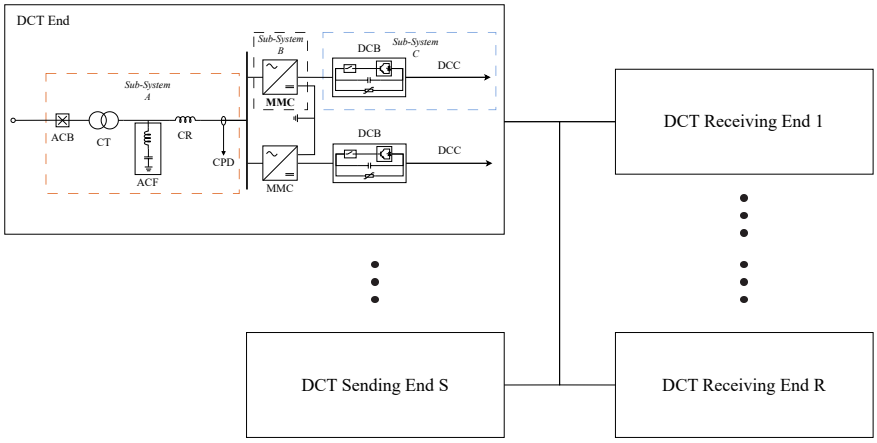

Figure 5.1: Reliability network block diagram of an MTDC system

To construct a model based on the state of each DCT end, the state space of the entire system must be determined by modelling each end. Traditional binary models, categorising states as either up or down, are insufficient. Instead, a ternary state space emerges, where each end can exist in one of three states: N, P, or F. Consequently, the complete state space of an MTDC system is of size 3^{S+R}, where S and R denote the number of sending and receiving DCT ends, respectively. Figure 5.2 illustrates a representative section of the state space for a 4-terminal MTDC system.

This state space is developed similarly to the logic used in a failure tree analysis for a single DCT end. However, in this state space, failures of sending and receiving ends are carried out separately—sending ends to the left and receiving ends to the right. Additionally, each state can undergo two different types of transitions, since each DCT end can move from one state to either of the other two states (e.g., transitioning from N to either P or F). Therefore, the transition rates in this state space are governed by the transition rates of a single equivalent DCT end 3-state model, as shown in Table 4.3. These rates, however, are not depicted in the figure to avoid clutter. The state space representation of this system is

complex and difficult to interpret pictorially due to its sheer size and high degree of interconnection. Nevertheless, three key considerations can be extracted:

1. **Sequential Transitions:** No two DCT ends transition simultaneously, as the probability of two events occurring at the exact same time is extremely low.
2. **Separate Evaluation of Ends:** The states and capacities of the receiving and sending ends must be considered separately, as they result in different outcomes for nodal reliability evaluations.
3. **Limiting System Capacity:** In mixed states where either the sending or receiving end has partial capacities, the capacity of the entire system is limited by the lowest capacity in the chain.

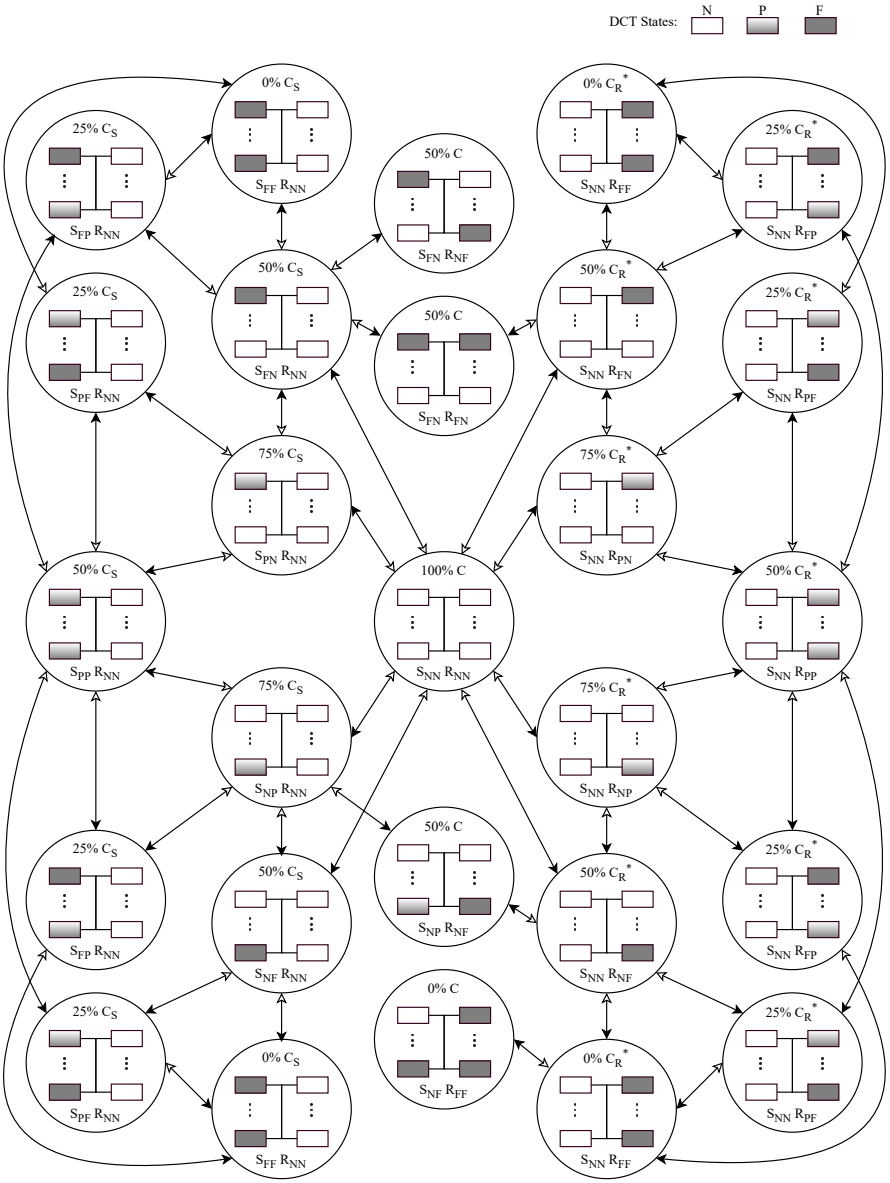

Figure 5.2: Representative section of the state space diagram of a 4-terminal MTDC system

The size of an MTDC state space can become unmanageable for reliability evaluation purposes. Fortunately, many states yield identical capacity and can be merged using equations (2.29) and (2.30) into a reduced equivalent state space. Figure 5.3 illustrates the equivalent state space of a 4-terminal MTDC system. This figure is much easier to interpret, highlighting the advantages of MTDC systems.

Firstly, the presence of numerous intermediate states compared to the original DCT model, or a single-link bipolar HVDC interconnector, increases the probability of maintaining an adequate transmission capacity. Additionally, because these intermediate states exist, there is no direct transition rate from full capacity to zero. This significantly reduces the probability of residing in lower capacity states.

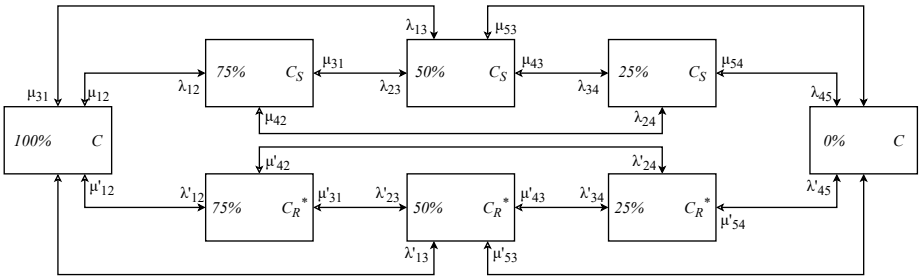

Figure 5.3: Equivalent 8 state space model of a 4-terminal MTDC system

Similarly to the previous models, the multi-state model of an MTDC can be represented in both a probability table and a probability distribution. The *MTDC capacity output probability table* or *MTDCCOPT* is presented in Table 5.1. The probability distribution of this system is depicted in Figure 5.4. These outputs reflect the model for a 4-terminal system with $S = 2$ sending and $R = 2$ receiving DCT ends, where each DCT end has a capacity of 2000 MW. Furthermore, this model uses a cost-optimal MMC reliability strategy with $l = 149$ SMs per arm and minimum MMC availability $A_{MMC_{min}} = 99.5\%$, a redundancy level of $n = 8$ SMs, and a maintenance period of $T_m = 3.5$ years.

States	C_{MTDC} (MW)	P_i (-)	α_{+i} (occ/day)	α_{-i} (occ/day)	f_i (occ/day)
100%	4000	0.76	0.00	1.18×10^{-2}	8.92×10^{-3}
75%	3000	0.19	2.67×10^{-2}	8.16×10^{-3}	6.59×10^{-3}
50%	2000	0.05	1.06×10^{-1}	3.36×10^{-3}	5.33×10^{-3}
25%	1000	~ 0	1.42×10^{-1}	2.54×10^{-3}	3.70×10^{-4}
0%	0	~ 0	2.29×10^{-1}	0.00	6.19×10^{-5}
Sum		1.00			

Table 5.1: 4-terminal MTDC capacity output probability table MTDCCOPT

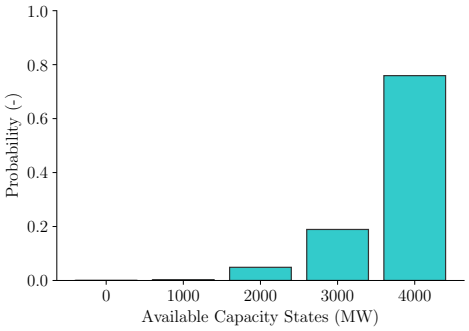

Figure 5.4: 4-terminal MTDC model output probability distribution

Evidently, the probability of the two lowest states is negligible since this would require that at least two DCT ends in the system reside in a failed or partial state simultaneously. The same logic applies to the lower probability of achieving full capacity with respect to a single DCT end, as the likelihood of all DCT ends being in a full state is also lower.

An index that summarises the data depicted in the output probability distribution of the model, similar to the previous models, is the *expected available MTDC transmission capacity*. The resulting expectation for a 4-terminal model is 3704.57 MW, which is significantly higher than the expectation for a single point-to-point HVDC transmission model, which is 1848.23 MW. To compare these figures, normalisation with respect to the installed capacity can be performed, yielding an *expected available transmission capacity factor* of 92.61% for the 4-terminal system and 92.41% for the 2-terminal system. A more detailed analysis of how this expected capacity factor varies with an increasing number of ends—referred to as the *coupling degree* of an MTDC system—is provided in Section 5.3.1.

5.1.2. HLII Composite Model of Offshore Wind Energy

The systematic process of developing composite models, as outlined in Section 2.2.1, follows the principle of a minimum distribution, where capacity states are limited by the lower capacity state of either generation or transmission models. Consequently, the state space of the MTDC system model evolves into a multilayered structure, as illustrated in Figure 5.5. This figure depicts the states of a rounded 5-state space model of an offshore wind farm, developed in Chapter 3 and shown in Figure 3.17, superimposed as five distinct layers on the equivalent 8-state space of a 4-terminal MTDC system.

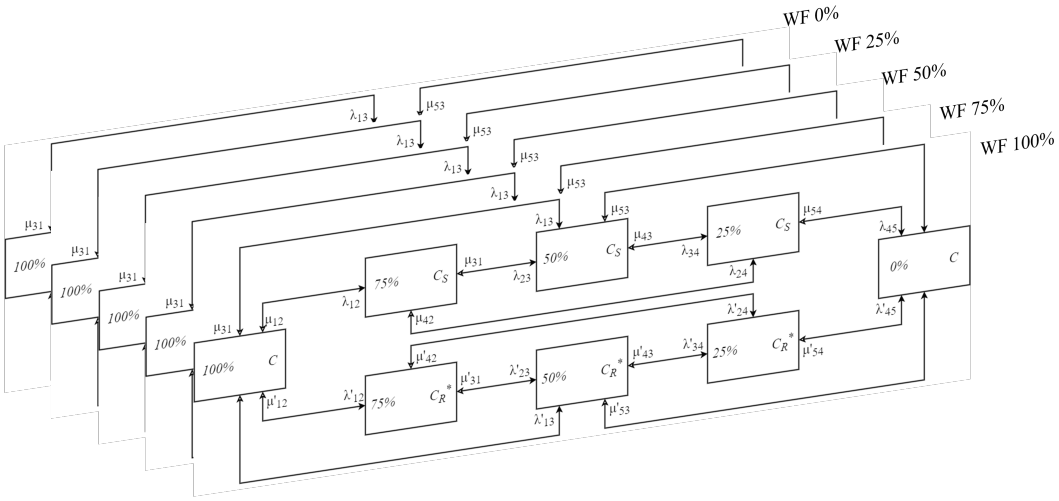

Figure 5.5: State space representation of HLII composite model of a 4-terminal MTDC and rounded 5-state offshore wind farm

Since there is complete independence between the probability distributions of each model, i.e., the available wind power is not dependent on the available transmission capacity, the probabilities P_i of each state can be determined by Equation 2.46 and the resulting state capacity C_{gt} is given by Equation 2.45. This procedure is applied to the rounded 5-states model of two 2010 MW wind farms composed of 15 MW IEA wind turbines located 100 km offshore and a 4-terminal MTDC system with cost-optimal MMC reliability strategy of $A_{MMC_{min}} = 99.5\%$, $l = 149$, $n = 8$, and $T_m = 3.5$ years. This yields the *composite wind-transmission capacity output probability table* or $COMPCOPT$ shown in Table 5.2. In addition, the probability distribution of this model is shown in Figure 5.6.

Since the capacity of the MTDC system is designed to match the total installed wind power capacity, the complete state space produces the same 5-state capacity levels as the previously developed 5-state rounded WF model and the 4-terminal MTDC model. Evidently, the highest capacity is seldom achieved

during the operation of these systems. This is due to the very low probability of residing in a state with rated wind speed, where all turbines are operational, and full transmission capacity is available. By examining the distributions of both models separately, it becomes clear that the primary factor contributing to this low probability is the rounded wind farm probability distributions.

States	C_{gt} (MW)	P_i (-)	α_{+i} (occ/day)	α_{-i} (occ/day)	f_i (occ/day)
100%	4020	~ 0	0.00	29.93	2.68×10^{-19}
75%	3015	0.51	5.21×10^{-19}	1.69	0.85
50%	2010	0.16	4.66	3.84	1.37
25%	1005	0.26	2.63	1.33	1.04
0%	0	0.07	5.67	0.00	0.39
Sum		1.00			

Table 5.2: 4-terminal MTDC + 2×2010 MW wind farms composite capacity output probability table COMPCOPT

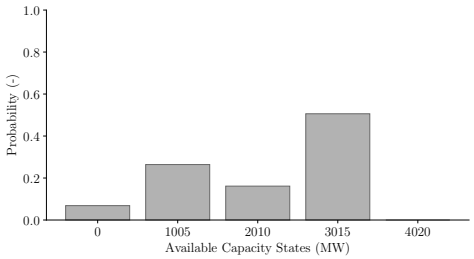

Figure 5.6: Composite model output probability distribution

The expectation of this distribution, in comparison, yields a capacity of 2115.47 MW which signifies an expected capacity factor of 52.62%. In comparison, disregarding the transmission layer would yield an expected available capacity of 2145.30 MW and a capacity factor of 53.37%. Furthermore, if a dedicated 2-terminal system for each wind farm is considered this would yield an expectation of 1056.95 MW for each link and a capacity factor of 52.58%. In this comparison it becomes clear that the coupling degree has a lower effect on the capacity factor, since the intermittence of wind power plays a bigger role in the reduction of the capacity factor.

Another observation from this result is the impact of rounding wind farm power to discrete states on the model's accuracy. To address this, a comparison with the exact number of states was performed. For a 4020 MW system, this amounts to a total of 269 states, yielding an expectation of 2166.24 MW and a capacity factor of 53.89%. This results in a significant difference of $\sim 1\%$ in the capacity factor compared to the rounded 5-state model. However, to reduce the state space for reliability evaluation and thereby decrease computational effort, this error is considered tolerable.

Finally, the *HLII model of offshore power providers* has been developed by integrating both transmission and generation models. The reduction in capacity factor attributable to these models is 0.75% due to limited transmission probability, compared to a 46.63% reduction caused by the variability of wind power. Therefore, it is evident that the greatest threat to the reliability of supply in power systems is the stochastic nature of wind power. This issue is further examined in the following section.

5.2. Reliability Evaluation of a Hybrid AC/DC Power System

The purpose of power systems is the supply of power from its generation points, e.g., offshore, to its demand nodes. Therefore, to perform a reliability evaluation of a power system including VSC-based MTDC offshore power, the previous HLII model must be connected to another AC grid model. This is illustrated in Figure 5.7. In this case, the chosen AC grid is the already developed and extensively researched standard IEEE RTS 24 model [8, 57, 7]. This model depicts a conventional power system with 24 nodes, including its own conventional generators and load models. It is therefore the purpose of this

section to evaluate how the reliability of this original system changes when the previously developed composite model substitutes conventional coal fired generators.

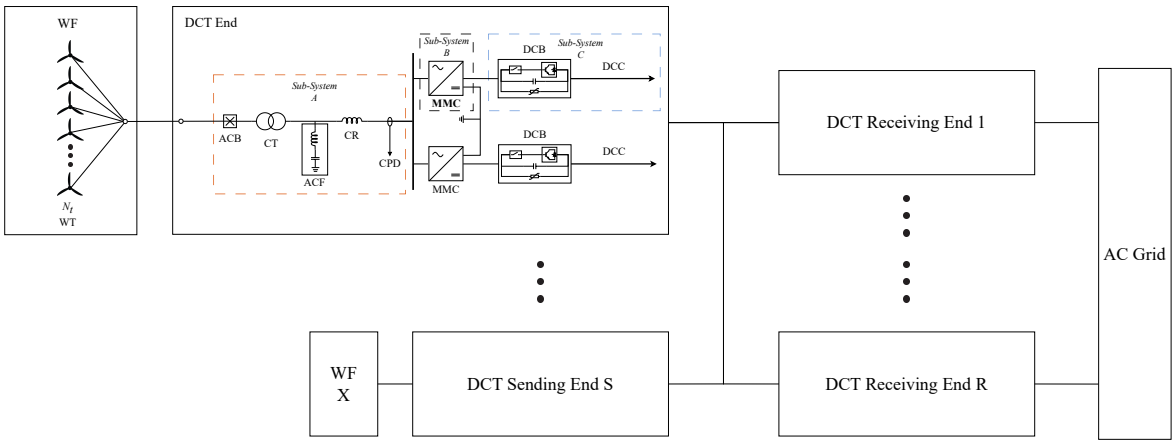

Figure 5.7: Hybrid AC/DC system reliability evaluation topology diagram

One aspect of probabilistic reliability evaluation involves the development of generation and transmission models, which have been extensively covered in previously. However, another crucial probabilistic model to consider is the load model. As explained in Section 2.2.3, frequency and duration methods are effective for developing these models. Consequently, the load model based on the standardised system is presented in Table 5.3 and Figure 5.8. This load model includes daily peak load values as well as a base load state. Notably, the transition probability from the base load state to a lower state is non-existent, and the transition probability to higher peak states is also zero which is expected of a daily peak load model. Furthermore, it is assumed that these peaks have a half day duration, hence an exposure factor $e = 0.5$.

States	L_i (MW)	P_i (-)	α_{+i} (occ/day)	α_{-i} (occ/day)	f_i (occ/day)
1	2687	0.0164	0	2	0.0329
2	2454	0.1123	0	2	0.2247
3	2188	0.1479	0	2	0.0329
4	1953	0.1589	0	2	0.3178
5	1593	0.0644	0	2	0.0329
6	1485	0.5000	2	0	1.0000
Sum		1.00			

Table 5.3: Load model considering an exposure factor $e = 0.5$

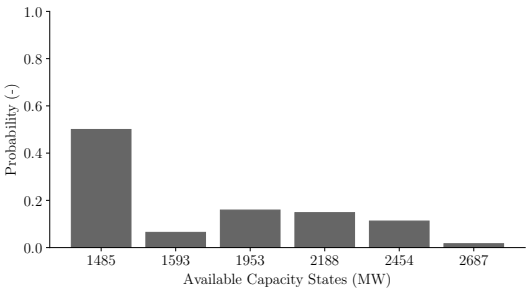

Figure 5.8: Load model demand probability distribution

In addition to the load model, this system consists of multiple generators already connected to supply this load. Therefore, the addition of the composite offshore generation must be recursively incorporated into the existing capacity model, using the methods explained in Section 2.2.2.

The original generation mix of this model has a very low share of sustainable energies. Consequently, the evaluation of this system is performed in three distinct cases, where the energy transition is modelled in this mix as shown in Table 5.4. Case 1 is the original scenario in which no wind power has been

added. In Case 2, a single 350 MW steam fossil-coal fired generator is substituted by 600 MW of offshore wind power. Lastly, in Case 3, the same 350 MW generator is decommissioned, and additionally, four more 155 MW generators are decommissioned. Thus, in total 970 MW of steam coal-fired generation is substituted by 2010 MW of wind power in Case 3.

Generators (MW)	Case 1	Case 2	Case 3
Offshore Wind	0	600	2010
Hydro	300	300	300
Nuclear	800	800	800
Steam Fossil-oil	951	951	951
Steam Fossil-coal	1274	924	304
Combustion Turbine	80	80	80
Total	3405	3655	4445

Table 5.4: Generation mix of three cases

The reliability data of the decommissioned generators is shown in Table 5.5. In their place, an offshore wind farm model is introduced, utilising the 5-state composite model of wind farms and transmission, which is composed of 15 MW IEA turbines located 100 km offshore and a 4-terminal MTDC interconnecting transmission system. Furthermore, the MTDC system is characterised by a cost-optimal MMC reliability design with $A_{MMC_{min}}$ = 99.5% and a 525 kV voltage DC link.

Units size (MW)	Number of units	Forced outage rate (FOR)
350	1	0.08
155	4	0.04

Table 5.5: Decommissioned steam coal fired gerators in cases 2 & 3

Once the available capacity model has been developed recursively according to the mix of generators in each case, the convolution of the generation and load models, as explained in Section 2.2.4, is performed to evaluate the system's reliability indices. The probabilistic indicators of loss of load probability $LOLP$, loss of load expectation $LOLE$, and loss of energy expected $LOEE$ are shown in the table below. However, these indices are hard to compare, therefore the energy index of reliability EIR is the easier metric to interpret in Table 5.6. Additionally, given the extensive detail of the models, complementary metrics involving the expected surplus wind energy $ESWE$, offshore O&M variable costs (*affordability*), and wind energy penetration (*sustainability*) is determined for the three cases.[1]

Case	LOLP (-)	LOLE (d/y)	LOEE (MWh/y)	ESWE (GWh/y)	EIR (%)	Sustainability (%)	O&M Costs ($/MWh)
1	0.0016	1.17	1706.16	-	**99.989**	**-**	**-**
2	0.0021	1.53	2329.16	38.46	**99.985**	**17.40**	**53.93**
3	0.0163	11.95	27571.68	181.03	**99.825**	**58.53**	**53.26**

Table 5.6: System indices for three distinct cases

These results reveal a clear decreasing pattern in system reliability as conventional generators are substituted by offshore wind. From an LOLP perspective, the probabilities of failure in case 3 increase

[1]Each one of these indices and the way they are determined is explained thoroughly in Section 2.2.4

tenfold compared to the baseline case 1. Similarly, the increase in LOLE indicates a tenfold rise in the frequency of blackouts within the system. The LOEE quantifies un-reliability in terms of energy not supplied to loads which increases non-linearly, even more than tenfold. However, the ESWE, i.e., the amount of wind power curtailed, is much higher than the total LOEE in both case 2 & 3. This suggests that developing storage capacity offshore is a potential partial solution to address the intermittency and reliability issues in these sustainable power systems. Consequently, there is a correlation between surplus wind energy and the expected available storage capacity in these offshore systems, as will be discussed in Section 5.3.2.

Moreover, these findings highlight the trilemma of reliability, sustainability, and affordability. As sustainability increases, the EIR, which is the ratio of power supplied to power demanded, significantly decreases. Conversely, the expected O&M costs per MWh show a small decreasing variation. Therefore, system operators must balance these three factors, weighing benefits, costs and risks. Further analysis of this trilemma, including its behaviour across various ranges of wind power capacity and reliability strategy, is presented in Section 5.3.3.

5.3. Reliability Evaluation Analysis

The reliability evaluation of a hybrid AC/DC power system has been performed in the previous section. However, it is important to note that the resulting system indices are contingent upon the selected parameters of the composite wind farm and MTDC system. Therefore, this section is dedicated to analysing these system indices across various degrees of freedom within the model. Specifically, Section 5.3.1 examines the impact of coupling degrees on the expected available capacity factor of MTDC systems. Following this, Section 5.3.2 explores how the expected surplus wind energy $ESWE$ and loss of energy expected $LOEE$ change as additional wind power is integrated into the system. Finally, Section 5.3.3 investigates the overall behaviour of the system indices, with a particular emphasis on the interplay between reliability, sustainability, and affordability.

5.3.1. Effect of Coupling Degrees on MTDC Reliability

In Section 5.1.1, it is highlighted that the state space of an MTDC system expands by 3^{S+R} as additional sending ends S and receiving ends R are incorporated into a meshed topology. The degree of this meshing is referred to as the coupling degree of the system.

While increasing the coupling degree of a power system offers numerous benefits, this analysis concentrates on the reliability indices of the MTDC system, particularly considering that the transmission capacity becomes less dependent on the availability of any single DCT end. Consequently, the expected available transmission capacity factor is assessed as the number of both sending and receiving ends is varied. This evaluation is depicted in Figure 5.9.

In this figure, the coupling degree—and thus the system's capacity, assuming each DCT end maintains a capacity of 2000 MW—is increased from the simplest 2-terminal topology to the more complex 12-terminal topology. Across this range, multiple intermediate combinations of S and R are possible, and each combination is thoroughly evaluated.

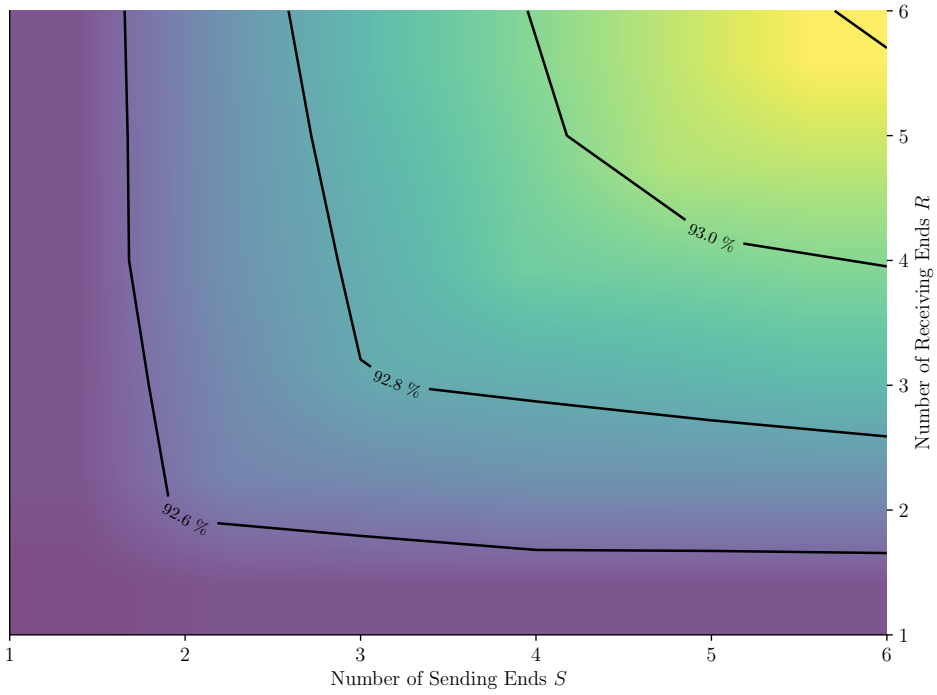

Figure 5.9: Expected available transmission capacity factor of an MTDC system considering different coupling degrees

As anticipated, the expected capacity factor rises with an increase in the coupling degree. However, this improvement in reliability is not linear. Additionally, the contour lines reveal that configurations where the number of sending ends differs from the number of receiving ends are less effective in enhancing reliability compared to configurations with an equal number of ends on each side, especially at small coupling degrees. For example, an 8-terminal configuration with $S = 2$ and $R = 6$ has a lower capacity factor than one with $S = 4$ and $R = 4$. This discrepancy arises because the side with the fewer ends becomes the bottleneck, limiting the overall transmission capacity.

A more detailed analysis of the percentage gains in availability reveals that, while increasing the coupling degrees of the MTDC system does yield improvements, these gains are marginal, not exceeding 1%. In the context of nodal reliability evaluation, however, these small gains can become significantly more meaningful, especially when the importance of each receiving node varies. In such cases, a higher number of receiving ends—even if imbalanced relative to the number of sending ends—might be preferable. Nevertheless, this specific consideration falls outside the scope of the current analysis.

Although this analysis has focused on the MTDC system in isolation, a more comprehensive evaluation of the overall reliability of a power system incorporating an MTDC model is discussed in the following section. Given that the differences in expected available capacity between simpler and more complex MTDC configurations are minimal, the subsequent sections will employ an intermediate 4-terminal MTDC topology for further analysis. This choice strikes a balance between computational effort and complexity, facilitating a more practical assessment of system performance.

5.3.2. Expected Offshore Storage Capacity and Surplus Wind Energy

The convolution of the available generation capacity model and the load demand model produces negative margin states, leading to loss of load situations. However, this convolution also identifies instances where available wind power must be curtailed, either because the transmission system is unable to transmit the excess power or because the available wind power exceeds the total power demand. To avoid losing this surplus energy entirely, one possible solution is to store it offshore.

Moreover, storing this energy when it is not immediately needed or when there is insufficient transmission capacity can enhance the system's flexibility and reliability. Figure 5.10 demonstrates how $ESWE$ and, consequently, the associated storage potential, increase as the installed offshore power capacity on the RTS-24 system (Case 2) grows. Additionally, the figure shows a corresponding decrease in $LOEE$ as the installed capacity increases. To address potential inaccuracies arising from rounding in the composite model, a parallel evaluation is conducted without rounding, depicted with dotted lines for comparison.

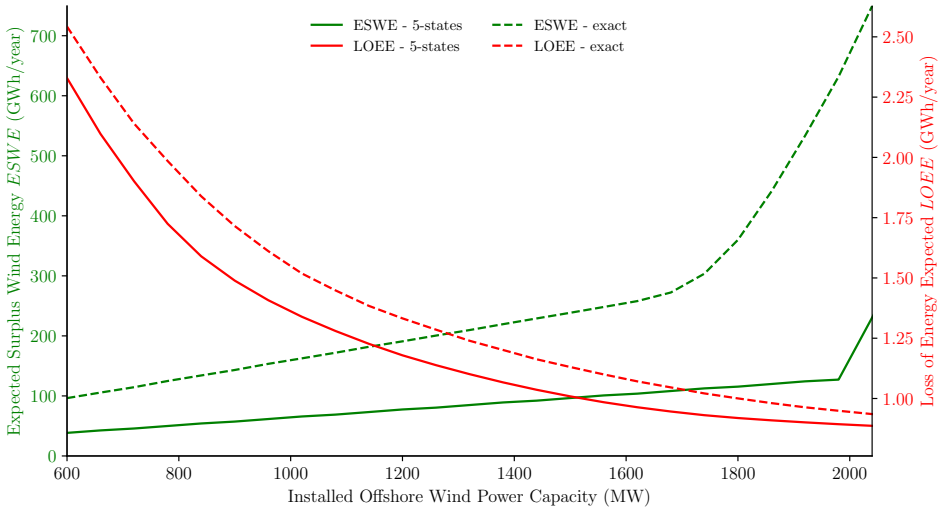

Figure 5.10: Offshore storage potential considering ESWE and LOEE

Given that the composite model rarely operates at 100% output capacity, the $ESWE$ appears to increase linearly until the total installed capacity reaches a threshold, since before this threshold curtailment is primarily due to the limited availability of transmission capacity. In the 5-state rounded model, this threshold is reached when the installed capacity hits 1980 MW. At this point, the 75% state of the model aligns with the base load state, which has the highest probability and duration within the load model. Beyond this threshold, the probability of wind energy curtailment due to excess supply over demand increases significantly, leading to a sharp rise in $ESWE$.

The differences between the exact and 5-state rounded composite models indicate that as more states are considered, a greater amount of wind energy is curtailed. This outcome is expected because the exact model includes more intermediate states between the natural (unrounded) 5 states of a 4-terminal MTDC transmission system. Consequently, more energy is lost due to the limited transmission capacity. Moreover, the threshold transition starts at lower capacities and becomes smoother in the exact model, since the distribution of states is more dispersed.

While it is evident that surplus energy significantly exceeds lost energy in both the rounded and exact

models, this does not imply that offshore storage alone can resolve the reliability issues. To fully assess the impact of storage on power system reliability, it is essential to incorporate energy-limited systems—such as storage systems modelled based on their available energy states—into the reliability evaluation.

This scenario, which does not account for storage capacity, presents significant challenges in power system sizing, as it indicates lower utilisation of offshore capacity, particularly beyond installed capacities of the 75% threshold. However, this outcome may be somewhat unrealistic because the base load is not a constant value; it varies throughout the year, just as the wind energy resource fluctuates seasonally. As a result, the limitations of this model for assessing storage capacity become evident, particularly at this level of installed capacity. To achieve more accurate storage sizing, time-sequential simulations are required, where energy states are tracked over time, and more detailed load models are incorporated.

5.3.3. Reliability-Sustainability-Affordability Trilemma in Hybrid AC/DC Power Systems

Reliability measures the ability of a power system to fulfil its function of supplying power consistently. However, environmental and economic aspects are equally crucial, giving rise to the trilemma of reliability-sustainability-affordability. It is therefore essential to consider the inter-dependencies and interactions among these indices, especially in hybrid AC/DC power systems where sustainable offshore power sources can be modelled using the previously developed composite model.

Until now, only isolated analyses of these complementary system indices have been conducted under two distinct scenarios with fixed model parameters. However, a more nuanced understanding of how these indices evolve as installed offshore wind power capacity and MMC availability vary can be achieved with these models. Figure 5.11 illustrates the behaviour of the RTS-24 system (Case 2) as the installed offshore wind capacity increases from 600 to 2040 MW. Additionally, the system indices are evaluated across a range of minimum MMC availabilities, from 98% to the maximum achievable 99.91%.

Interestingly, the system exhibits a converging pattern in reliability and cost as wind energy penetration increases. This suggests that as the share of offshore power in the system grows, it becomes increasingly challenging to enhance reliability merely by adding more wind capacity. This trend is particularly evident when comparing the initial significant improvements in system reliability resulting from small increases in wind power with the diminishing returns observed at higher levels of wind energy penetration. This behaviour can be attributed to the previously discussed analyses of $LOEE$ and $ESWE$. After a certain threshold of installed wind capacity, $LOEE$ stabilises, while $ESWE$ sharply grows due to the increased likelihood of excess wind energy generation.

On the other hand, variable costs have a very subtle impact on system reliability. These costs tend to decrease as the scale of generation increases, demonstrating the effect of economies of scale. Moreover, the influence of reliability of the MMC and HVDC system on the overall power system reliability diminishes as wind power increases, since, beyond the threshold mentioned in the previous section, the loss of power due to transmission limitations becomes less significant. This understanding can guide the appropriate sizing of additional offshore wind capacity, based on policies that balance cost and reliability for society.

An optimal sizing method can be employed by applying constraints on the desired minimum indices across this surface. For example, maintaining the same level of reliability as before the substitution of

the conventional 350 MW generator could serve as a benchmark. In the figure, this is represented by a flat surface where the EIR is 99.989%. The intersection of this surface with the system's performance curve determines the appropriate sizing for the offshore system. According to this policy, the optimal total installed wind capacity would be 780 MW, with an MMC availability of 98.25%. This corresponds to an MMC reliability strategy with a redundancy level of $n = 7$ SMs and a maintenance interval of $T_m = 4.5$ years. All of this resulting in an offshore O&M variable cost of 53.512 \$/MWh and a wind energy penetration level of 22.60% in the system. The implication of this sizing method and its further opportunities are discussed in Chapter 6.

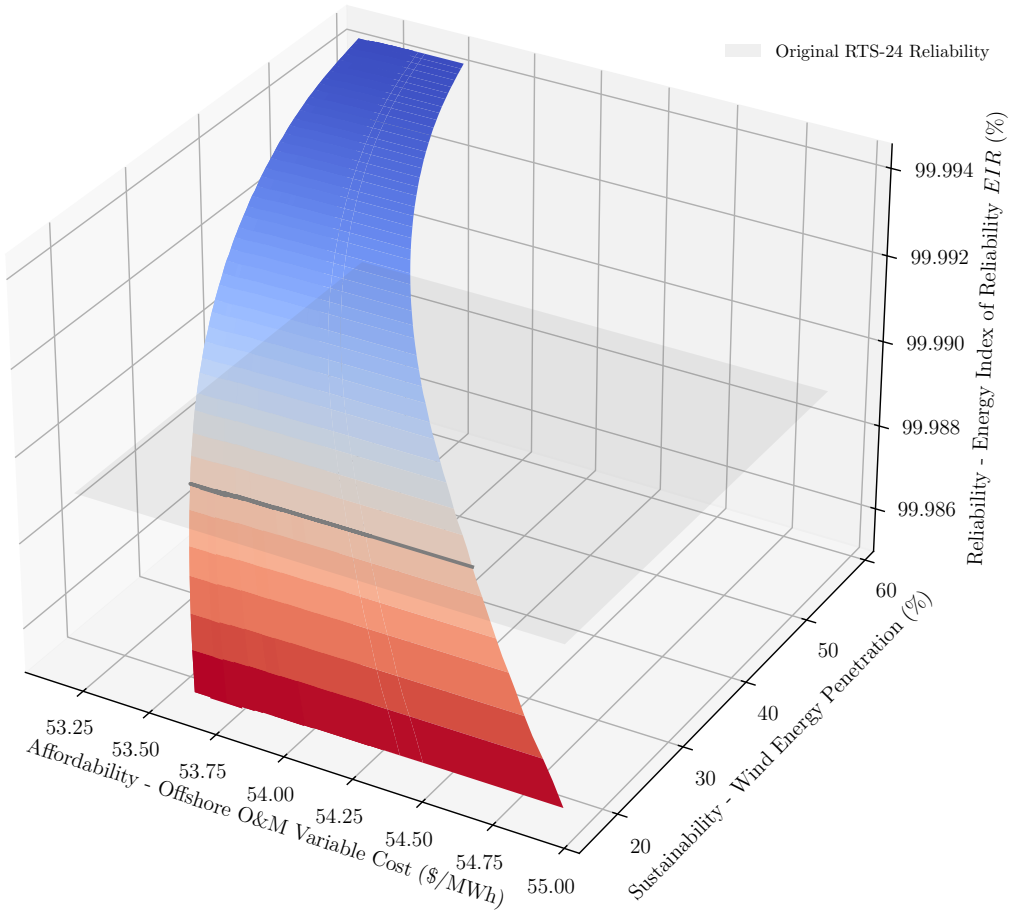

Figure 5.11: System indices sensitivity to installed offshore wind energy and transmission system reliability strategy

5.4. Summary and Conclusions

This chapter focused on the reliability evaluation of hybrid AC/DC power systems, integrating offshore wind energy generation with MTDC transmission systems. It aimed to address several sub-research questions: the impact of offshore wind energy penetration on system adequacy when conventional generators are decommissioned, the quantification of surplus wind energy using probabilistic indices, the modelling MTDC HVDC system reliability and its sensitivity to coupling degrees, and the extent to which HVDC system availability limits offshore energy supply and affects overall power system

reliability.

A significant portion of this chapter was dedicated to developing a composite model to evaluate the reliability of offshore generation and transmission across various degrees of coupling in MTDC systems. The analysis revealed that increasing the degree of coupling within the MTDC system—by incorporating more sending and receiving ends—improves in $\leq 1\%$ the system's expected available transmission capacity factor by increasing the number of possible intermediate states from 1 to 11 as the MTDC meshing is increased from a 2-terminal to a 12-terminal topology. It was also found that configurations with unequal numbers of sending and receiving ends are less effective in enhancing reliability compared to balanced configurations, as the side with fewer ends becomes a bottleneck, limiting overall transmission capacity and reliability.

The developed composite model was recursively added to the standardised IEEE RTS24 load and generation models to assess the overall system reliability when conventional generators are replaced with offshore wind generation. The convolution of these models indicated a significant decrease in system reliability, as demonstrated by increased LOLP, LOLE and LOEE metrics. This decline in reliability was particularly pronounced in scenarios where higher capacities of conventional generators were substituted without a strategic policy or sizing method to manage the transition. The findings underscore the increased risk associated with integrating large-scale offshore wind capacity into existing power systems, highlighting the necessity for careful planning and sizing to maintain system reliability.

Further analysis explored the gradient in reliability and cost as offshore wind energy penetration increases and the minimum MMC availability constraint was varied. The results revealed a converging behaviour, indicating that simply increasing offshore wind capacity does not linearly improve the security of supply. This suggests that the appropriate sizing of offshore wind capacity should be determined based on a balance between cost and reliability, acknowledging the diminishing returns in reliability improvements as wind capacity increases.

To address the challenge of optimally sizing offshore wind capacity and designing of the MMC reliability strategy, a constant risk policy was developed and applied to the RTS-24 system where 350 MW of coal fired generation was decommissioned. This policy determined that an optimal total installed wind capacity of 780 MW, with an MMC availability of 98.25%, would effectively maintain system reliability while replacing the conventional generator. This configuration, which includes an MMC reliability strategy with $n = 7$ redundant sub-modules and a maintenance interval of $T_m = 4.5$ years, results in an offshore O&M variable cost of 53.512 \$/MWh and achieves a wind energy penetration level of 22.60% within the system.

In conclusion, this chapter established a comprehensive reliability model for hybrid AC/DC power systems that incorporate offshore wind energy and MTDC transmission systems. The findings highlight the complexities and challenges of integrating renewable energy sources into existing power systems, particularly in terms of balancing reliability, sustainability, and affordability. The insights gained from this study provide a foundation for future strategies aimed at optimising hybrid power systems as they increasingly rely on power electronics and sustainable energies.

6

Discussion

Through the development of probabilistic models and detailed reliability evaluation, this thesis identified critical elements that influence system reliability. These include the optimal use of the impact of drivetrain technologies on offshore wind turbines, redundancy and maintenance in MMCs, the coupling degree and topology of an MTDC system, and the share of offshore wind power within a hybrid AC/DC power system. The results highlight that a careful balance of these factors is essential for maintaining reliability as renewable energy becomes more integral to power systems. This discussion chapter will delve into the implications of these findings, considering their broader relevance to future power system designs and further opportunities for future research.

Chapter 3 highlights the significance of drivetrain technology and offshore distance in the reliability and cost-effectiveness of offshore wind farms. The probabilistic model developed in the study demonstrates the advantages of direct drive systems, particularly in deeper offshore locations, due to their enhanced reliability and lower operation and maintenance costs compared to geared systems. These findings are crucial for optimising offshore wind farm designs as renewable energy integration increases. However, the study also reveals the need for further refinement of the model, particularly in improving accuracy related to the rounding of the 5-state space model, nevertheless increased distance enhances model precision due to a higher likelihood of turbines operating in lower capacity states.

Another key area for future research involves addressing the parametric uncertainties associated with drivetrain components, particularly in failure and repair rates that vary with operational conditions such as wind speed and turbine load. Incorporating mission profiling into reliability models could provide a more accurate assessment of how environmental stresses impact turbine performance and reliability. Additionally, while the current study did not incorporate real-world logistical constraints, particularly those in the North Sea, this presents a significant opportunity for future research. Understanding how these regional constraints, such as resource availability and maintenance logistics, influence the economic viability of different drivetrain options could be pivotal in making more informed decisions.

Finally, the study indicates the necessities of further exploring wind farm array topology and the risk of dependent failures within these systems. While the existing model offers valuable insights, future research could focus on how interactions between array topology, and protection schemes might be

optimised to develop more robust and resilient offshore wind energy designs. Addressing these aspects could significantly enhance the optimisation of offshore wind farms reliability, ensuring they are better suited to various environmental and logistical challenges.

Chapter 4 underscores the crucial role that MMCs play in the reliability of DC transmission systems. By developing a detailed probabilistic model, the study examined the sensitivity of MMC reliability to various strategies, including redundancy levels and maintenance intervals. The findings revealed that while redundancy significantly enhances converter reliability, the most cost-effective strategy combines both redundancy and maintenance. This balance is essential for achieving high reliability without incurring excessive costs. The analysis highlighted that, with the optimal strategy, the system could closely approach maximum reliability, demonstrating that carefully planned reliability strategies can significantly improve the performance of DC transmission systems.

Despite the robustness of the developed model, the research also has areas where further refinement is needed. For instance, the current model assumes a perfect periodic maintenance schedule, which may not fully capture the complexities of real-world maintenance activities. More nuanced strategies, such as Reliability-Centered Maintenance (RCM) or Condition-Based Maintenance (CBM), could offer a more accurate representation by considering the gradual wear and tear of components and the varying effectiveness of maintenance interventions. Additionally, the study could benefit from incorporating parametric uncertainties and mission profiling to better account for the operational conditions that impact component failure rates. These enhancements would provide a more comprehensive understanding of the long-term reliability of MMCs in DC transmission systems.

Further research could also explore the dynamic aspects of converter operation, such as the impact of varying load conditions and the implementation of protection schemes on overall system reliability and dynamic security. Understanding how these factors interact with the converter's reliability strategies could lead to more resilient system designs. Additionally, the integration of long-term assessments, which consider the ageing and wear-out of components, would provide valuable insights into the reliability of the transmission system over its operational lifespan. These areas of further investigation are essential for advancing the reliability modelling of DC transmission systems and ensuring their robust performance in increasingly complex power grids.

Chapter 5 examines the combined effects of generation and transmission models within a hybrid AC/DC power system, focusing on the integration of an MTDC topology with an AC system. Using the standardised IEEE RTS-24 model, the study evaluates system reliability, highlighting how increasing the coupling degrees in the MTDC system enhances reliability by improving the probability of having available DC transmission ends. The chapter also examines the challenges of probabilistacally sizing offshore storage capacity to manage surplus wind energy and investigates the complex interplay between reliability, sustainability, and affordability, particularly as these factors are influenced by wind energy penetration and O&M costs.

The results revealed that while increasing the coupling degrees within an MTDC system does improve system reliability, these benefits are primarily due to the enhanced likelihood of available transmission paths. However, this evaluation was limited by the degree of resolution in the system topology, and future research could extend this approach to a real Dutch power system nodal reliability evaluation. Incorporating a nodal reliability evaluation, where the importance of each receiving end varies, could provide a more nuanced understanding of how uneven coupling degrees could be optimised based on specific system needs. Additionally, further research could explore dynamic security and power

flow optimisation for reliability, considering the topology of the AC/DC system. This would involve addressing dynamic constraints such as angle and frequency stability, which become increasingly critical as system inertia decreases with higher renewable energy penetration.

A significant outcome of the chapter is the observed converging behaviour of power system reliability in relation to both O&M costs and wind energy penetration. As offshore wind capacity increases, the initial gains in system reliability diminish, highlighting the reliability-sustainability-affordability trilemma. This convergence indicates that beyond a certain point, merely adding more wind capacity does not linearly enhance system reliability. Instead, a strategic balance must be achieved between these factors. The research illustrates how applying a constant risk policy can help navigate this trilemma, providing a framework for optimising the integration of renewable energy sources. However, the chapter also suggests that other policies and strategies could be explored in future research to further refine the balance between reliability, sustainability, and affordability in sustainable power systems.

In summary, this thesis has identified and analysed critical factors influencing the reliability of hybrid AC/DC power systems, with a particular focus on offshore wind energy integration and the role of MMCs in DC transmission systems. The research highlights the importance of optimising drivetrain technologies, redundancy and maintenance strategies, MTDC system topologies, and wind energy penetration to enhance system reliability. While the findings provide valuable insights, they also point to the need for further research in areas such as nodal reliability evaluation, dynamic security and power flow optimisation, and the strategic sizing of storage and wind capacity. By addressing these areas, future work can continue to refine the balance between reliability, sustainability, and affordability, ultimately supporting the development of more resilient and sustainable power systems.

7

Conclusion

In this thesis, the central research question explored how to *assess and enhance the reliability of an AC/VSC-MTDC system based on MMC technology for offshore wind energy generation and transmission while balancing redundancy, modularity, and maintenance costs*. The research involved the development of composite probabilistic models and a detailed analysis of system components, revealing that system reliability can be significantly improved by carefully evaluating these factors. Strategic redundancy in MMCs, optimised maintenance intervals, wind turbine drivetrain technologies and appropriate sizing of offshore wind capacities were used as key elements in a methodology maintaining a reliable power supply while integrating renewable energy sources into the grid.

To address how the expected available capacity of offshore wind energy generators can be probabilistically modelled under various meteorological conditions, a composite probabilistic model was developed, incorporating wind speed characteristics, turbine power output curves, and the stochastic nature of component failures. The model's accuracy was carefully evaluated, revealing that a 5-state model led to an approximate 10% accuracy loss of expected capacity in the worst-case scenario, particularly at the IJmuiden Ver Alpha location. This loss was primarily due to conservative rounding methods that did not merge other states with the 100% output state, which therefore lead to worse reliability indices rather than overly optimistic ones. Despite the similar wind profiles across different chosen locations in the North Sea, offshore distances contributed to a decrease in expected available capacity, which the model was able to account for effectively. Moreover, as locations moved further offshore, the model's accuracy improved due to increased probabilities of intermediate states. This accuracy was balanced against the computational expense required to evaluate the reliability of a hybrid AC/DC power system, ensuring that the assessment remained both precise and efficient at the 100 km distance further used. Future work could enhance these models by incorporating real-world logistical constraints, such as resource availability and maintenance logistics, which would further refine the economic viability of different drivetrain options.

The analysis of drivetrain technology and offshore distance showed that direct drive DD systems offer superior reliability and lower operation and maintenance $O\&M$ costs compared to geared systems, particularly in deep offshore locations and high installed capacities. For instance, the $O\&M$ costs for DD turbines at far-offshore locations were found to be significantly lower than those for geared turbines,

with the cost gap widening as offshore distance increased. Moreover, the geared drivetrain showed approximately a 2% reduction in availability compared to DD systems due to the absence of the gearbox component with this gap widening as turbines were placed further offshore. The increased reliability and lower maintenance costs make the DD systems more favourable in deep offshore applications. The analysis also highlighted that the expected capacity factor for DD systems declines more gradually than for DFIG systems, especially as installed capacity increases because of the generally higher capacity in DD wind turbines. Through this model an O&M cost difference criterion that is sensitive to both offshore distance and installed capacity was established, underscoring the importance of selecting appropriate drivetrain technologies based on specific offshore conditions to optimise both performance and cost-efficiency.

A detailed reliability model for a Modular Multilevel Converter (MMC) was developed, based on the fundamental failure rates of sub-module components and the impact of various redundancy schemes. The model compared stand-by redundancy with active redundancy. The analysis demonstrated that stand-by redundancy is more effective, particularly at high levels of redundancy. Moreover, the sensitivity analysis of the model revealed that by implementing an optimised MMC reliability strategy, the expected available capacity of the entire DC transmission end can be improved by 20%, demonstrating the substantial system-wide impact of targeted reliability enhancements in the converter level. The sensitivity analysis further revealed that the effectiveness of redundancy in improving MMC reliability is significantly amplified when paired with shorter maintenance intervals. Additionally, the model identified a maximum achievable MMC availability of 99.91%, highlighting the necessary balance between cost and reliability.

The cost-effective optimisation of MMC reliability was achieved by balancing redundancy, modularity, and maintenance costs. The study identified an optimal strategy involving a redundancy level of $n = 7$ sub-modules and a maintenance interval of $T_m = 4.5$ years. This strategy was based on a minimum MMC availability of 99.5% criterion which yields an annual cost increment of 40.943 k$ per year in O&M costs. This approach ensured that the MMC could achieve high reliability at the minimum cost, making it suitable for integration into HVDC systems where both reliability and cost-efficiency are critical. Future research could further enhance these strategies by incorporating dynamic aspects of converter operation, such as varying load conditions and the implementation of protection schemes, to ensure long-term reliability under changing operational demands.

The reliability of a complete multi-terminal HVDC MTDC system was modelled using a probabilistic approach that was based on the 3-state model of a single DCT end, with careful consideration of the state space building process. This involved ensuring sequential transitions, separate evaluation of sending and receiving ends, and limiting system capacity by the lowest capacity in the sending and receiving chain. The analysis found that increasing the degree of coupling within the MTDC system improves the expected available transmission capacity factor by up to 1%, but the benefits diminish beyond a certain level of coupling. Furthermore, configurations with unequal numbers of sending and receiving ends were less effective in enhancing reliability compared to balanced configurations, highlighting the importance of a well-designed system topology. However, the research also showed that further refinement is possible by extending this analysis to a real power system nodal reliability evaluation, where the importance of each receiving end can be better understood and optimised.

In quantifying expected surplus wind energy (ESWE) and the associated offshore storage potential as offshore wind capacity increased, the study found that after a threshold point, where the 75% state

of the 5-state HLII composite model aligns with the base load state, the probability of wind energy curtailment due to excess supply over demand rises sharply. Beyond this threshold, ESWE increases significantly. Furthermore, the differences between the exact and 5-state rounded composite models revealed that as more states are considered, a greater amount of wind energy is curtailed due to limited transmission capacity, and this threshold transition smooths out. However, this outcome may be somewhat unrealistic because the base load is not constant; it varies throughout the year, just as the wind energy resource fluctuates seasonally. This suggests that more accurate storage sizing necessitates time-sequential simulations that incorporate energy state tracking and more detailed load models, alongside a thorough analysis of load forecast uncertainties.

The integration of large-scale offshore wind capacity into existing power systems presents significant challenges to system reliability, particularly when conventional generators are replaced without a well-defined strategic policy or sizing method. The convolution of the composite model with the standardised IEEE RTS24 load and generation model revealed a notable decline in reliability, moreover it is demonstrated that merely increasing wind capacity does not linearly improve reliability indices. The results, however, exhibited a converging behaviour as more offshore wind capacity was added, highlighting the necessity for careful planning and optimal sizing of wind capacity to balance sustainability, cost and reliability. The application of a constant risk policy to the RTS-24 system identified an optimal offshore wind capacity of 780 MW, combined with an MMC availability of 98.25%, as an effective solution for maintaining system reliability while substituting 350 MW of conventional generation. This approach resulted in an offshore O&M variable cost of 53.512 $/MWh and achieved a wind energy penetration level of 22.60% within the system. Future research could explore additional policies to further optimise this balance, ensuring that the integration of renewable energy sources continues to meet the evolving demands of power systems.

In conclusion, this thesis provides a comprehensive analysis of the reliability of hybrid AC/DC power systems that incorporate offshore wind energy and MTDC transmission systems. The findings emphasise the critical influence of careful topology planning, strategic redundancy, optimised maintenance intervals, and the appropriate sizing of offshore wind capacities to ensure system reliability while integrating renewable energy sources. The research explores the intricate balance between reliability, sustainability, and affordability in modern power systems, and introduces the constant risk sizing method as a strategic approach for optimising wind energy penetration while minimising O&M costs. These insights offer a valuable foundation for future designs and strategies aimed at safeguarding the reliability of the power grid as it increasingly depends on sustainable energy and advanced power electronics.

References

[1] National Renewable Energy Laboratory (NREL). *IEA 15MW 240 RWT Offshore Wind Turbine Data*. https://github.com/NREL/turbine-models/blob/master/Offshore/IEA_15MW_240_RWT.csv. Accessed: 2024-07-08. National Renewable Energy Laboratory (NREL), 2020. URL: https://github.com/NREL/turbine-models/blob/master/Offshore/IEA_15MW_240_RWT.csv.

[2] Gayan Abeynayake et al. "Reliability and cost-oriented analysis, comparison and selection of multi-level MVDC converters". In: *IEEE Transactions on Power Delivery* 36.6 (2021), pp. 3945–3955.

[3] Hamza Abunima et al. "A systematic review of reliability studies on composite power systems: a coherent taxonomy motivations, open challenges, recommendations, and new research directions". In: *Energies* 11.9 (2018), p. 2417.

[4] Miad Ahmadi, Aditya Shekhar, and Pavol Bauer. "Impact of the various components consideration on choosing optimal redundancy strategy in mmc". In: *2022 IEEE 20th International Power Electronics and Motion Control Conference (PEMC)*. IEEE. 2022, pp. 21–26.

[5] Miad Ahmadi, Aditya Shekhar, and Pavol Bauer. "Mixed Redundancy Strategy for Modular Multilevel Converters in High-Power Applications". In: *IEEE Open Journal of the Industrial Electronics Society* 5 (2024), pp. 535–546. DOI: 10.1109/OJIES.2024.3415007.

[6] Miad Ahmadi, Aditya Shekhar, and Pavol Bauer. "Switch voltage rating selection considering cost-oriented redundancy and modularity-based trade-offs in modular multilevel converter". In: *IEEE Transactions on Power Delivery* 38.4 (2023), pp. 2831–2842.

[7] Ronald N Allan et al. *Reliability evaluation of power systems*. Springer Science & Business Media, 2013.

[8] Ronald N Allan, Roy Billinton, and NMK Abdel-Gawad. "The IEEE reliability test system-extensions to and evaluation of the generating system". In: *IEEE Transactions on Power Systems* 1.4 (1986), pp. 1–7.

[9] O. Anaya-Lara. "12 - Offshore wind farm arrays". In: *Offshore Wind Farms*. Ed. by Chong Ng and Li Ran. Woodhead Publishing, 2016, pp. 389–417. ISBN: 978-0-08-100779-2. DOI: https://doi.org/10.1016/B978-0-08-100779-2.00012-X. URL: https://www.sciencedirect.com/science/article/pii/B978008100779200012X.

[10] Jake Badger et al. *Global Wind Atlas 3.0*. https://globalwindatlas.info/es/. Developed with financial support from the Energy Sector Management Assistance Program (ESMAP), a multi-donor trust fund administered by The World Bank. 2023.

[11] Christian Bak et al. "The DTU 10-MW reference wind turbine". In: *Danish wind power research 2013*. 2013.

[12] Reinhold Bayerer et al. "Model for power cycling lifetime of IGBT modules-various factors influencing lifetime". In: *5th international conference on integrated power electronics systems*. VDE. 2008, pp. 1–6.

[13] François Besnard, Katharina Fischer, and Lina Bertling Tjernberg. "A model for the optimization of the maintenance support organization for offshore wind farms". In: *IEEE Transactions on Sustainable Energy* 4.2 (2012), pp. 443–450.

[14] R Billinton, CL Wee, and G Hamoud. "Digital computer algobithms for the calculation of generating capacity reliability indices". In: *IEEE Transactions on Power Apparatus and Systems* 1 (1982), pp. 203–211.

[15] Roy Billinton and Ronald Norman Allan. *Reliability evaluation of engineering systems*. Vol. 792. Springer, 1992.

[16] Roy Billinton and Guang Bai. "Generating capacity adequacy associated with wind energy". In: *IEEE transactions on energy conversion* 19.3 (2004), pp. 641–646.

[17] Roy Billinton, Hua Chen, and R Ghajar. "Time-series models for reliability evaluation of power systems including wind energy". In: *Microelectronics Reliability* 36.9 (1996), pp. 1253–1261.

[18] Roy Billinton and Yi Gao. "Multistate wind energy conversion system models for adequacy assessment of generating systems incorporating wind energy". In: *IEEE Transactions on Energy Conversion* 23.1 (2008), pp. 163–170.

[19] Roy Billinton and Dange Huang. "Effects of Load Forecast Uncertainty on Bulk Electric System Reliability Evaluation". In: *IEEE Transactions on Power Systems* 23.2 (2008), pp. 418–425. DOI: 10.1109/TPWRS.2008.920078.

[20] James Carroll, Alasdair McDonald, and David McMillan. "Failure rate, repair time and unscheduled O&M cost analysis of offshore wind turbines". In: *Wind energy* 19.6 (2016), pp. 1107–1119.

[21] James Carroll et al. "Availability, operation and maintenance costs of offshore wind turbines with different drive train configurations". In: *Wind Energy* 20.2 (2017), pp. 361–378.

[22] James Carroll et al. "Drivetrain availability in offshore wind turbines". In: *European Wind Energy Association 2014 Annual Conference*. 2014.

[23] Christopher J Crabtree, Donatella Zappalá, and Simon I Hogg. "Wind energy: UK experiences and offshore operational challenges". In: *Proceedings of the Institution of Mechanical Engineers, Part A: Journal of Power and Energy* 229.7 (2015), pp. 727–746.

[24] Ahmad Salehi Dobakhshari and Mahmud Fotuhi-Firuzabad. "A reliability model of large wind farms for power system adequacy studies". In: *IEEE Transactions on energy conversion* 24.3 (2009), pp. 792–801.

[25] European Commission. *Delivering on the EU Offshore Renewable Energy Ambitions*. Communication from the Commission to the European Parliament, the Council, the European Economic and Social Committee and the Committee of the Regions, Brussels, 24 October 2023, COM(2023) 668 final. 2023. URL: https://eur-lex.europa.eu/legal-content/EN/TXT/?uri=COM:2023:668:FIN.

[26] Johannes Falck et al. "Reliability of power electronic systems: An industry perspective". In: *IEEE Industrial Electronics Magazine* 12.2 (2018), pp. 24–35.

[27] Katharina Fischer, Francois Besnard, and Lina Bertling. "Reliability-centered maintenance for wind turbines based on statistical analysis and practical experience". In: *IEEE Transactions on Energy Conversion* 27.1 (2011), pp. 184–195.

[28] Evan Gaertner et al. *Definition of the IEA 15-Megawatt Offshore Reference Wind Turbine*. Technical Report NREL/TP-5000-75698. Sponsored by the U.S. Department of Energy and the European Union's H2020 Program. National Renewable Energy Laboratory (NREL), Mar. 2020. URL: https://www.nrel.gov/docs/fy20osti/75698.pdf.

[29] Anastasios Golnas. "PV system reliability: An operator's perspective". In: *2012 IEEE 38th Photovoltaic Specialists Conference (PVSC) PART 2*. IEEE. 2012, pp. 1–6.

[30] M. Grigoriu. "Methods for approximate reliability analysis". In: *Structural Safety* 1.2 (1982), pp. 155–165. ISSN: 0167-4730. DOI: https://doi.org/10.1016/0167-4730(82)90022-4. URL: https://www.sciencedirect.com/science/article/pii/0167473082900224.

[31] Libang Guo et al. "Nodal reliability evaluation for a VSC-MTDC-based hybrid AC/DC power system". In: *IEEE Transactions on Power Systems* 35.3 (2019), pp. 2300–2312.

[32] Yifei Guo, Houlei Gao, and Qiuwei Wu. "A combined reliability model of VSC-HVDC connected offshore wind farms considering wind speed correlation". In: *IEEE Transactions on Sustainable Energy* 8.4 (2017), pp. 1637–1646.

[33] Berthold Hahn, Michael Durstewitz, and Kurt Rohrig. "Reliability of wind turbines". In: *Wind Energy: Proceedings of the Euromech Colloquium*. Springer. 2007, pp. 329–332.

[34] Frederik Hahn et al. "Mission profile based reliability evaluation of building blocks for modular power converters". In: *PCIM Europe 2017; International Exhibition and Conference for Power Electronics, Intelligent Motion, Renewable Energy and Energy Management*. VDE. 2017, pp. 1–7.

[35] T.J. Hammons et al. "Role of HVDC transmission in future energy development". In: *IEEE Power Engineering Review* 20.2 (2000), pp. 10–25. DOI: 10.1109/MPER.2000.819913.

[36] Military Handbook. "Reliability prediction of electronic equipment (mil-hdbk-217f)". In: *US Government Printing Office, Washington DC* (1986).

[37] Guoqiang Ji et al. "A renewal-process-based component outage model considering the effects of aging and maintenance". In: *International Journal of Electrical Power & Energy Systems* 44.1 (2013), pp. 52–59. ISSN: 0142-0615. DOI: https://doi.org/10.1016/j.ijepes.2012.07.035. URL: https://www.sciencedirect.com/science/article/pii/S014206151200395X.

[38] Kailash C Kapur and Michael Pecht. *Reliability engineering*. Vol. 86. John Wiley & Sons, 2014.

[39] G.A. Klutke, P.C. Kiessler, and M.A. Wortman. "A critical look at the bathtub curve". In: *IEEE Transactions on Reliability* 52.1 (2003), pp. 125–129. DOI: 10.1109/TR.2002.804492.

[40] KNMI. *WINS50 - wind at 10-600 meter height for the Netherlands from HARMONIE-AROME as daily files*. https://dataplatform.knmi.nl/dataset/wins50-ctl-nl-daily-3d-2. Winds of the North Sea in 2050 (WINS50): wind speed, wind direction, temperature, pressure and relative humidity at 10-600 meter height from a reanalysis for 2019-2021 with the NWP model HARMONIE-AROME nested in the ECMWF reanalysis ERA5. Data are stored as daily files for a subdomain covering the Netherlands. More information on: www.wins50.nl. Koninklijk Nederlands Meteorologisch Instituut (KNMI), 2024. URL: https://dataplatform.knmi.nl/dataset/wins50-ctl-nl-daily-3d-2.

[41] Andréa P Leite, Carmen LT Borges, and Djalma M Falcao. "Probabilistic wind farms generation model for reliability studies applied to Brazilian sites". In: *IEEE Transactions on Power Systems* 21.4 (2006), pp. 1493–1501.

[42] Hui Liu, Poh Chiang Loh, and Frede Blaabjerg. "Review of fault diagnosis and fault-tolerant control for modular multilevel converter of HVDC". In: *IECON 2013-39th Annual Conference of the IEEE Industrial Electronics Society*. IEEE. 2013, pp. 1242–1247.

[43] Callum MacIver, Keith RW Bell, and Duško P Nedić. "A reliability evaluation of offshore HVDC grid configuration options". In: *IEEE transactions on power delivery* 31.2 (2015), pp. 810–819.

[44] N. Unnikrishnan Nair, P.G. Sankaran, and N. Balakrishnan. "Chapter 2 - Basic Reliability Concepts". In: *Reliability Modelling and Analysis in Discrete Time*. Ed. by N. Unnikrishnan Nair, P.G. Sankaran, and N. Balakrishnan. Boston: Academic Press, 2018, pp. 43–106. ISBN: 978-0-12-801913-9. DOI: https://doi.org/10.1016/B978-0-12-801913-9.00002-6. URL: https://www.sciencedirect.com/science/article/pii/B9780128019139000026.

[45] Saeed Peyghami, Peter Palensky, and Frede Blaabjerg. "An overview on the reliability of modern power electronic based power systems". In: *IEEE Open Journal of Power Electronics* 1 (2020), pp. 34–50.

[46] Saeed Peyghami, Zhongxu Wang, and Frede Blaabjerg. "Reliability modeling of power electronic converters: A general approach". In: *2019 20th workshop on control and modeling for power electronics (COMPEL)*. IEEE. 2019, pp. 1–7.

[47] Marvin Rausand and Arnljot Hoyland. *System reliability theory: models, statistical methods, and applications*. Vol. 396. John Wiley & Sons, 2003.

[48] Johan Ribrant and Lina Bertling. "Survey of failures in wind power systems with focus on Swedish wind power plants during 1997-2005". In: *2007 IEEE power engineering society general meeting*. IEEE. 2007, pp. 1–8.

[49] F Castro Sayas and RN Allan. "Generation availability assessment of wind farms". In: *IEE Proceedings-Generation, Transmission and Distribution* 143.5 (1996), pp. 507–518.

[50] Pieter Schavemaker and Lou Van der Sluis. *Electrical power system essentials*. John Wiley & Sons, 2017.

[51] Kamran Sharifabadi et al. *Design, control, and application of modular multilevel converters for HVDC transmission systems*. John Wiley & Sons, 2016.

[52] L Shen et al. "A review on VSC-HVDC reliability modeling and evaluation techniques". In: *IOP Conference Series: Materials Science and Engineering*. Vol. 199. 1. IOP Publishing. 2017, p. 012133.

[53] C Singh and A Lago-Gonzalez. "Reliability modeling of generation systems including unconventional energy sources". In: *IEEE Transactions on Power Apparatus and Systems* 5 (1985), pp. 1049–1056.

[54] Yantao Song and Bingsen Wang. "Survey on reliability of power electronic systems". In: *IEEE transactions on power electronics* 28.1 (2012), pp. 591–604.

[55] Andrei Stan, Sorina Costinaș, and Georgiana Ion. "Overview and Assessment of HVDC Current Applications and Future Trends". In: *Energies* 15.3 (2022). ISSN: 1996-1073. DOI: 10.3390/en15031193. URL: https://www.mdpi.com/1996-1073/15/3/1193.

[56] Tyler Stehly, Philipp Beiter, and Patrick Duffy. *2019 cost of wind energy review*. Tech. rep. National Renewable Energy Lab.(NREL), Golden, CO (United States), 2020.

[57] Probability Methods Subcommittee. "IEEE reliability test system". In: *IEEE Transactions on power apparatus and systems* 6 (1979), pp. 2047–2054.

[58] TenneT. *2GW Program: More Wind Energy for Europe*. TenneT TSO B.V., TenneT TSO GmbH, April 2023. 2023. URL: https://www.tennet.eu.

[59] B.W. Tuinema. "Reliability Evaluation of Offshore Wind Energy Networks and the Dutch Power System". Master's thesis. Delft, Netherlands: Delft University of Technology, Dec. 2009. URL: http://resolver.tudelft.nl/uuid:c93519c6-164f-43e8-a684-3b8e6125c4fc.

[60] Bart Tuinema. "Reliability of transmission networks: Impact of EHV underground cables & interaction of offshore-onshore networks". English. Dissertation (TU Delft). Delft University of Technology, 2017. ISBN: 978-94-6299-778-3. DOI: 10.4233/uuid:98c73893-a400-4fb2-9266-a9b5e19ccc69.

[61] Bart W Tuinema, Alexandru I Stefanov, and Francisco M Gonzalez-Longatt. *Probabilistic reliability analysis of power systems*. Springer.

[62] Katsumi Uchida et al. "Study on detection for the defects of XLPE cable lines". In: *IEEE transactions on power delivery* 11.2 (1996), pp. 663–668.

[63] Biyang Wang et al. "Reliability model of MMC considering periodic preventive maintenance". In: *IEEE Transactions on Power Delivery* 32.3 (2016), pp. 1535–1544.

[64] Shaoping Wang, Mileta Tomovic, and Hong Liu. *Commercial Aircraft Hydraulic Systems: Shanghai Jiao Tong University Press Aerospace Series*. Academic Press, 2015.

[65] Shuaishuai Wang, Amir R Nejad, and Torgeir Moan. "On initial design and modelling of a 10 MW medium speed drivetrain for offshore wind turbines". In: *Journal of Physics: Conference Series*. Vol. 1356. 1. IOP Publishing. 2019, p. 012024.

[66] Shaoyong Yang et al. "An industry-based survey of reliability in power electronic converters". In: *IEEE transactions on Industry Applications* 47.3 (2011), pp. 1441–1451.

[67] Roy D Yates and David J Goodman. *Probability and stochastic processes: a friendly introduction for electrical and computer engineers*. John Wiley & Sons, 2014.

[68] Pengfei Yu et al. "Reliability-centered maintenance for modular multilevel converter in HVDC transmission application". In: *IEEE Journal of Emerging and Selected Topics in Power Electronics* 9.3 (2020), pp. 3166–3176.

[69] Donatella Zappalá and Peter J Tavner. "2.11-Wind Turbine Reliability-Maintenance Strategies". In: *Comprehensive Renewable Energy (Second Edition): Volume 1-9*. Elsevier, 2022, pp. 353–370.